UNIVERSITY OF SOUTHAMPTON

FACULTY OF ENGINEERING, SCIENCE & MATHEMATICS

School of Physics and Astronomy

Lattice QCD calculations of K_{l3} and pion form factors using partially twisted boundary conditions

by

Hugo Pedroso de Lima

Thesis submitted for the degree of
Doctor of Philosophy

September 2010

UNIVERSITY OF SOUTHAMPTON

<u>ABSTRACT</u>

FACULTY OF ENGINEERING, SCIENCE & MATHEMATICS

SCHOOL OF PHYSICS AND ASTRONOMY

<u>Doctor of Philosophy</u>

LATTICE QCD CALCULATIONS OF K_{l3} AND PION FORM FACTORS USING PARTIALLY TWISTED BOUNDARY CONDITIONS

Hugo Pedroso de Lima

This thesis presents results of lattice QCD computations of the $K \to \pi$ semi-leptonic (K_{l3}) and pion electromagnetic form factors using partially twisted boundary conditions. These form factors parameterize low-energy non-perturbative strong interaction effects and cannot therefore be calculated in perturbative QCD. The pion electromagnetic form factor provides information on its charge distribution. The K_{l3} form factor at zero momentum transfer ($q^2 = 0$) can be used in the determination of the $|V_{us}|$ element of the CKM matrix. An accurate determination of these form factors is therefore important. Using partially twisted boundary conditions we calculate the K_{l3} form factor directly at $q^2 = 0$, removing the need for the q^2 interpolation required in previous lattice QCD simulations, thus eliminating one source of systematic error in this calculation. We also use partially twisted boundary conditions to calculate the pion form factor at values of q^2 close to $q^2 = 0$ allowing for a direct evaluation of the charge radius of the pion. The simulations are performed on an ensemble of the RBC/UKQCD collaboration's gauge configurations with Domain Wall Fermions and the Iwasaki gauge action with an inverse lattice spacing of 1.73(3) GeV at light quark masses corresponding to a pion mass of 330 MeV. We calculate the form factors at these simulated quark masses and then use chiral perturbation theory to extrapolate our results to physical light quark masses. We find for the charge radius of the physical pion $\langle r_\pi^2 \rangle = 0.418(31)\,\text{fm}^2$, in agreement with the experimentally determined result. For the value of the K_{l3} form factor, $f_+^{K\pi}(q^2)$, at $q^2 = 0$ and physical quark masses we find $f_+^{K\pi}(0) = 0.960(^{+5}_{-6})$. This result is then used to determine a value for $|V_{us}|$. Together with a recent determination of $|V_{ud}|$ we find that the current results are consistent with unitarity of the CKM matrix.

Contents

List of Tables

iv

List of Figures

Declaration

This thesis was composed by myself and presents work that was carried out as part of the RBC-UKQCD collaboration. Some of the results presented here have been published in:

- P. Boyle, J. Flynn, A. Jüttner, C. Kelly, C. Maynard, H. Pedroso de Lima, C. Sachrajda, and J. Zanotti, *The pion's electromagnetic form factor at small momentum transfer in full lattice QCD*, JHEP **07** (2008) 112, [0804.3971]

- P. Boyle, J. Flynn, A. Jüttner, C. Kelly, C. Maynard, H. Pedroso de Lima, C. Sachrajda, and J. Zanotti, *$K \to \pi$ form factors with reduced model dependence*, *The European Physical Journal C - Particles and Fields* **69** (2010) 159–167, [1004.0886]

and have also appeared in the conference proceedings:

- P. Boyle, J. Flynn, A. Jüttner, C. Kelly, C. Maynard, H. Pedroso de Lima, C. Sachrajda, and J. Zanotti, *K_{l3} and pion form factors using partially twisted boundary conditions*, *PoS* **LATTICE2008** (2008) 287, [0812.4265]

Chapters 1-5 present background material compiled using a number of sources as well as my own description of both established techniques and techniques proposed by our collaboration which were used in this work for the calculations of the form factors presented in this thesis. The material presented in these chapters has been appropriately referenced in the text.

The results for the form factor computations performed in this work are presented in chapters 6 and 7. Of the original material presented in these chapters, I played a major role in the measurements of correlation functions using the QCDOC and HECToR supercomputers as well as their analysis for the calculations of the form factors. The correlation function measurements were carried out on gauge configuration ensembles generated

by the RBC-UKQCD collaboration. I also worked directly on the pion form factor chiral extrapolations and contributed to the chiral extrapolation calculations of the K_{l3} form factor.

Acknowledgments

Firstly, I would like to thank my supervisor Chris Sachrajda for his guidance and supervision over the last four years and in particular for his comments and suggestions on this thesis. I would also like to thank my advisor Jonathan Flynn for all his help in all things lattice QCD.

I would particularly like to thank Andreas Jüttner for numerous helpful discussions and for all his help in getting me started on lattice QCD analysis techniques.

I also thank my collaborators James Zanotti, Chris Maynard, Peter Boyle and Chris Kelly.

My experience over the last four years would not have been the same without Asia, to whom I will always be grateful for all her love and support.

Lastly, I thank my mother who has always been supportive and understanding throughout the years.

x

Chapter 1

Introduction

The idea that all matter is composed of elementary particles has been around since the sixth century BC. It was first suggested by the Greek philosopher Democritus who proposed that all matter is comprised of tiny "atoms", from the Greek word "átomos" meaning indivisible. Today we know that atoms are not the smallest building blocks of nature. With the discovery of the electron by J. J. Thompson in 1898 and the atomic nucleus by Rutherford in 1911 it became clear that in fact atoms are mostly empty space with a small positively charged nucleus containing most of the mass of the atom and small mass negatively charged electrons orbiting this nucleus. It was later discovered that the nucleus itself is composed of protons and neutrons, which themselves belong to a large family of particles called "hadrons".

During the 1950's and 1960's a huge number of hadrons were discovered in particle experiments. Physicists literate in group theory, most notably M. Gell-Mann [7], were able to see that the patterns of symmetries in this 'zoo' of particles suggested that the huge number of hadrons being discovered could be neatly organized by the principles of group theory, and that the resulting patterns could be explained in terms of a quark model of particles with fractional electric charge, carrying some other type of charge that physicists now call colour. This led to the development of quantum chromodynamics, or QCD for short, the quantum field theory of the strong interaction, which describes the interactions of quarks and gluons (the force carriers of the strong interaction). Quarks and gluons have however never been observed as free particles in nature, a phenomenon known as *confinement*. They are permanently bound inside hadrons due to the strongly interacting forces between them.

Meanwhile during the 1960's Glashow, Weinberg and Salam [8–10] were successful in combining two of the fundamental forces of nature, the electromagnetic and weak interactions, into a single unified quantum field theory known as the quantum electroweak theory, for which they shared the 1979 Nobel prize in physics. According to the Glashow, Weinberg and Salam (GSW) model the electroweak force is carried by the photon, the Z^0 and the $W^\pm$ bosons. An additional scalar field is however also required in the electroweak theory to generate the masses of the quarks, leptons and the W and Z bosons via spontaneous symmetry breaking. This additional spin-0 boson is the famous Higgs boson, which to this day has not been discovered, and the mechanism of mass generation is known as the Higgs mechanism [11–14].

The combined QCD and quantum electroweak theories became known as the Standard Model (SM) of particle physics. The SM embodies our current understanding of all the known fermionic matter particles (plus the Higgs boson) and their interactions via three of the four fundamental forces of nature: electromagnetic, weak and strong, mediated by spin-1 gauge bosons. The SM however, falls short of being a complete theory of fundamental interactions because it does not incorporate gravity. Furthermore, it also does not correctly account for neutrino oscillations and their masses. Nevertheless, despite these and other shortcomings, the SM has been highly successful in explaining a huge range of experimental data and has been tested to remarkable precision.

If QCD correctly accounts for the quark-gluon interactions, confinement of quarks and the observed hadron spectrum should naturally follow from it. However, as was first proved by Gross and Wilczek [15], QCD exhibits *asymptotic freedom* which implies that the coupling constant of QCD increases with decreasing energy scale. This means that we cannot study low energy physics such as the hadron spectrum using the usual perturbative techniques of quantum field theory and must resort to non-perturbative methods. Furthermore, the study of various weak interaction processes is also burdened by the influence of non-perturbative effects from the strong interaction. Of relevance to this work is the study of the semi-leptonic weak decay $K \to \pi l \nu_l$ (known as a K_{l3} decay, where l is a lepton and ν_l the corresponding neutrino), where the non-perturbative features of the strong interaction are prominent due to the typical energy scales of the particles involved. To correctly account for the low energy non-perturbative effects

of the strong interaction, we employ lattice QCD.

Lattice QCD is based on the Euclidean formulation of QCD and can be understood as a regularization method that discretises spacetime with a finite lattice spacing a. The advance of modern computer technologies, together with Monte Carlo methods allows us to numerically evaluate, within a reasonable amount of time, the path integral of lattice QCD formulated in a finite volume.

It turns out however that the computational cost of simulating fully dynamical fermions in lattice QCD increases as $1/m_f^2$, where m_f is the fermion mass. This means that at present we are unable to simulate QCD on a lattice with physical light quark masses. Instead we have to do lattice simulations with light quark masses heavier than the physical ones and resort to chiral perturbation theory, an effective field theory based on the approximate chiral symmetry of the light quark QCD Lagrangian, to extrapolate to the physical point.

In this work we use lattice QCD with $N_f = 2 + 1$ dynamical flavours of quarks (i.e. 2 light degenerate quarks and 1 heavy quark) at light quark masses corresponding to a pion with mass $m_\pi = 330\,\text{MeV}$ to calculate the pion electromagnetic (e.m.) form factor and the form factors for K_{l3} decays. We then make use of chiral perturbation theory formulae to extrapolate the results to physical light quark masses.

The $K \to \pi l \nu_l$ decay channel is an important channel for precision studies of SM parameters. As we will discuss later in this introductory chapter, the K_{l3} form factor at zero momentum transfer ($q^2 = 0$) can be used in the determination of $|V_{us}|$, an element of the Cabbibo-Kobayashi-Maskawa (CKM) matrix [16, 17] that relates the strong and weak interaction eigenstates. An accurate determination of $|V_{us}|$ is important as it allows us to impose constraints on some unknown parameters of possible physics models beyond the SM that are relevant to guide direct searches at high energy particle colliders, e.g. those planned at the Large Hadron Collider (LHC) at CERN (see for example [18, 19]). In particular, an accurate determination of $|V_{us}|$ allows us to test the unitarity of the CKM matrix. The situation prior to the work presented in this thesis began, pointed towards a possible violation of unitarity of the CKM matrix with the lattice results and experimental measurements at the time (see for example [20] for a review of these results).

Precise determinations of the K_{l3} form factor are therefore important.

Previous lattice calculations of the K_{l3} form factor were not able to calculate it directly at $q^2 = 0$ due to the use of periodic boundary conditions. They relied on an interpolation between $q^2_{\max} = (m_K - m_\pi)^2$ and several negative values of q^2, as allowed by periodic boundary conditions, to determine the form factor at $q^2 = 0$. This introduces a systematic error due to the choice of interpolating function used. In this work we update and improve on previous lattice calculations of the K_{l3} form factor by using partially twisted boundary conditions to calculate the form factor directly at $q^2 = 0$ thus eliminating this source of systematic error.

In this work we also use partially twisted boundary conditions in a lattice QCD calculation of the pion e.m. form factor. The pion e.m. form factor has previously been studied on the lattice using periodic boundary conditions. This limits the momentum resolution that one can achieve to the discrete Fourier momentum values that result from periodic boundary conditions. The use of partially twisted boundary conditions allows us to calculate the form factor at any desired value of the momentum transfer q^2 and in particular at low values of q^2 below the minimum value obtainable with periodic boundary conditions. In contrast to previous studies this allows for a direct evaluation of the charge radius of the pion.

The rest of this thesis will be structured as follows:

- For the remainder of this chapter, I will briefly introduce the aspects of the SM that are relevant to this thesis, namely QCD, electroweak interactions and the CKM matrix. I will also introduce in this chapter the form factors that are investigated in this thesis.

- In chapter 2, I will briefly describe lattice QCD. I will introduce the gauge field and fermion actions used in the generation of the configurations used for the measurements done in this work, namely the Iwasaki gauge action and the Domain Wall fermion action.

- In chapter 3, I introduce Monte Carlo methods for gauge field configuration generation and discuss how to measure the required correlation functions on these gauge configurations, for the calculation of pseudo-scalar meson form factors. I finish the chapter with a brief discussion of the techniques used for analyzing the resulting data.

- Chapter 4 gives an overview of chiral perturbation theory and its applications to the pion electromagnetic and the K_{l3} form factors.

The derivation of the relevant chiral perturbation theory formulae is outlined.

- Chapter 5 introduces twisted and partially twisted boundary conditions and discusses their application in the calculation of pseudoscalar meson form factors at any desired value of q^2.

- The results of the lattice simulations carried out in this work at light quark masses corresponding to a pion with mass $m_\pi = 330 \, \text{MeV}$ are presented in chapter 6.

- In chapter 7 we extrapolate our data to physical light quark masses using the chiral perturbation theory formulae discussed in chapter 4. A discussion of the systematic errors in our results is also given in this chapter.

- Chapter 8 presents the conclusions as well as future prospects for the calculations presented in this work.

1.1   Standard Model

The Standard Model (SM) of particle physics describes the interaction of the known fundamental matter particles (plus the Higgs boson) via the strong, electromagnetic and weak forces. In the SM there are three generations of quarks and leptons. The Standard Model Lagrangian is constructed by imposing a local $\text{SU}(3)_C \times \text{SU}(2)_L \times \text{U}(1)_Y$ internal gauge symmetry. The local $\text{SU}(3)_C$ gauge symmetry gives rise to the strong interaction and the $\text{SU}(2)_L \times \text{U}(1)_Y$ local gauge symmetry gives rise to the electroweak interaction. The matter and gauge fields fall into different representations of the various symmetry groups of the SM. An additional scalar field, the Higgs boson, is also included to generate the fermion and gauge boson masses. Upon writing the most general Lagrangian invariant under this symmetry group, one finds that the dynamics depend on 19 parameters, whose numerical values are established by experiment. We now describe the different sectors of the SM, namely the quantum chromodynamics and electroweak sectors.

1.1.1 Quantum Chromodynamics

Quantum chromodynamics (QCD) is the theory of the strong nuclear force, which describes the interactions of quarks (spin-$\frac{1}{2}$ fermions) and gluons (spin-1 massless gauge bosons). In QCD there are six quark flavours (u, d, c, s, t, b), split into three generations (u, d), (c, s) and (t, b). QCD is a non-abelian SU(3) gauge theory. Each quark has a hidden three-valued quantum number known as colour and transforms as the fundamental triplet representation of SU(3) in colour space. There are eight gluons that transform as the adjoint representation of SU(3) in colour space.

The QCD Lagrangian density is given by

$$\mathcal{L}_{QCD} = \sum_f \bar{\psi}_{f,a}(x)(i\gamma^\mu D_\mu - m_f)_{ab}\psi_{f,b}(x) - \frac{1}{4}F^{c,\mu\nu}F^c_{\mu\nu}, \qquad (1.1)$$

where a, b and c are colour indices and a and b run from 1 to 3 (fundamental representation) while c runs from 1 to 8 (adjoint representation), the sum over f is taken over the six flavours of quarks $f \in (u, d, c, s, t, b)$ and spinor indices have been suppressed.

The covariant derivative is defined as

$$(D_\mu)_{ab} = \partial_\mu \delta_{ab} - ig(A_\mu)_{ab}, \qquad (1.2)$$

where g is the bare strong coupling constant. The gauge field A_μ comprises of eight gluon fields

$$A_\mu = A_\mu^a \lambda^a, \qquad (1.3)$$

where λ^a are the eight generators of SU(3) satisfying the commutation relations $[\lambda^a, \lambda^b] = if^{abc}\lambda^c$ (where f^{abc} are the structure constants) and the normalization condition $\text{Tr}(\lambda^a\lambda^b) = \frac{\delta_{ab}}{2}$.

The gauge field strength tensor $F_{\mu\nu}$ is given in terms of the gluon fields by

$$F^a_{\mu\nu} = \partial_\mu A^a_\nu - \partial_\nu A^a_\mu + g[A^b_\mu, A^c_\nu]f^{abc}. \qquad (1.4)$$

We can readily check that the QCD Lagrangian is invariant under the local gauge transformations:

$$\psi(x) \quad \to \quad \psi'(x) = \Lambda(x)\psi(x), \qquad (1.5)$$

$$A_\mu(x) \quad \to \quad A'_\mu(x) = \Lambda(x)A_\mu(x)\Lambda^\dagger(x) + \frac{i}{g}\Lambda(x)\partial_\mu\Lambda^\dagger(x), \qquad (1.6)$$

$$\Lambda(x) \quad = \quad e^{-i\lambda^a \alpha^a(x)} \in \mathrm{SU}(3). \tag{1.7}$$

Since the gluons also carry colour charge, they are self-interacting. The way that the gluons interact among themselves has dramatic effects. The strength of the strong coupling increases as the distance scale increases. This means that it is not possible to observe quarks or gluons as free particles and they are permanently confined in bound states known as hadrons, such as the proton or neutron. This is a property known as *confinement*. However, at very high energies (corresponding to short distances) the strength of the interaction is small. This is known as *asymptotic freedom*. This means that at high energies we can use perturbation theory to do calculations in QCD. At low energies however we must use non-perturbative methods to study the bound states of the theory. The dominant non-perturbative method used for the study of QCD at low energies is the lattice formulation of QCD.

1.1.2 Symmetries of the light quark QCD Lagrangian

The six quark flavours in QCD can be split into two groups according to their masses as there is a substantial mass difference between the light (u, d, s) quarks and the heavy (c, b, t) quarks. We will now look at the symmetries of the QCD Lagrangian in flavour space that arise from considering only the light quark part of the QCD Lagrangian.

SU(3) flavour symmetry and isospin

The light quark part of the QCD Lagrangian is given by

$$\mathcal{L}_{QCD} = \bar{\psi}(\gamma_\mu D_\mu - M)\psi, \tag{1.8}$$

where

$$\psi = \begin{pmatrix} u \\ d \\ s \end{pmatrix}, \quad M = \begin{pmatrix} m_u & 0 & 0 \\ 0 & m_d & 0 \\ 0 & 0 & m_s \end{pmatrix}, \tag{1.9}$$

and we have dropped colour indices for simplicity.

If we make the assumption that all the light quarks are degenerate in mass $m_u = m_d = m_s = m_l = (m_u + m_d + m_s)/3$, then

$$M = m_l I, \tag{1.10}$$

where I is the identity matrix, and the light quark QCD Lagrangian is invariant under global U(3) transformations in flavour space

$$\psi \to \psi' = U\psi, \quad U = e^{i\beta^a\lambda^a}, e^{i\alpha} \in \mathrm{U}(3), \tag{1.11}$$

where the λ^a are the generators of SU(3). The light QCD Lagrangian therefore has a symmetry group SU(3)×U(1). The U(1) symmetry leads to conservation of baryon number. The SU(3) flavour symmetry classifies the spectrum of hadrons made up of u, d and s quarks, all of which can be grouped into different representations of SU(3), like for example the octets of 0^- mesons $(\pi^+, \pi^-, \pi^0, \eta, K^+, K^-, K^0, \bar{K}^0)$ and $\frac{1}{2}^+$ baryons $(n, p, \Sigma^+, \Lambda^0, \Sigma^0, \Sigma^+, \Xi^-, \Xi^0)$. SU(3) flavour symmetry is only an approximate symmetry. Since $\hat{m}/m_s \approx 1/25$ (where $\hat{m} = (m_u + m_d)/2$), the dominant contribution to SU(3) flavour symmetry breaking is the mass of the strange quark. A much better symmetry comes from considering only the u and d quarks since m_u and m_d are much closer together. The light quark QCD Lagrangian is then invariant under global SU(2) transformations in flavour space, and this symmetry is known as isospin symmetry.

Chiral symmetry

Define the left and right handed fermion fields

$$\psi_L = P_L\psi = \frac{1-\gamma_5}{2}\psi \quad ; \quad \psi_R = P_R\psi = \frac{1+\gamma_5}{2}\psi \tag{1.12}$$

$$\bar{\psi}_{L/R} = \bar{\psi}P_{R/L}. \tag{1.13}$$

In terms of these fields the light quark QCD Lagrangian can be written as

$$\bar{\psi}(i\gamma^\mu D_\mu - M)\psi = \bar{\psi}_L i\gamma^\mu D_\mu \psi_L + \bar{\psi}_R i\gamma^\mu D_\mu \psi_R - \bar{\psi}_R M\psi_L - \bar{\psi}_L M\psi_R. \tag{1.14}$$

If we now set the light quark masses to zero, then we can see that the light quark QCD Lagrangian is invariant under the independent U(3) global transformations of left and right handed fermion fields

$$\psi_L \to \psi'_L = \mathrm{U}_L\psi \; ; \quad \psi_R \to \psi'_R = \mathrm{U}_R\psi \tag{1.15}$$

where

$$\mathrm{U}_L = e^{i\beta^a_L\lambda^a}, e^{i\alpha_L} \; ; \quad \mathrm{U}_R = e^{i\beta^a_R\lambda^a}, e^{i\alpha_R}. \tag{1.16}$$

8

The Lagrangian therefore has a symmetry group $SU(3)_L \times SU(3)_R \times U(1)_L \times U(1)_R$ and each of the above transformations has an associated Noether current

$$
\begin{aligned}
J_{\mu,L}^a(x) &= \bar{\psi}_L(x)\gamma_\mu\lambda^a\psi_L(x), & (1.17) \\
J_{\mu,R}^a(x) &= \bar{\psi}_R(x)\gamma_\mu\lambda^a\psi_R(x), & (1.18) \\
J_{\mu,L}(x) &= \bar{\psi}_L(x)\gamma_\mu\psi_L(x), & (1.19) \\
J_{\mu,R}(x) &= \bar{\psi}_R(x)\gamma_\mu\psi_R(x). & (1.20)
\end{aligned}
$$

Equivalently we can transform the ψ and $\bar{\psi}$ fields by

$$
\psi \rightarrow V\psi ; \quad \bar{\psi} \rightarrow \bar{\psi}V \qquad (1.21)
$$

where

$$
V = U_L P_L + U_R P_R, \quad U_{L,R} \in U(3)_{L,R} \qquad (1.22)
$$

which leads to the conserved vector and axial vector currents

$$
\begin{aligned}
J_\mu^a(x) &= J_{\mu,L}^a(x) + J_{\mu,R}^a(x) = \bar{\psi}(x)\gamma_\mu\lambda^a\psi(x), & (1.23) \\
J_{\mu 5}^a(x) &= J_{\mu,L}^a(x) - J_{\mu,R}^a(x) = \bar{\psi}(x)\gamma_\mu\gamma_5\lambda^a\psi(x), & (1.24) \\
J_\mu(x) &= J_{\mu,L}(x) + J_{\mu,R}(x) = \bar{\psi}(x)\gamma_\mu\psi(x), & (1.25) \\
J_{\mu 5}(x) &= J_{\mu,L}(x) - J_{\mu,R}(x) = \bar{\psi}(x)\gamma_\mu\gamma_5\psi(x). & (1.26)
\end{aligned}
$$

Note that the axial current (1.26) is only conserved in the classical theory. Quantum effects lead to a non-zero divergence of the axial current, a phenomenon known as the axial anomaly [21]. The Lagrangian therefore has a symmetry group $SU(3)_V \times SU(3)_A \times U(1)_V$. This chiral symmetry, which should be approximately satisfied in the light quark sector, is however not seen in the hadronic spectrum. Although hadrons can be classified in $SU(3)_V$ representations, degenerate multiplets with opposite parity do not exist. Furthermore, the octet of pseudo-scalar mesons is much lighter than all other hadronic states. To be consistent with experiment, the $SU(3)_L \times SU(3)_R$ symmetry must be broken by the ground state of QCD and thus the symmetry is spontaneously broken down to $SU(3)_V$, which leads to eight Goldstone bosons, one for each generator of the broken $SU(3)$ symmetry. Since $m_f \neq 0$ chiral symmetry is only an approximate symmetry, and the Goldstone bosons have non-zero masses. These eight Goldstone bosons are identified as the pseudo-scalar meson octet, which have much lighter masses

than the rest of the hadron spectrum. Similar considerations with the u and d quarks only, lead to an SU(2) chiral symmetry which leads to the isospin triplet of the relatively light pions. The approximation $m_s = 0$ is less accurate than assuming zero mass for the u and d quarks and consequently the pions are lighter than the kaons or the η. The question of whether chiral SU(3) or chiral SU(2) is a better approximation has important implications for the application of chiral perturbation theory to lattice calculations. We will discuss the applications of chiral SU(3) and SU(2) perturbation theory to the K_{l3} and pion form factors in this thesis.

1.1.3 Electroweak theory

In the GSW electroweak model [8–10], unification of the electromagnetic and weak interactions is accomplished through a Lagrangian invariant under a local $\mathrm{SU}(2)_L \times \mathrm{U}(1)_Y$ internal gauge symmetry with the corresponding gauge bosons $(W_\mu^1, W_\mu^2, W_\mu^3)$ in the adjoint representation of the weak isospin group $\mathrm{SU}(2)_L$ and the gauge boson B_μ of the weak hypercharge group $\mathrm{U}(1)_Y$. The W_μ^i gauge bosons couple only to doublets of the left-handed components of quark and lepton fields,

$$\begin{pmatrix} \nu_e \\ e^- \end{pmatrix}_L \begin{pmatrix} \nu_\mu \\ \mu^- \end{pmatrix}_L \begin{pmatrix} \nu_\tau \\ \tau^- \end{pmatrix}_L \begin{pmatrix} u \\ d' \end{pmatrix}_L \begin{pmatrix} c \\ s' \end{pmatrix}_L \begin{pmatrix} t \\ b' \end{pmatrix}_L , \quad (1.27)$$

where d', s' and b' are weak interaction eigenstates, which are related to the strong interaction eigenstates d, s and t via the CKM matrix which we will describe in section (1.1.4).

The B_μ gauge field couples to both left and right handed fermions with an interaction strength proportional to the weak hypercharge Y defined by

$$Y = Q - I_3, \quad (1.28)$$

where Q is the electromagnetic charge and I_3 is the third component of weak isospin, i.e. $\pm\frac{1}{2}$ for the upper/lower component of a weak isospin doublet (left-handed) and 0 for a weak isospin singlet (right-handed).

Since the left-handed fermions are weak isospin doublets and the right-handed ones are singlets a Lagrangian constructed in this way does not allow for fermion mass terms. Furthermore the gauge bosons of this theory are massless which is inconsistent with experiment. For these reasons, an additional scalar field Φ, the Higgs boson [11–14], has to be introduced into

the Lagrangian. The Higgs field is a weak isospin doublet of complex scalar fields and has a non-zero vacuum expectation value v. With the addition of the Higgs field, the vacuum state of the theory is no longer invariant under $\text{SU}(2)_L \times \text{U}(1)_Y$. The $\text{SU}(2)_L \times \text{U}(1)_Y$ symmetry is spontaneously broken down to the group $\text{U}(1)_Q$ of electromagnetism. The gauge bosons W_μ^3 and B_μ mix to form the Z_μ^0 boson and the photon A_μ. The $W_\mu^\pm$ gauge bosons are given by $W_\mu^\pm = \frac{1}{\sqrt{2}}(W_\mu^1 \mp iW_\mu^2)$. The $W^\pm$ and the Z^0 bosons acquire a mass through this Higgs mechanism by absorbing the Goldstone bosons of the broken symmetry while the photon remains massless corresponding to the unbroken $\text{U}(1)_Q$ symmetry. The Higgs field couples to the fermions via Yukawa type interactions and generates their masses through its vacuum expectation value.

Of the many terms in the electroweak Lagrangian after spontaneous symmetry breaking, the only ones of relevance to this work are the charged current interactions $\mathcal{L}_{CC}$ and the electromagnetic current interactions $\mathcal{L}_{\text{em}}$ given by

$$
\begin{aligned}
\mathcal{L}_{CC} &= -\frac{g_w}{\sqrt{2}} \left[\bar{u}_i \gamma^\mu \frac{1}{2}(1 - \gamma^5)d_i' + \bar{\nu}_i \gamma^\mu \frac{1}{2}(1 - \gamma^5)l_i \right] W_\mu^+ + h.c., \quad (1.29) \\
\mathcal{L}_{\text{em}} &= eQ_f \sum_f \bar{f}\gamma_\mu f A^\mu, \quad (1.30)
\end{aligned}
$$

where the u_i are up-type quarks, namely the u, c and t quarks, the d_i' are down-type weak interaction eigenstate quarks, namely the d', s' and b' quarks, the l_i are the leptons e^-, μ^- and τ^- with their corresponding neutrinos ν_i, g_w is the weak coupling constant and f is a fermion with charge Q_f. The charged current interactions allow for flavour changing via the exchange of $W^\pm$ bosons.

1.1.4   The CKM matrix

The Cabibbo-Kobayashi-Maskawa (CKM) matrix [16,17] is a matrix that relates the quark flavour eigenstates of the weak interaction to the quark mass eigenstates (the eigenstates of the strong interaction). The CKM matrix is a unitary matrix that parameterizes the relative strength of transitions between different quark flavours. It is defined by

$$
\begin{pmatrix} d' \\ s' \\ b' \end{pmatrix} = \begin{pmatrix} V_{ud} & V_{us} & V_{ub} \\ V_{cd} & V_{cs} & V_{cb} \\ V_{td} & V_{ts} & V_{tb} \end{pmatrix} \begin{pmatrix} d \\ s \\ b \end{pmatrix} = V_{\text{CKM}} \begin{pmatrix} d \\ s \\ b \end{pmatrix}, \qquad (1.31)
$$

where the elements V_{ij} are complex. The CKM matrix is a unitary matrix, so it has at most N^2 components, where N is the number of generations of quark flavours. $2N - 1$ of these parameters are not physically significant, because one phase can be absorbed into each quark field but an overall common phase is unobservable. Hence, the total number of free parameters independent of the choice of the phases of basis vectors is $(N - 1)^2$. The CKM matrix is therefore described by only four free parameters one of which is a complex phase which allows for CP violation within the SM. Unitarity of the CKM matrix implies that the sum of the squares of the row (or column) elements is one. Of particular interest to this thesis is the unitarity relation

$$
|V_{ud}|^2 + |V_{us}|^2 + |V_{ub}|^2 = 1. \qquad (1.32)
$$

Weak decays are normalized to the Fermi coupling $G_F = \sqrt{2}g_w^2/8m_W^2$, which is determined from muon decay $\mu^- \to e^- \nu_e \nu_\mu$. In the SM, G_F is universal for quarks and leptons, thus as well as testing the unitarity of the CKM matrix, equation (1.32) also tests the universality of weak interactions between quarks and leptons. Any deviation from one in equation (1.32) would be a sign for physics beyond the SM.

In the unitarity relation (1.32), the contribution from $|V_{ub}|^2$ is at least an order of magnitude smaller than the current errors on $|V_{ud}|^2$ or $|V_{us}|^2$ and can therefore be safely neglected ($|V_{ub}| = 0.00389(44)$ [22]). Thus with the currently achievable precision the unitarity relation (1.32) reduces to

$$
|V_{ud}|^2 + |V_{us}|^2 = 1. \qquad (1.33)
$$

The $|V_{ud}|$ matrix element can be determined very precisely from super allowed $0^+ \to 0^+$ nuclear beta decays (see [23] for a recent determination giving $|V_{ud}| = 0.97425(22)$). The $|V_{us}|$ matrix element can be determined using the following two methods:

1. From the ratio of the kaon and pion leptonic decay rates we obtain [24,

12

25]

$$\frac{\Gamma_{K\to l\nu}}{\Gamma_{\pi\to l\nu}} = \frac{|V_{us}|^2}{|V_{ud}|^2}\frac{f_K^2}{f_\pi^2}\frac{m_K(1-m_l^2/m_K^2)^2}{m_\pi(1-m_l^2/m_\pi^2)^2}(1+\delta_{\text{EM}}), \qquad (1.34)$$

where f_K and f_π are the kaon and pion decay constants and δ_{EM} denotes the effect of long-distance electromagnetic effects. The ratio of the decay rates can thus be used to extract the ratio

$$\frac{|V_{us}|^2}{|V_{ud}|^2}\frac{f_K^2}{f_\pi^2}, \qquad (1.35)$$

and one can then extract $|V_{us}|$ using lattice determinations of the ratio f_K/f_π and experimental measurements of $|V_{ud}|$.

2. The decay rate of the semi-leptonic decay $K \to \pi l\nu_l$ (K_{l3}) is given by [26]

$$\Gamma_{K_{l3}} = \frac{G_F^2 m_K^5}{192\pi^3}C_K^2 I S_{\text{EW}}\left[1+\delta_{\text{EM}}+\delta_{SU(2)}\right]^2|V_{us}|^2|f_+^{K\pi}(0)|^2, \quad (1.36)$$

where G_F is the Fermi coupling constant, I is a phase-space integral, $\delta_{SU(2)}, S_{\text{EW}}, \delta_{\text{EM}}$ contain the isospin breaking, short distance electroweak and long distance electromagnetic corrections respectively, C_K is a Clebsch-Gordan coefficient (1 for K^0 and $1/\sqrt{2}$ for $K^\pm$ decays) and $f_+^{K\pi}(0)$ is the $K \to \pi$ vector form factor at zero momentum transfer which we will define in section 1.2.1. From the measured decay rate one can extract $|V_{us}f_+^{K\pi}(0)|$ and a theoretical calculation of $f_+^{K\pi}(0)$ is then required to extract $|V_{us}|$.

Prior to the work presented in this thesis was carried out the experimental measurements and lattice QCD results at that time showed signs of a possible deviation from one in the unitarity relation (1.33) (see for example [20]). This highlights the importance for precision calculations of $f_+^{K\pi}(0)$ for the determination of $|V_{us}|$. In this work we calculate the $f_+^{K\pi}(0)$ form factor in lattice QCD using partially twisted boundary conditions.

1.2 Pseudo-scalar meson form factors

The matrix element $\langle P_f(p_f)|j_\mu|P_i(p_i)\rangle$ of the vector current j_μ between initial and final states consisting of pseudo-scalar mesons P_i and P_f respectively, must by Lorentz invariance, be a four-vector function of only the two momentum four-vectors p_i^μ and p_f^μ as the pseudo-scalar mesons

have spin zero. The most general such four-vector function takes the form of a linear combination of p_i^μ and p_f^μ, or equivalently of $p_i^\mu + p_f^\mu$ and $p_i^\mu - p_f^\mu$, with scalar coefficients. As we will be considering only mesons that are on-shell the scalars p_i^2 and p_f^2 are fixed at the values $p_i^2 = m_i^2$ and $p_f^2 = m_f^2$. Thus the scalar variables that can be formed from p_i^μ and p_f^μ can only be functions of $p_i \cdot p_f$, or equivalently of the momentum transfer $q^2 = (p_i - p_f)^2 = (m_i^2 + m_f^2) - 2p_i \cdot p_f$. Thus the matrix element must take the general form

$$\langle P_f(p_f)|j_\mu|P_i(p_i)\rangle = f_+^{P_i P_f}(q^2)(p_i + p_f)_\mu + f_-^{P_i P_f}(q^2)(p_i - p_f)_\mu, \quad (1.37)$$

where the functions $f_+^{P_i P_f}(q^2)$ and $f_-^{P_i P_f}(q^2)$ are known as the vector form factors of the transition $P_i \to P_f$. The form factors $f_+^{P_i P_f}(q^2)$ and $f_-^{P_i P_f}(q^2)$ parameterize the non-perturbative QCD effects and cannot therefore be calculated using perturbative QCD methods.

1.2.1 K_{l3} form factor

For $K \to \pi l \nu_l$ semi-leptonic decays, j_μ is the weak current $\bar{s}\gamma_\mu u$ and the hadronic matrix element is

$$\langle \pi(p_f)|j_\mu|K(p_i)\rangle = (p_i + p_f)_\mu f_+^{K\pi}(q^2) + (p_i - p_f)_\mu f_-^{K\pi}(q^2). \quad (1.38)$$

As we will discuss in chapter 4, the form factors can be calculated in chiral perturbation theory. In the SU(3) flavour limit ($m_u = m_d = m_s$) the conservation of the vector current implies that $f_+^{K\pi}(0) = 1$. We can thus expand around the SU(3) chiral limit ($m_u = m_d = m_s = 0$) in powers of the light quark masses

$$f_+^{K\pi}(0) = 1 + f_2 + f_4 + ... \quad (1.39)$$

where $f_n = \mathcal{O}(m_{u,d,s}^n/(4\pi f_0)^n)$ and f_2 and f_4 are the next-to-leading order (NLO) and next-to-next-to-leading order (NNLO) corrections in chiral perturbation theory (see section 4.3.1 for an expression for f_2). The Ademollo-Gatto Theorem [27], implies that f_2 is completely specified in terms of light pseudo-scalar meson masses and the decay constant f_0 in the chiral limit. Furthermore, $|f_+^{K\pi}(0) - 1|$ will be at least of second order in the expansion in powers of the mass difference $m_s - m_{u,d}$ and therefore f_2 and f_4 will be *small* ($f_2 = -0.023$ [26] using the physical pion decay

14

constant $f_\pi = 131$ MeV as an estimate for f_0). Difficulties arise in the calculation of Δf, the sum of the corrections beyond NLO

$$\Delta f = f_+^{K\pi}(0) - (1 + f_2), \qquad (1.40)$$

to the sub-1% precision level using analytical methods only. The quantity Δf depends on the low energy constants of chiral perturbation theory and thus requires model input. A model independent determination of Δf with a reliable error estimate is required.

The standard approach of computing $f_+^{K\pi}(0)$ in lattice QCD uses periodic boundary conditions and was first developed by Becirevic et al. in [28, 29]. It involves determining the scalar form factor $f_0^{K\pi}(q^2)$ defined by

$$f_0^{K\pi}(q^2) = f_+^{K\pi}(q^2) + \frac{q^2}{m_K^2 - m_\pi^2} f_-^{K\pi}(q^2), \qquad (1.41)$$

at $q_{\max}^2 = (m_K - m_\pi)^2$ and several negative values of q^2 as allowed by the periodic boundary conditions and then interpolating the results to $q^2 = 0$ to calculate $f_+^{K\pi}(0) = f_0^{K\pi}(0)$. In [2] this method is used at a variety of quark masses and the result is then chirally extrapolated to the physical pion and kaon masses. The final result quoted is $f_+^{K\pi}(0) = 0.9644(33)(34)(14)$ where the first error is statistical, and the second and third are estimates of the systematic errors due to the choice of parameterization for the interpolation and lattice artefacts respectively.

In this work we use partially twisted boundary conditions to calculate the form factor directly at $q^2 = 0$, thereby removing the systematic error due to the choice of parameterization for the interpolation in q^2.

1.2.2 Pion electromagnetic form factor

For the $\pi \to \pi$ transition, j_μ is the electromagnetic current $\frac{2}{3}\bar{u}\gamma_\mu u - \frac{1}{3}\bar{d}\gamma_\mu d$, both P_i and P_f are pions and current conservation implies that $f_-^{\pi\pi}(q^2) = 0$. Thus we have a single form factor, the electromagnetic form factor of the pion $f^{\pi\pi}(q^2)$, defined by

$$\langle \pi(p_f)|j_\mu|\pi(p_i)\rangle = (p_i + p_f)_\mu\, f^{\pi\pi}(q^2). \qquad (1.42)$$

Clearly $f^{\pi\pi}(0) = 1$ as we can see by setting $p_i = p_f$. $f^{\pi\pi}(q^2)$ provides information on the internal structure of the pion and in particular on its

charge distribution. From the slope of the form factor at $q^2 = 0$ we can calculate the pion's electromagnetic charge radius, which is defined by

$$\langle r_\pi^2 \rangle \equiv 6 \frac{d}{dq^2} f^{\pi\pi}(q^2)\big|_{q^2=0}. \tag{1.43}$$

Prior to the work presented in this thesis the pion form factor had been studied in lattice QCD using periodic boundary conditions (the European Twisted Mass Collaboration (ETMC) did however present preliminary results with $N_f = 2$ dynamical flavours using twisted boundary conditions in [30] before the work presented in this thesis was published. Their final results were then later published in [31]). As will be discussed in chapter 5, this limits the momentum resolution that one can achieve. In particular the smallest non-zero value of $Q^2 = -q^2$, obtainable with periodic boundary conditions is $Q^2_{\text{min}} = 2m_\pi(\sqrt{m_\pi^2 + (2\pi/L)^2} - m_\pi)$. In our simulations this corresponds to $Q^2_{\text{min}} \approx 0.15 \text{ GeV}^2$. In this work we use partially twisted boundary conditions to calculate the form factor at arbitrarily small values of the momentum transfer and explore the region $0 < Q^2 < Q^2_{\text{min}}$. The smallest values of Q^2 at which we calculate the form factor are lower than those explored by any other collaboration so far (we calculate the form factor down to $Q^2 = 0.013 \text{ GeV}^2$, while the smallest value at which the ETMC collaboration calculates the form factor is $Q^2 \approx 0.05 \text{ GeV}^2$).

Chapter 2

Lattice QCD

QCD is an asymptotically free theory. This means that at low energies the strength of the interaction is large and we cannot therefore use perturbation theory. We are thus forced to use non-perturbative methods to do calculations in QCD in this regime. One such method is lattice QCD, where we simulate QCD on a discrete Euclidean spacetime lattice, with the quarks placed on lattice sites and the gluons on the links connecting the lattice sites. Discretizing spacetime regulates both the infrared and ultraviolet divergences in the path integrals that we will describe in section 2.1. Furthermore, on a finite spacetime lattice path integrals become finite dimension integrals (albeit with a large number of dimensions) which we can evaluate using Monte Carlo techniques.

When we discretise the QCD action, we must ensure that two conditions are met. First, we must preserve gauge invariance and secondly the lattice QCD action must have the correct continuum limit.

In this chapter we begin by showing how one can evaluate observables in QCD using path integrals in section 2.1. We then proceed to discretise the gauge field part and fermion part of the QCD action in sections 2.2 and 2.3 respectively, in order to turn the path integral into a finite dimensional integral which we can then evaluate using Monte Carlo methods.

2.1   Path integral formulation

In the path integral formulation of QCD we can calculate the vacuum expectation value of an operator $\mathcal{O}$ by starting from the generating func-

tional [21]:

$$Z[\eta, \bar{\eta}, J] = \int \mathcal{D}A_\mu \mathcal{D}\psi \mathcal{D}\bar{\psi} \exp\left[i \int d^4x [\mathcal{L}_{QCD} + JA_\mu + \bar{\eta}\psi + \bar{\psi}\eta]\right], \quad (2.1)$$

and taking functional derivatives with respect to the source terms J, η, $\bar{\eta}$

$$\begin{aligned}
\langle 0 | \mathcal{O} | 0 \rangle &= \left. \frac{1}{Z} \frac{\delta}{\delta J} \frac{\delta}{\delta \eta} \frac{\delta}{\delta \bar{\eta}} Z[J, \eta, \bar{\eta}] \right|_{J=\eta=\bar{\eta}=0} \qquad (2.2) \\
&= \frac{1}{Z} \int \mathcal{D}A_\mu \mathcal{D}\psi \mathcal{D}\bar{\psi} \mathcal{O} \exp\left[i \int d^4x \mathcal{L}_{QCD}\right]. \qquad (2.3)
\end{aligned}$$

In lattice QCD we evaluate these path integrals numerically in a finite volume, using statistical techniques. To do so we must first perform a Wick rotation from Minkowski spacetime into Euclidean spacetime,

$$t_M \rightarrow -it_E. \qquad (2.4)$$

The path integral (2.3) then becomes

$$\langle 0 | \mathcal{O} | 0 \rangle = \frac{1}{Z} \int \mathcal{D}A_\mu \mathcal{D}\psi \mathcal{D}\bar{\psi} \mathcal{O} e^{-S^E_{QCD}}, \qquad (2.5)$$

where the Euclidean QCD action S^E_{QCD}, is given by

$$S^E_{QCD} = \int d^4x \left[\sum_f \bar{\psi}_{f,a}(x)(\gamma^{E,\mu}D_\mu + m_f)_{ab}\psi_{f,b}(x) + \frac{1}{4}F^{a,\mu\nu}F^a_{\mu\nu} \right]. \quad (2.6)$$

Here γ^E_μ are the Euclidean gamma matrices, which satisfy $\gamma^{E\dagger}_\mu = \gamma^E_\mu$, $\{\gamma^E_\mu, \gamma^E_\nu\} = 2\delta_{\mu\nu}$ and γ^E_5 is defined as $\gamma^E_5 = \gamma^E_1 \gamma^E_2 \gamma^E_3 \gamma^E_4$. From now on we will be working in Euclidean space only and therefore we drop the superscript E.

The quark fields ψ and $\bar{\psi}$ are Grassmann variables and we can integrate them out. The partition function in Euclidean space then becomes

$$Z[\eta, \bar{\eta}, J] = \int \mathcal{D}A_\mu \mathcal{D}\psi \mathcal{D}\bar{\psi} \exp\left[-\int d^4x[\mathcal{L}_{QCD} + JA_\mu + \bar{\eta}\psi + \bar{\psi}\eta]\right] \quad (2.7)$$

$$= \int \mathcal{D}A_\mu \det(D) \exp\left[-\int d^4x[\bar{\eta}D^{-1}\eta + \mathcal{L}_G + JA_\mu]\right]. \qquad (2.8)$$

Here $\mathcal{L}_G$ is the gauge field kinetic term part of the Euclidean QCD La-

18

grangian density and for one fermion flavour D is

$$D = \gamma^\mu D_\mu + m_f. \tag{2.9}$$

We can now calculate vacuum expectation values of operators from the partition function by functional differentiation. For example, we can calculate the quark propagator

$$\langle 0| \psi(x)\bar{\psi}(y) |0\rangle = \frac{\delta}{\delta\eta(x)} \frac{\delta}{\delta\bar{\eta}(y)} Z \Big|_{\eta=\bar{\eta}=0} \tag{2.10}$$

$$= \frac{1}{Z} \int \mathcal{D}A_\mu G(x,y) \det(D) e^{-S_G}, \tag{2.11}$$

where

$$G(x,y) = D^{-1}(x,y), \tag{2.12}$$

is the Feynman quark propagator, which is the amplitude of propagation of a quark from one point in spacetime to another. The quark propagator is of particular importance, as we will show later in section 3.2, as we can write any observable involving quark fields in terms of the quark propagator.

The Euclidean formulation of the path integral thus takes the form of a statistical ensemble average with a Boltzmann factor $\det D e^{-S_G}$. We can therefore use statistical mechanics techniques to evaluate the path integral.

2.2 Gauge bosons on the lattice

2.2.1 Wilson gauge action

To represent the gauge field $A_\mu(x)$ on a lattice we use a link variable $U(x, x + a\hat{\mu})$ related to the gauge field by

$$U(x, x + a\hat{\mu}) \equiv U_\mu(x) = e^{iagA_\mu^b(x)\lambda_b}. \tag{2.13}$$

Here a is the lattice spacing, $\hat{\mu}$ is a unit vector in one of the four space-time directions, g is the bare coupling constant and λ_b are the eight generators of SU(3). The link variable $U_\mu(x)$ is thus an SU(3) matrix and provides a path-dependent connection between the lattice site x and the lattice site $x + a\hat{\mu}$. The conjugate $U_\mu^\dagger(x)$ connects the two lattice sites in

the opposite direction

$$U_\mu^\dagger(x) = e^{-iagA_\mu^b(x)\lambda_b} = U(x + a\hat\mu, x). \tag{2.14}$$

Each link matrix transforms according to

$$U_\mu(x) \rightarrow \Lambda(x)U_\mu(x)\Lambda^\dagger(x + a\hat\mu). \tag{2.15}$$

where $\Lambda(x) \in$ SU(3). We can construct a gauge invariant action from the trace of a closed loop of gauge links. The simplest such loop is the plaquette

$$P_{\mu\nu} = U_\mu(x)U_\nu(x + a\hat\mu)U_\mu^\dagger(x + a\hat\nu)U_\nu^\dagger(x). \tag{2.16}$$

The plaquette is used to define the Wilson gauge action [32] as follows:

$$S_G^W = \frac{\beta}{N_c} \sum_{x;\mu<\nu} ReTr[1 - P_{\mu\nu(x)}], \tag{2.17}$$

where $\beta = 2N_c/g^2$ and N_c is number of colours ($N_c = 3$ in this case). It is easy to check that this action is invariant under the SU(3) gauge transformation (2.15). Inserting (2.13) into (2.16) and expanding as a series in the lattice spacing a we get

$$P_{\mu\nu}(x) = 1 + iga^2 F_{\mu\nu}(x) - \frac{g^2a^4}{2}F_{\mu\nu}^2(x) + ... \tag{2.18}$$

Plugging this into the Wilson gauge action (2.17) and taking the limit $a \rightarrow 0$

$$S_G^W = a^4\left(\sum_x \frac{1}{4}F^{a,\mu\nu}(x)F_{\mu\nu}^a(x) + \mathcal{O}(a^2)\right) \tag{2.19}$$

$$\rightarrow \int d^4x \frac{1}{4}F^{a,\mu\nu}(x)F_{\mu\nu}^a(x). \tag{2.20}$$

we see that the Wilson gauge action has the correct continuum limit and is thus an appropriate lattice gauge action. We can also see from the above equation that with the Wilson action lattice artifacts contribute at $\mathcal{O}(a^2)$.

2.2.2 Iwasaki gauge action

The Wilson gauge action is not a unique lattice gauge action. Other gauge invariant choices are possible. Any arbitrary closed loop of links can be

used to construct a lattice gauge action. Consequently it is possible to design lattice gauge actions from linear combinations of closed loops such that the discretization errors are reduced.

One example is to add a term based on a six link rectangle to the Wilson action

$$R_{\mu\nu} = U_\mu(x)U_\mu(x+a\hat{\mu})U_\nu(x+2a\hat{\mu})U_\mu^\dagger(x+a\hat{\mu}+a\hat{\nu})U_\mu^\dagger(x+a\hat{\nu})U_\nu^\dagger(x). \quad (2.21)$$

The gauge action is then given by [33, 34]

$$S_G = \frac{\beta}{N_c} \sum_{x;\mu<\nu} ReTr[1 - c_{pl}P_{\mu\nu(x)} - c_{rt}R_{\mu\nu}(x)]. \quad (2.22)$$

where the constants c_{pl} and c_{rt} satisfy $c_{pl} + 8c_{rt} = 1$ in order to preserve the correct continuum limit.

In this work we used the renormalization group improved gauge action of Iwasaki, defined by setting $c_{rt} = -0.331$ [35, 36]. As well as reducing discretization errors this gauge action is also chosen because it has been shown to reduce the residual chiral symmetry breaking that arises from the domain wall fermion action [37, 38] which we will describe in section 2.3.3.

2.3 Fermions on the lattice

2.3.1 Naive fermions

The simplest way to construct a lattice action for fermions is to replace derivatives in the continuum Euclidean fermion action by symmetric differences. We define the lattice difference operator

$$\Delta_\mu^+(x,y) = \frac{1}{a}\left[\delta_{y,x+a\hat{\mu}} - \delta_{y,x}\right], \quad (2.23)$$

and the lattice symmetric difference operator

$$\Delta_\mu(x,y) \equiv \frac{1}{2}[\Delta_\mu^+(x,y) + \Delta_\mu^-(x,y)] = \frac{1}{2a}\left[\delta_{y,x+a\hat{\mu}} - \delta_{y,x-a\hat{\mu}}\right]. \quad (2.24)$$

In analogy with the covariant derivative for the continuum theory we define a lattice covariant difference operator by using link variables to con-

nect neighboring sites as follows:

$$\nabla_\mu^+(x,y) = \frac{1}{a}\left[U_\mu(x)\delta_{y,x+a\hat\mu} - \delta_{y,x}\right], \tag{2.25}$$

and a symmetric lattice covariant difference operator

$$\nabla_\mu(x,y) = \frac{1}{2}[\nabla_\mu^+(x,y) + \nabla_\mu^-(x,y)] = \frac{1}{2a}\left[U_\mu(x)\delta_{y,x+a\hat\mu} - U_\mu^\dagger(x)\delta_{y,x-a\hat\mu}\right]. \tag{2.26}$$

The naive lattice fermion action is then given by

$$S_F = a^4 \sum_{x,y} \bar\psi(x)D(x,y)\psi(y), \tag{2.27}$$

where

$$D(x,y) = \sum_\mu \gamma_\mu \nabla_\mu(x,y) + m_f \delta_{x,y}. \tag{2.28}$$

It is easy to check that this action has the correct continuum limit by Taylor expanding in small lattice spacing a. This will also show that the discretization errors are of $\mathcal{O}(a^2)$ [39]. A problem with this action occurs however if we calculate the quark propagator in the free field theory, where $U_\mu(x) = 1$. In this case the free quark propagator is given by

$$G(x,y) = D^{-1}(x,y) = \int_{-\pi/a}^{\pi/a} \frac{d^4k}{(2\pi)^4} e^{-ik.(x-y)}G(k), \tag{2.29}$$

where

$$G(k) = D^{-1}(k) = \left(i\sum_\mu \gamma_\mu \tilde k_\mu + m_f\right)^{-1}, \quad \tilde k_\mu = \frac{1}{a}\sin(ak_\mu). \tag{2.30}$$

We see that in addition to the poles of the continuum theory at $k_\mu = 0$ the propagator also has poles at the corners of the Brillouin Zone $k_\mu = \pm\pi/a$. Therefore we see that such an action describes a theory with $2^4 = 16$ fermions. This is known as the *fermion doubling problem.* Several improvements over the naive fermion action have been proposed in order to remove the doubling problem. Here we will discuss two of them: Wilson fermions and Domain Wall fermions.

2.3.2 Wilson fermions

In order to overcome the fermion doubling problem Wilson introduced an extra dimension five term. The addition of this term is irrelevant in the continuum limit as it vanishes linearly as $a \to 0$. The Wilson fermion action [40] is given by

$$S_F^W = S_F + \frac{ar}{2} \sum_{x,y,z,\mu} \nabla_\mu^+(x,y) \bar{\psi}(y) \nabla_\mu^+(x,z) \psi(z), \qquad (2.31)$$

where r is the Wilson parameter $0 \le r \le 1$. The Wilson action can be rewritten as

$$S_F^W = a^4 \sum_{x,y} \bar{\psi}(x) D^W(x,y) \psi(y), \qquad (2.32)$$

where

$$D^W(x,y) = -\frac{1}{2} \sum_{\mu} \left[\left(\frac{r}{a} - \gamma_\mu \right) U_\mu(x) \delta_{y,x+a\hat{\mu}} + \left(\frac{r}{a} + \gamma_\mu \right) U_\mu^\dagger(x) \delta_{y,x-a\hat{\mu}} \right]$$

$$+ \left(m_f + \frac{4r}{a} \right) \delta_{x,y}. \qquad (2.33)$$

If we again consider the fermion propagator in the free field theory, where $U_\mu(x) = 1$ we get

$$G(k) = D^{-1}(k) = \left(i \sum_{\mu} \gamma^\mu \tilde{k}_\mu + \mathcal{M}(k) \right)^{-1}, \qquad (2.34)$$

where

$$\mathcal{M}(k) = m_f + \frac{2r}{a} \sum_{\mu} \sin^2 \frac{ak_\mu}{2}. \qquad (2.35)$$

We can see that for $k_\mu \approx \pm \pi/a$, $\mathcal{M}(k)$ diverges for $a \to 0$. Thus the addition of the Wilson term has the effect of raising the masses of the unwanted doublers to the order of the cutoff $\mathcal{O}(1/a)$ and they are therefore eliminated in the continuum limit.

The Wilson fermion action can therefore remove doublers from the naive discretization of the QCD action. However, it does so at the expense of breaking chiral symmetry at finite lattice spacing, as we can see that the second term in (2.31) is not invariant under chiral transformations. This makes it difficult to do calculations where chiral symmetry is important, as is the case for the calculation of the pion and K_{l3} form factors. It is

23

therefore more desirable to use an action that preserves chiral symmetry.

For a long time it was thought that preserving chiral symmetry and simultaneously removing doublers was not possible, due to the Nielsen and Ninomiya no-go theorem [41]. Ginsparg and Wilson however, found a way to circumvent this no-go theorem [42] by imposing that the lattice Dirac operator D with $m_f = 0$, satisfy the following condition,

$$\{\gamma^5, D\} = 2aD\gamma^5 D, \tag{2.36}$$

and defining a lattice chiral transformation as

$$\psi \to e^{i\alpha\gamma^5(1-aD)}\psi; \quad \bar{\psi} \to \bar{\psi}e^{i\alpha(1-aD)\gamma^5}, \tag{2.37}$$

which becomes the usual chiral transformation in the continuum limit. It is easy to verify that the massless lattice QCD Lagrangian is indeed invariant under this transformation if (2.36) is satisfied. This violates one of the assumptions of the no-go theorem where the right hand side of (2.36) is zero, allowing for the possibility of chiral symmetry while simultaneously removing doublers. One fermion Lagrangian formulation that satisfies the Ginsparg-Wilson relation is the domain wall fermion formulation, which we will discuss in the next section.

For convenience we will use lattice units as defined by

$$
\begin{aligned}
\tilde{\psi} &= a^{3/2}\psi, \\
\tilde{m}_f &= am_f, \\
\tilde{x} &= x/a.
\end{aligned}
\tag{2.38}
$$

(and drop the $\sim$'s) from here onwards, unless otherwise stated.

2.3.3 Domain wall fermions

The domain wall fermion (DWF) formulation is a method of simulating fermions on a lattice that preserves chiral symmetry at finite lattice spacing and simultaneously removes doublers. DWF was first introduced by Kaplan [43] who showed that it was possible to have light chiral fermions in 2n dimensions as surface states in a 2n+1 dimensional theory. The DWF action used in this work is a variant of Kaplan's formulation, originally proposed by Shamir [44, 45]. In the following I will give a brief description of

the theory and describe how these surface states originate. For a more comprehensive treatment of the theory, the reader is referred to [44–46]. I will follow the conventions of Shamir [45] and denote coordinates in the usual four dimensions by x, and the coordinate in the fifth dimension by s. The number of sites in the fifth dimension will be denoted by L_s and s will run from 0 to $L_s - 1$. The five-dimensional fermion fields are denoted by $\Psi(x, s)$ and $\bar{\Psi}(x, s)$.

The domain wall fermion action is then given by [45]

$$S_F^{DW} = - \sum_{x, x', s, s'} \bar{\Psi}(x, s) D(x, s; x', s') \Psi(x', s'), \tag{2.39}$$

where

$$D(x, s; x', s') = \delta(s - s') D^{\|}(x, x') + \delta(x - x') D^{\perp}(s, s'), \tag{2.40}$$

$$D^{\|}(x, x') = \frac{1}{2} \sum_{\mu=1}^{4} \left[(1 - \gamma_\mu) U_\mu(x) \delta(x + \hat{\mu} - x') + (1 + \gamma_\mu) U_\mu^\dagger(x') \delta(x' + \hat{\mu} - x) \right]$$
$$+ (M_5 - 4) \delta(x - x'), \tag{2.41}$$

$$\begin{aligned} D^{\perp}(s, s') &= \left[P_L \delta(s + 1 - s') + P_R \delta(s - 1 - s') - 2\delta(s - s') \right] \\ &\quad - m_f \left[P_L \delta(s - L_s - 1) \delta(0 - s') + P_R \delta(s - 0) \delta(L_s - 1 - s') \right] \\ &= P_L M(s, s') + P_R M^\dagger(s, s') - \delta(s - s'), \end{aligned} \tag{2.42}$$

where M is the $L_s \times L_s$ matrix [46]

$$M(s, s') = \delta(s + 1 - s') - m_f \delta(s - L_s - 1) \delta(0 - s'). \tag{2.43}$$

Here, m_f is the 4-d bare quark mass that explicitly couples the $s = 0$ and $s = L_s - 1$ walls. Note the $D^{\|}$ is just the Wilson fermion action with $r = 1$ and a negative mass $-M_5$. M_5 is the domain wall height in Kaplan's original formulation [43]. In the free field case, if $0 < M_5 < 1$, there will be a single fermion flavour with the left-hand chirality state bound to $s = 0$ and the right-hand chirality state bound to $s = L_s - 1$.

The four-dimensional quark fields $\psi(x)$ and $\bar{\psi}(x)$ are then constructed from the five-dimensional fermion fields $\Psi(x, s)$ and $\bar{\Psi}(x, s)$ as

$$\begin{aligned} \psi(x) &= P_L \Psi(x, 0) + P_R \Psi(x, L_s - 1) \\ \bar{\psi}(x) &= \bar{\Psi}(x, L_s - 1) P_L + \bar{\Psi}(x, 0) P_R. \end{aligned} \tag{2.44}$$

To understand how the states bound to the four dimensional walls at the boundaries of the fifth dimension arise, let us look at the spectrum of the free field DWF Dirac operator. In the free field case $U_\mu(x) = 1$, and we can see that in momentum space (2.40) is

$$D(k; s, s') = P_L M(s, s') + P_R M^\dagger(s, s') - (b(k) + i\gamma_\mu \tilde{k}^\mu)\delta(s - s'), \quad (2.45)$$

where

$$b(k) = 1 - M_5 + \sum_\mu (1 - \cos k_\mu). \quad (2.46)$$

The operator D is not hermitian. We will consider instead the second order operator $DD^\dagger$ as this operator is hermitian and non-negative and look at its eigenvalue spectrum. The propagator for D can then be constructed from the propagator for $DD^\dagger$ from $G_F = D^\dagger G$, where G_F is the propagator of D and G is the propagator of the second order operator $DD^\dagger$ [44]. We can show that [46]

$$DD^\dagger = P_L \Omega_- + P_R \Omega_+, \quad (2.47)$$

where

$$\Omega_+ = MM^\dagger - b(M + M^\dagger) + b^2 + \tilde{k}^2, \quad (2.48)$$
$$\Omega_- = M^\dagger M - b(M + M^\dagger) + b^2 + \tilde{k}^2. \quad (2.49)$$

Writing M in explicit matrix form

$$M = \begin{pmatrix} 0 & 1 & 0 & ... & 0 \\ 0 & 0 & 1 & ... & 0 \\ ... & ... & ... & ... & ... \\ 0 & 0 & 0 & ... & 1 \\ -m_f & 0 & 0 & ... & 0 \end{pmatrix}, \quad (2.50)$$

we can see that $M^\dagger = R_5 M R_5^{-1} \Rightarrow \Omega_- = R_5 \Omega_+ R_5^{-1}$ where R_5 is a reflection in the s-direction about the midpoint $s = (L_s - 1)/2$. Thus if Ω_+ has an eigenvector ϕ with eigenvalue λ then Ω_- has a corresponding eigenvector $R_5 \phi$ with the same eigenvalue λ. Thus we can write an eigenvector Ψ of $DD^\dagger$ as

$$\Psi = P_L R_5 \phi + P_R \phi, \quad (2.51)$$

and it suffices to solve the eigenvalue equation $\Omega_+ \phi = \lambda \phi$ to find the spec-

26

trum of the operator $DD^\dagger$.

In explicit matrix form Ω_+ is given by

$$\Omega_+ = \begin{pmatrix} 1 + b^2 + \tilde{k}^2 & -b & \dots & 0 & m_f b \\ -b & 1 + b^2 + \tilde{k}^2 & \dots & 0 & 0 \\ \dots & \dots & \dots & \dots & \dots \\ 0 & 0 & \dots & 1 + b^2 + \tilde{k}^2 & -b \\ m_f b & 0 & \dots & -b & m_f^2 + b^2 + \tilde{k}^2 \end{pmatrix}. \tag{2.52}$$

We can diagonalize Ω_+ by choosing

$$\phi(s) = Ae^{\alpha s} + Be^{-\alpha s}, \tag{2.53}$$

and we can then show that λ is given by

$$\lambda = 1 + b^2 + \tilde{k}^2 - 2b \cosh \alpha. \tag{2.54}$$

λ must be real since Ω_+ is hermitian, but since α appears in the expression for λ as $\cosh \alpha$, α can be real, imaginary or $\alpha = i\pi + \beta$ where β is real and non-zero. If α is imaginary then we have eigenvectors that propagate in the s-direction. If α is real then we have eigenvectors that decay exponentially in the s-direction and are bound to the s-direction boundaries. If $\alpha = i\pi + \beta$ then we also have decaying bound states, but they change sign from one site to the next in the s-direction.

We can see that the decaying state ϕ is bound to the wall at $s = L_s - 1$ by looking at the ratio of the eigenvector's amplitudes at $s = 0$ and $s = L_s - 1$:

$$\frac{A + B}{Ae^{\alpha(L_s-1)} + Be^{-\alpha(L_s-1)}} = \frac{e^\alpha - e^{-\alpha}}{e^{\alpha L_s} - e^{-\alpha L_s}}. \tag{2.55}$$

For the decaying states where α is not pure imaginary this ratio is very small. We conclude then that for the decaying states of $DD^\dagger$ the right-handed component is bound to the $s = L_s - 1$ boundary. Similarly the left-handed component will be bound to the $s = 0$ boundary. This is consistent with how we defined the 4-d quark field $\psi(x)$. All physical observables are defined on the s-direction boundaries. Physics is therefore represented by the decaying states in the DWF formalism. It can be shown that the operator D has these same types of states as $DD^\dagger$ [44,46]. Furthermore, by considering the spectrum of $DD^\dagger$ it can be shown that if $0 < M_5 < 1$, then

we have exactly just one decaying state at the origin of the Brillouin zone, while all other states are propagating states in the s-direction [44]. The DWF action with the condition $0 < M_5 < 1$ is therefore free of doublers.

Since the chiral states decay exponentially in the fifth dimension, at finite L_s there is a finite overlap between them and the fermion theory is not fully chiral. Full lattice chiral symmetry is recovered however in the limit $L_s \to \infty$ where there is no overlap. At finite L_s the degree of chiral symmetry is governed by the overlap between these states. The degree of chiral symmetry breaking is measured by the residual mass m_{res} which can be found through the Ward-Takahashi identity [45]. This leads to an additive quark mass renormalization $m_q = m_f + m_{res}$, where m_q is the true quark mass and m_f is the bare mass parameter that appears in the DWF action [47]. Thus for DWF at finite L_s the chiral limit is defined as $m_f + m_{res} = 0$ as opposed to $m_f = 0$ as is the case in the continuum limit.

As well as describing a light decaying state with opposite chiralities bound to the boundaries of the fifth dimension, DWF formulation also describes an extra $L_s - 1$ propagating heavy states that can propagate in the fifth dimension. These must be canceled out as they lead to bulk type infinities in the $L_s \to \infty$ limit [45]. Regulator fields are introduced to remove these infinities. One way to do this is to introduce a set of bosonic Pauli-Villars fields into the lattice QCD action which share the same Dirac matrix as the fermionic fields but have a mass m_{pv} [46]. The partition function then gets an extra determinant in the denominator and becomes

$$Z = \int \mathcal{D}U \frac{\det D(m_f)}{\det D(m_{pv})} e^{-S_g[U]}. \tag{2.56}$$

Chapter 3

Numerical Methods

In chapter 2 we discussed how to design lattice gauge boson and fermion actions. In this chapter we describe how to compute physical observables given a lattice QCD action. We begin with a brief discussion of Monte Carlo methods. For a more comprehensive introduction to Monte Carlo methods for dynamical fermions the reader is referred to [48]. We then go on to show how the problem of computing correlation functions on the lattice can be reduced to that of computing the quark propagator and we proceed to show how to obtain phenomenologically relevant observables, such as meson masses and hadronic matrix elements, from correlation functions. We finish the chapter with a discussion of the data analysis techniques used for dealing with statistical errors and model fitting to lattice data.

3.1   Monte Carlo Methods

As we saw in section 2.1 we can calculate any physical observable $\mathcal{O}$ in QCD from the path integral

$$\langle \mathcal{O} \rangle = \frac{1}{Z} \int \mathcal{D}U \mathcal{D}\psi \mathcal{D}\bar{\psi} \mathcal{O}(U, \psi, \bar{\psi}) e^{-S_F(U,\psi,\bar{\psi})-S_G(U)} \tag{3.1}$$

where the partition function Z is given by

$$\begin{aligned} Z &= \int \mathcal{D}U \mathcal{D}\psi \mathcal{D}\bar{\psi} e^{-S_F(U,\psi,\bar{\psi})-S_G(U)} \\ &= \int \mathcal{D}U \det[D(U)] e^{-S_G(U)} \end{aligned} \tag{3.2}$$

and U is the gauge field, S_G is the gauge action and $S_F = \bar{\psi}D\psi$ is the fermion action. In the second line of equation (3.2) we perform the integration over the Grassman variables ψ and $\bar{\psi}$ to bring down the determinant of the matrix D in the fermion action.

In the lattice formulation of QCD this path integral has a finite number of integration variables since spacetime has been discretized. However, its exact evaluation is computationally prohibitive due to the huge number of integration variables. We can resort to Monte Carlo methods to evaluate such integrals numerically. Monte Carlo methods use the average on randomly selected points within the integration domain to estimate the integral. These sample points are called "gauge field configurations". One configuration specifies the value of the gauge field on all lattice points.

In order to efficiently calculate the integral, "importance sampling" techniques are used which, instead of using the simple average from points drawn from a uniform distribution of the configurations, select a representative subset of points $\{U^{(0)}, U^{(1)}, ..., U^{(N)}\}$ drawn from a probability distribution $P(U) \propto \det[D(U)]e^{-S_G(U)}$ such that the path integral is well estimated on this subset. This ensures that more points are drawn from where the path integral is large and therefore more important to the ensemble average. The vacuum expectation value $\langle \mathcal{O} \rangle$ can then be estimated from the ensemble average over the N gauge configurations:

$$\langle \mathcal{O} \rangle \approx \frac{1}{N} \sum_{n=1}^{N} \mathcal{O}(U^{(n)}). \tag{3.3}$$

The law of large numbers then tells us that the configuration average tends to the expectation value $\langle \mathcal{O} \rangle$ as N tends to infinity. Furthermore, by the central limit theorem, the sample average tends to become Gaussian distributed with expectation value $\langle \mathcal{O} \rangle$ and standard deviation that falls of as $\sim 1/\sqrt{N}$.

In order to perform this sampling of gauge configurations a Markov chain technique can be used (see for example [48]). In generating a Markov Chain, one starts with an initial field configuration and approaches the desired probability distribution through a series of prescribed random updates of the field values. The limiting probability distribution is called the "equilibrium distribution" and the process of reaching it is called "equilibration". The expectation value of the observable is then calculated after the distribution is first suitably equilibrated. A sufficient (but not neces-

sary) condition for the generated sequence of gauge configurations to be a Markov chain is detailed balance

$$R(U' \leftarrow U)P(U) = R(U \leftarrow U')P(U')$$ (3.4)

where $R(U' \leftarrow U)$ is the transition probability from configuration U to U'. A simple way of implementing detailed balance is using the Metropolis algorithm [49], where we select a candidate configuration U' at random and then accept it with probability

$$R(U' \leftarrow U) = \min\left(1, \frac{P(U')}{P(U)}\right)$$ (3.5)

or otherwise reject it and keep the initial configuration U as the next configuration in the Markov chain. It is easy to show that this method generates a transition probability that satisfies detailed balance.

Another method of achieving detailed balance is to update the gauge links at different lattice sites one by one according to the probability distribution $P(U')$. As each update is independent of the previous configuration, the transition probability is just

$$R(U' \leftarrow U) \propto P(U').$$ (3.6)

This method is called the heatbath algorithm.

Generating gauge configurations by Markov chain methods however means that consecutive gauge field configurations are 'autocorrelated' i.e. they are not independent and one must therefore take care when estimating the statistical error. Only configurations with an adequate separation in Monte Carlo time can be taken as independent.

The fermion determinant in the probability distribution $P(U)$ is highly non-local, so computing its change under a change in the gauge field is very expensive. One solution, used in the early days of lattice QCD, is to set the fermion determinant to 1. This is known as the quenched approximation [50] and in perturbation theory, it is equivalent to ignoring the fermion loops to all orders. This results in uncontrolled systematic errors that can be as large as 30% [51].

With advances in computing power it became possible to include the fermion determinant into the simulations. Various methods have been developed and refined to deal with the fermion determinant. A full treat-

ment of such methods is beyond the scope of this thesis and the reader is referred to [48] for an introduction into Monte Carlo algorithms for dynamical fermions. Typically such methods re-express the fermion determinant as an integration over bosonic-valued fields ϕ and $\phi^\dagger$, known as 'pseudo-fermions', via

$$\det D(U) = \int \mathcal{D}\phi^\dagger \mathcal{D}\phi \exp(-\phi^\dagger D^{-1}\phi) \tag{3.7}$$

or make use of the matrix identity $\ln(\det A) = \text{Tr} \ln A$ to absorb the fermion determinant into an effective gauge action. The condition number of the fermion matrix increases as $1/m_f^2$ and the resulting increase in computational cost of inverting the fermion matrix means that at present simulations at physical light quark masses are not possible.

The current state-of-the-art for gauge configuration generation is the Rational Hybrid Monte Carlo (RHMC) algorithm [52–55]. The gauge configurations used for the correlation function measurements in this thesis were generated by the RBC-UKQCD collaboration using the RHMC algorithm.

3.2 Correlation functions on the lattice

3.2.1 Propagators as building blocks

Consider the lattice hadron two-point correlation function with a momentum $\vec{p}$ at time $t = t_f - t_i$ defined by

$$C_H(t, \vec{p}) = \sum_{\vec{x}_f, \vec{x}_i} e^{i\vec{p}\cdot(\vec{x}_f - \vec{x}_i)} \langle O_H(t_f, \vec{x}_f) O_H^\dagger(t_i, \vec{x}_i) \rangle, \tag{3.8}$$

where the operator $O_H^\dagger(t_i, \vec{x}_i)$ creates a hadron H at the source $(t_i, \vec{x}_i)$ and $O_H(t_f, \vec{x}_f)$ destroys it at the sink $(t_f, \vec{x}_f)$.

For mesons the operator $O_H(t, \vec{x})$ takes the form

$$O_H(t, \vec{x}) = \bar{\psi}_2(t, \vec{x})\Gamma\psi_1(t, \vec{x}), \tag{3.9}$$

where Γ is a combination of γ matrices that gives the desired spin and parity quantum numbers for the meson (see table 3.1 for the possible γ-matrix structures). In this work we will only consider pseudo-scalar mesons for which the operator has the structure $O_H = \bar{\psi}_2\gamma_5\psi_1$ for general momentum $\vec{p}$ (e.g. for the pion and kaon $O_\pi = \bar{q}\gamma_5 q$ and $O_K = \bar{s}\gamma_5 q$ respectively).

State	J^P	Γ
scalar	0^+	I, γ_4
pseudoscalar	0^-	$\gamma_5, \gamma_4\gamma_5$
vector	1^-	$\gamma_i, \gamma_i\gamma_4$
axial vector	1^+	$\gamma_i\gamma_5$
tensor	2^+	$\sigma_{\mu\nu}$

Table 3.1: Table of the possible γ-matrix structures for the different meson states at $\vec{p} = \vec{0}$. The tensor γ-matrix structure is given by $\sigma_{\mu\nu} = \frac{1}{2}(\gamma_\mu\gamma_\nu - \gamma_\nu\gamma_\mu)$.

Inserting (3.9) into (3.8) and performing Wick contractions we get

$$
\begin{aligned}
C_H(t, \vec{p}) &= \sum_{\vec{x}_f, \vec{x}_i} e^{i\vec{p}\cdot(\vec{x}_f - \vec{x}_i)} \langle \bar{\psi}_2(t_f, \vec{x}_f)\Gamma\psi_1(t_f, \vec{x}_f)\bar{\psi}_1(t_i, \vec{x}_i)\Gamma^\dagger\psi_2(t_i, \vec{x}_i)\rangle \\
&= \sum_{\vec{x}_f, \vec{x}_i} e^{i\vec{p}\cdot(\vec{x}_f - \vec{x}_i)} \mathrm{Tr}\left[\Gamma G_2(t_i, \vec{x}_i; t_f, \vec{x}_f)\Gamma^\dagger G_1(t_f, \vec{x}_f; t_i, \vec{x}_i)\right] (3.10)
\end{aligned}
$$

where $G_j(t_f, \vec{x}_f; t_i, \vec{x}_i)$ is the propagator for a quark of flavour j from $(t_i, \vec{x}_i)$ to $(t_f, \vec{x}_f)$ as defined in equation (2.12) and the trace is over spin and colour indices. Note that for flavour-singlet mesons, where $\psi_1 = \psi_2$, there is a second term consisting of disconnected self-contractions of quark fields. We will however not consider these here.

The Dirac operator satisfies $\gamma_5 D^\dagger \gamma_5 = D$, thus we can relate the backward propagator $G_j(t_i, \vec{x}_i; t_f, \vec{x}_f)$ to the forward one by

$$
G_j(t_i, \vec{x}_i; t_f, \vec{x}_f) = \gamma_5 G_j^\dagger(t_f, \vec{x}_f; t_i, \vec{x}_i)\gamma_5, \tag{3.11}
$$

and the expression for the meson two-point correlation function becomes

$$
C_H(t, \vec{p}) = \sum_{\vec{x}_f, \vec{x}_i} e^{i\vec{p}\cdot(\vec{x}_f - \vec{x}_i)} \mathrm{Tr}\left[\Gamma\gamma_5 G_2^\dagger(t_f, \vec{x}_f; t_i, \vec{x}_i)\gamma_5\Gamma^\dagger G_1(t_f, \vec{x}_f; t_i, \vec{x}_i)\right].
$$
$$\tag{3.12}$$

Thus we only need to compute one quark propagator for each quark flavour to determine the two-point function.

In order to calculate form factors we will also need to consider pseudoscalar meson three-point correlation functions of the form

$$
C_{P_i P_f}^{(\mu)}(t_i, t, t_f, \vec{p}_i, \vec{p}_f) = \sum_{\vec{x}_f, \vec{x}, \vec{x}_i} e^{i\vec{p}_f\cdot(\vec{x}_f - \vec{x})} e^{i\vec{p}_i\cdot(\vec{x} - \vec{x}_i)} \langle O_{P_f}(t_f, \vec{x}_f)\, j_\mu(t, \vec{x})\, O_{P_i}^\dagger(t_i, \vec{x}_i)\rangle,
$$
$$\tag{3.13}$$

33

where the operator $O_{P_i}^\dagger = \bar\psi_1\gamma_5\psi_3$ creates a pseudo-scalar meson P_i at $(t_i, \vec{x}_i)$, $O_{P_f}^\dagger = \bar\psi_3\gamma_5\psi_2$ destroys a pseudo-scalar meson P_f at $(t_f, \vec{x}_f)$ and we insert the vector current $j_\mu = \bar\psi_2\gamma_\mu\psi_1$ at $(t, \vec{x})$ to allow for the transition $P_i \to P_f$.

After Wick contraction the three-point function becomes

$$
C_{P_iP_f}^{(\mu)}(t_i, t, t_f, \vec{p}_i, \vec{p}_f) = \sum_{\vec{x}_f, \vec{x}, \vec{x}_i} e^{i\vec{p}_f\cdot(\vec{x}_f-\vec{x})}e^{i\vec{p}_i\cdot(\vec{x}-\vec{x}_i)} \times
$$
$$
\times \mathrm{Tr}\left[G_3(t_i, \vec{x}_i; t_f, \vec{x}_f)\gamma_5 G_2(t_f, \vec{x}_f; t, \vec{x})\gamma^\mu G_1(t, \vec{x}; t_i, \vec{x}_i)\gamma_5\right]. \quad (3.14)
$$

In lattice QCD calculations we typically work in the isospin limit $m_u = m_d$ and thus we only need two different quark propagators in the expression for the three-point function.

3.2.2 Point Sources

In order to compute the quark propagator from any source spacetime point $(t_i, \vec{x}_i)$ to any sink spacetime point $(t, \vec{x})$ we must invert the Dirac matrix

$$
D_{\alpha\gamma}^{ac}(t_y, \vec{y}; t, \vec{x})G_{\gamma\beta}^{cb}(t, \vec{x}; t_i, \vec{x}_i) = \delta_{\alpha\beta}\delta^{ab}\delta_{t_y,t_i}\delta^3_{\vec{y},\vec{x}_i}, \quad (3.15)
$$

where α, β, γ are spin indices and a, b, c are colour indices and summation is implied over repeated indices. The dimension of the Dirac matrix in lattice QCD simulations is usually very large, and it is impractical to solve for the inverse directly. Instead, one usually calculates only a subset of the elements of the propagator matrix from a subset of source points to obtain a solution vector

$$
G_\alpha^a(t, \vec{x}) = \sum_{t_i, \vec{x}_i}\left[D_{\alpha\gamma}^{ac}(t, \vec{x}; t_i, \vec{x}_i)\right]^{-1}\eta_\gamma^c(t_i, \vec{x}_i) \quad (3.16)
$$

where η is a complex vector source in spin and colour spaces occupying some region of space. This equation can be solved using an iterative method, such as the conjugate gradient algorithm.

Traditionally this computation has been performed using the point source consisting of unit spin and colour vectors on a single lattice spacetime point $(t_0, \vec{x}_0)$. The 12 possible spin and colour source vectors are usually written as a unit matrix in spin-colour space at the single lattice

site $(t_0, \vec{x}_0)$

$$\eta_{AB}(\vec{x}) = \delta_{AB}\delta_{\vec{x},\vec{x}_0}\delta_{t,t_0} \tag{3.17}$$

where δ_{AB} are the components of the 12×12 unit matrix in spin-colour space.

The solutions $G_{AB}(t, \vec{x})$ evaluated from these sources are matrices consisting of the subset of elements of the propagator from a single lattice site to all other points on the lattice, for all combinations of spin and colour indices at source and sink, thus requiring 12 inversions of the Dirac matrix. These solutions are typically referred to as one-to-all propagators.

The propagators for the two-point correlation functions defined in section 3.2 can all be computed using point sources in this way. The meson-two point correlation function is then just given by

$$C_H(t, \vec{p}) = \sum_{\vec{x}_f} e^{i\vec{p}\cdot(\vec{x}_f - \vec{x}_0)} \text{Tr}\left[\Gamma\gamma_5 G_2^\dagger(t_f, \vec{x}_f)\gamma_5\Gamma^\dagger G_1(t_f, \vec{x}_f)\right]. \tag{3.18}$$

For the three-point correlation function we can compute $G_1(t, \vec{x}; t_i, \vec{x}_i)$ and $G_3(t_i, \vec{x}_i; t_f, \vec{x}_f)$ using a single point source. However, the propagator $G_2(t_f, \vec{x}_f; t, \vec{x})$ involves many source points and cannot be computed in this way. We can however employ a trick where we re-express the three-point function in terms of the product of the propagator $G_1(t, \vec{x}; t_i, \vec{x}_i)$ and a sequential source propagator [56] defined by

$$G'(t_i, \vec{x}_i; t_f, \vec{p}_f; t, \vec{x}) = \sum_{\vec{x}_f} \gamma_5 \left(G_2(t, \vec{x}; t_f, \vec{x}_f)\gamma^5 G_3(t_f, \vec{x}_f; t_i, \vec{x}_i)\, e^{-i\vec{p}_f\cdot\vec{x}_f}\right)^\dagger \gamma_5. \tag{3.19}$$

The sequential source propagator can then be computed by inverting the Dirac matrix upon the source $G_{AB}(t, \vec{x})$.

3.2.3 Stochastic Sources

It has been shown in [57–59] that one can substantially reduce the computational cost of computing meson correlators by using stochastic vector sources, where the elements of the source vectors are randomly chosen from a distribution $\mathcal{D}$ that is symmetric about zero. A set $\{\eta_A^j(t_i, \vec{x}) \in \mathcal{D}|j = 1, \ldots, N\}$ of these sources has the property that in the limit $N \to \infty$,

$$\frac{1}{N}\sum_{j=0}^{N} \eta_A^j(t_i, \vec{x})\eta_B^{\dagger j}(t_i, \vec{y}) \to \delta_{\vec{x},\vec{y}}\, \delta_{A,B}. \tag{3.20}$$

The studies of [57,58,60] suggest that the optimal choice is to use source vectors with random elements from the set $\mathbb{Z}(2)$ for both real and imaginary components i.e. $\mathcal{D} = \mathbb{Z}(2) \otimes \mathbb{Z}(2)$. In [59] source vectors of this type are implemented into existing code designed for dealing with 12×12 matrices, such as those for point sources. In this way existing propagator contraction code can be reused without the need for further modifications. The source vectors are placed on the first column of an empty 12×12 matrix in spin-colour space for all sites $\vec{y}$ on the source time-slice. Thus we use matrix sources of the form: $\eta_{A,0}^{j}(t_i, \vec{y}) \in \mathbb{Z}(2) \otimes \mathbb{Z}(2)$. In this way the property of equation (3.20) is retained for these matrix sources. With sources of this form, the solution $G_{AB}(t, \vec{x})$ for pseudo-scalar mesons requires only a single inversion per valence quark mass rather than the 12 required for the point source solution (note that this is only true for the pseudo-scalar mesons, for the rest of the meson spectrum we require 4 inversions per valence quark mass [59]). Using equation (3.20) we can then show that the pseudo-scalar meson two-point correlator at zero momentum tends to the spatial average of the point source solution [57,58]

$$
\begin{aligned}
C_P(t, \vec{0}) &= \sum_{j=0}^{N} \sum_{\vec{x}} \mathrm{Tr} \left\{ \gamma^5 G_1^j(t, \vec{x}) \gamma^5 \left(\gamma^5 G_2^j(t, \vec{x}) \gamma^5 \right)^{\dagger} \right\} \\
&\rightarrow \sum_{\vec{x}, \vec{y}} \mathrm{Tr} \left\{ \gamma^5 G_1(t, \vec{x}; t_i, \vec{y}) \gamma^5 \left(\gamma^5 G_2(t, \vec{x}; t_i, \vec{y}) \gamma^5 \right)^{\dagger} \right\} .
\end{aligned}
\tag{3.21}
$$

Although this explicitly projects to zero momentum at source, partially twisted boundary conditions can be used to induce a non-vanishing meson momentum as we will see in chapter 5.

The properties of equation (3.20) are retained on average when the sources η^j reside on different *configurations*, provided a large enough ensemble of configurations is used, such that the stochastic sum can be included in the ensemble average [59]. Therefore we require only a single stochastic source per configuration, giving an overall factor of 12 cost reduction over the traditional point source method.

This technique can be extended simply to three-point correlators using the sequential source propagator method of equation (3.19), the solution of which is again non-zero only on a single source spin-colour index, thus requiring only one extra inversion. The stochastic cancellation with the other source occurs at the source timeslice t_i as in (3.21).

3.3 Phenomenology from lattice correlators

3.3.1 Meson masses

Consider again the meson two-point correlation function

$$C_i(t, \vec{p}) = \sum_{\vec{x}} e^{-i\vec{p}\cdot\vec{x}} \langle O_i(t, \vec{x}) O_i^\dagger(0, \vec{0}) \rangle \qquad (3.22)$$

where O_i is the interpolating operator for the meson i and we have used the translational symmetry of the lattice to shift the source to $(0, \vec{0})$. In Euclidean space the operator $O_i(t, \vec{x})$ evolves as $e^{Ht} O(0, \vec{x}) e^{-Ht}$ with time t. Thus if we insert a complete set of energy eigenstates normalized as $\langle n | n' \rangle = 2E_n \delta_{nn'}$ into (3.22) we get

$$
\begin{aligned}
C_i(t, \vec{p}) &= \sum_n \frac{\langle 0 | O_i(0, \vec{0}) | n \rangle \langle n | O_i^\dagger(0, \vec{0}) | 0 \rangle e^{-E_n t}}{2E_n} \\
&= \sum_n \frac{|Z_n|^2 e^{-E_n t}}{2E_n} \qquad (3.23)
\end{aligned}
$$

where $n = 0, 1, 2...$ represents the n-th excited state, $E_n = \sqrt{m_n^2 + |\vec{p}|^2}$ is the energy of the n-th excited state and $Z_n = \langle n | O_i^\dagger(0, \vec{0}) | 0 \rangle$.

The extent of the lattice is finite and there are therefore both forward and backward time propagating contributions to the correlators. The correlator therefore has the form

$$C_i(t, \vec{p}) = \sum_n \frac{|Z_n|^2}{2E_n} \left(e^{-E_n t} + e^{-E_n (T-t)} \right) , \qquad (3.24)$$

where T is the lattice size in the time direction. If t and $T - t$ are large enough, the contributions to the correlator from the heavier excited states will damp out exponentially leaving the main contribution to the correlator from the ground state

$$C_i(t, \vec{p}) = \frac{|Z_0|^2}{2E_0} \left(e^{-E_0 t} + e^{-E_0 (T-t)} \right) , \qquad (3.25)$$

In this work we will only be interested in the ground state and therefore we will drop the subscript 0 from (3.25) and just write the correlator as

$$C_i(t, \vec{p}) = \frac{|Z_i|^2}{2E_i} \left(e^{-E_i t} + e^{-E_i (T-t)} \right) , \qquad (3.26)$$

with $Z_i = \langle i|O_i^\dagger(0,\vec{0})|0\rangle$ and $i = \pi$ or K.

We can now fit a meson two-point correlation function computed on the lattice to the expression (3.26) to extract the ground state energy (or mass for $\vec{p} = \vec{0}$). In order to determine an appropriate lower bound to the time fitting range one can define the "effective mass":

$$m_{eff}(t) = \cosh^{-1}\left[\frac{C(t+1) + C(t-1)}{2C(t)}\right]. \tag{3.27}$$

which should be a constant (i.e. the ground state energy) if the contributions from excited states in equation (3.24) can be ignored. Thus, a natural criterion for the lower bound of the time fitting range is to check when the effective mass first becomes constant. The effective mass is used as an aid throughout this work to establish appropriate time fitting ranges for the meson energies.

3.3.2 Hadronic form factors

As we will now show the matrix element of the vector current between initial and final pseudo-scalar mesons P_i and P_f defined in equation (1.37) can be extracted from the time-dependence of combinations of Euclidean two- and three-point correlation functions.

As we did for the two-point function in section 3.3.1, for large enough time intervals such that the lightest mesons give the dominant contributions, the three-point function for pseudo-scalar mesons P_i and P_f can be written as [61]

$$
\begin{aligned}
C^{(\mu)}_{P_i P_f}(t_i, t, t_f, \vec{p}_i, \vec{p}_f) &= \\
&= Z_V \sum_{\vec{x}_f, \vec{x}} e^{i\vec{p}_f \cdot (\vec{x}_f - \vec{x})} e^{i\vec{p}_i \cdot \vec{x}} \langle\, O_f(t_f, \vec{x}_f)\, j_\mu(t, \vec{x})\, O_i^\dagger(t_i, \vec{0})\,\rangle \\
&= Z_V \frac{Z_i\, Z_f}{4 E_i E_f} \langle\, P_f(\vec{p}_f)\, |\, j_\mu(0)\, |\, P_i(\vec{p}_i)\,\rangle \\
&\quad \times \Big\{\theta(t_f - t)\, e^{-E_i(t - t_i) - E_f(t_f - t)} \\
&\quad + c_\mu\, \theta(t - t_f)\, e^{-E_i(T + t_i - t) - E_f(t - t_f)}\Big\}\,,
\end{aligned}
\tag{3.28}
$$

where we have defined $Z_f = \langle\, 0\, |\, O_f(0, \vec{0})|\, P_f\,\rangle$ and we have introduced the constant c_μ which is $c_4 = -1$ (time-direction) and $c_i = +1$ for $i = 1, 2, 3$. We have also introduced the vector current renormalization factor Z_V that relates the bare vector current to the renormalized one and can be obtained

as follows. For illustration we take $0 < t < t_f < T/2$, in which case Z_V is defined by

$$Z_V = \frac{\tilde{C}_\pi(t_f, \vec{0})}{C_{\pi\pi}^{(B,\mu)}(t_i, t, t_f, \vec{0}, \vec{0})} . \qquad (3.29)$$

In the numerator we use the function (here $i = \pi$) $\tilde{C}_i(t, \vec{p}) = C_i(t, \vec{p}) - \frac{|Z_i|^2}{2E_i} e^{-E_i(T-t)}$ where Z_i and E_i are determined from fits to $C_i(t, \vec{0})$ and using the dispersion relation $E_i = \sqrt{m_i^2 + |\vec{p}_i|^2}$ (for $t_f = T/2$ it is natural instead to use $\tilde{C}_i(t, \vec{p}) = \frac{1}{2}C_i(t, \vec{p})$ in (3.29)). The superscript B in the denominator indicates that we take the bare (unrenormalized) current in the three-point function. We chose to use $\tilde{C}_i(t, \vec{p})$ in place of $C_i(t, \vec{p})$ as we found that with this choice we were able to achieve better plateaus for Z_V as well as for the ratios defined below. In the following we drop the labels t_i and t_f (since they are fixed) and we combine the two- and three- point functions into the ratios

$$
\begin{aligned}
R_{1, P_i P_f}^{(\mu)}(\vec{p}_i, \vec{p}_f) &= \mathcal{N} \sqrt{\frac{C_{P_i P_f}^{(\mu)}(t, \vec{p}_i, \vec{p}_f)\, C_{P_f P_i}^{(\mu)}(t, \vec{p}_f, \vec{p}_i)}{\tilde{C}_{P_i}(t_f, \vec{p}_i)\, \tilde{C}_{P_f}(t_f, \vec{p}_f)}}, \\
R_{3, P_i P_f}^{(\mu)}(\vec{p}_i, \vec{p}_f) &= \\
&\mathcal{N} \frac{C_{P_i P_f}^{(\mu)}(t, \vec{p}_i, \vec{p}_f)}{\tilde{C}_{P_f}(t_f, \vec{p}_f)} \sqrt{\frac{C_{P_i}(t_f - t, \vec{p}_i)\, C_{P_f}(t, \vec{p}_f)\, \tilde{C}_{P_f}(t_f, \vec{p}_f)}{C_{P_f}(t_f - t, \vec{p}_f)\, C_{P_i}(t, \vec{p}_i)\, \tilde{C}_{P_i}(t_f, \vec{p}_i)}},
\end{aligned}
\qquad (3.30)
$$

where $\mathcal{N} = 4Z_V\sqrt{E_i E_f}$ and the ratios are constructed such that

$$R_{\alpha, P_i P_f}^{(\mu)}(\vec{p}_i, \vec{p}_f) = f_+^{P_i P_f}(q^2)(p_i + p_f)_\mu + f_-^{P_i P_f}(q^2)(p_i - p_f)_\mu, \qquad (3.31)$$

for $\alpha = 1, 3$. For the ratios we use the naming convention of [61] but we haven't made use of ratio R_2[1]. For the pion electromagnetic form factor $f_-^{\pi\pi}(q^2) = 0$ for all q^2 and thus $f_+^{\pi\pi}(q^2)$ is readily obtained. For the K_{l3} form factors once these ratios have been computed for some choices of $\vec{p}_i$ and $\vec{p}_f$ while keeping q^2 constant (of course we are particularly interested in $q^2 = 0$) the form factors $f_+^{K\pi}(q^2)$ and $f_-^{K\pi}(q^2)$ can be obtained as the solutions of the corresponding system of linear equations.

---

[1]We did not generate data for $C_{PP}^{(\mu)}(t, \vec{p}, \vec{p})|_{q^2=0}$ for $P = \pi, K$ from which the forward matrix elements $\langle P|V_\mu|P \rangle$ relevant for the construction of R_2 can be extracted.

3.4 Data analysis techniques

3.4.1 Correlations in simulation time

As described in section 3.1 the vacuum expectation value of an observable O is estimated from the average $\bar{O}$ over N measurements on gauge field configurations generated as a Markov Chain using Monte Carlo methods. The gauge field configurations are inherently correlated in the simulation time. This type of correlation is called 'autocorrelation'. Due to autocorrelations the usual 'naive' standard deviation for the observable O

$$\sigma_{\text{naive}} = \sqrt{\frac{1}{N(N-1)} \sum_{i=1}^{N} (O_i - \bar{O})^2} \qquad (3.32)$$

is typically an under-estimate of the true statistical error.

To deal with autocorrelations we usually bin the data into $N_{\text{bins}} = N/b$ bins, where b is the number of measurements in each bin. The optimal bin size b can be found by steadily increasing it until the statistical error estimate stops changing. The binned data is then considered to be independent and the usual standard deviation of equation (3.32) can be used with N_{bins} measurements to estimate the statistical error.

3.4.2 Correlations among observables

In lattice QCD calculations we often need to calculate physical observables that depend on more than one quantity calculated on the same ensemble of gauge field configurations. Such quantities will inevitably be correlated with one another and thus we need a method that will allow us to propagate the statistical errors in these quantities taking into account such correlations. One such method is the jackknife technique.

For the jackknife technique used in this work, we re-sample the original distribution of measurements $\{X_i; i = 1, ..., N\}$ by removing one measurement X_j and calculating the mean for the new distribution. We repeat the process each time removing one X_j and going through the whole distribution of measurements to obtain a distribution $\{\bar{X}_j; j = 1, ..., N\}$ of jackknife means. The jackknife means $\bar{X}_j$ are therefore given by

$$\bar{X}_j = \frac{1}{N-1} \left[\sum_{i=1}^{N} X_i - X_j \right] \quad \text{for} \ \ j = 1, ..., N \ , \qquad (3.33)$$

and we then calculate an error on the mean given by

$$\sigma_J = \sqrt{\frac{N-1}{N} \sum_{j=1}^{N} (\bar{X}_j - \langle \bar{X} \rangle)^2} \, , \tag{3.34}$$

where $\langle \bar{X} \rangle$ is the average mean value.

3.4.3 Least χ^2 fitting

We often need to fit lattice data $\{X_i\}$ to a model $F(Y, \alpha_1, \alpha_2, ...)$ where Y is some variable such as meson mass or momentum and the α_i's are unknown constants to be determined. The standard approach to fit correlated lattice data to a model and determine the unknown constants is to minimize the correlated χ^2 defined as

$$\chi^2 = \sum_{i,j=1}^{M} \left[\bar{X}_i - F(Y_i, \alpha_1, \alpha_2, ...) \right] \left(\mathrm{Cov}^{-1} \right)_{ij} \left[\bar{X}_j - F(Y_j, \alpha_1, \alpha_2, ...) \right]$$

$$\tag{3.35}$$

where M is the number of points included in the fit, $\bar{X}_i$ is the ensemble average of the ith data point

$$\bar{X}_i = \frac{1}{N} \sum_{k=1}^{N} X_{ik} \tag{3.36}$$

and Cov is the covariance matrix which can be approximated by

$$\mathrm{Cov}_{ij} = \frac{1}{N(N-1)} \sum_{k=1}^{N} (X_{ik} - \bar{X}_i)(X_{jk} - \bar{X}_j). \tag{3.37}$$

In the limit $N \to \infty$ this approaches the true covariance matrix. The covariance matrix accounts for the correlations between the different X_i's. Problems arise when the number of measurements N is not large enough, which results in large fluctuations of the covariance matrix. In this work we have used both *frozen* and *unfrozen* covariance matrices for correlated χ^2 fits. For the *unfrozen* case a covariance matrix is computed individually for each jackknife sample, while in the *frozen* case we calculate a single covariance matrix on the distribution of jackknife means. We also use uncorrelated χ^2 fits where the covariance matrix is just the unit matrix.

Chapter 4

Chiral Perturbation Theory

We saw in section 1.1.2 that the QCD Lagrangian with N_f massless quarks is invariant under the chiral group $G = \mathrm{SU}(N_f)_L \times \mathrm{SU}(N_f)_R$ and that the chiral group G is spontaneously broken down to the subgroup $H = \mathrm{SU}(N_f)_V$. This leads to $N_f^2 - 1$ pseudo-scalar Goldstone bosons identified as the light pseudo-scalar mesons. Since there is a large mass gap between the light pseudo-scalar mesons and the rest of the hadronic spectrum, we can build an effective field theory where the Goldstone fields are the fundamental fields of the theory and the rest of the hadronic spectrum has been integrated out. This effective field theory is known as Chiral Perturbation Theory (ChPT). ChPT can be used to calculate the quark mass and momentum dependence of hadronic observables, such as meson masses, decay constants and form factors. ChPT is thus particularly useful in lattice QCD for extrapolating lattice QCD results from unphysical quark masses to the physical points. In this chapter I will outline how to write down Chiral Lagrangians and then give a brief overview of the derivation of ChPT formulae for the pion and K_{l3} form factors to next-to-leading order (NLO). I will also briefly describe partially quenched ChPT as we have generated data partially quenched in the strange quark mass and used a partially quenched ChPT formula for the K_{l3} form factor extrapolation presented in section 7.2. I finish the chapter with a brief discussion of finite volume effects in ChPT.

4.1 Chiral Lagrangians

We want to construct a chiral Lagrangian that obeys the same symmetries as the QCD Lagrangian. To do this we need to know how the Goldstone

fields transform under G. The standard procedure to implement a symmetry transformation of a group G on Goldstone fields is to view the Goldstone fields ϕ as coordinates of the coset space G/H, where H is the conserved subgroup that G is spontaneously broken down to [62, 63]. An element g of G then induces a transformation on $\xi(\phi) \in G/H$ of the form

$$\xi(\phi) \xrightarrow{G} g\xi(\phi) = \xi(\phi')h(g,\phi). \tag{4.1}$$

The field $h(g,\phi) \in H$, known as a compensator field, accounts for the fact that a coset element is only defined up to an H transformation.

For the case of chiral symmetry $G = \mathrm{SU}(N_f)_L \times \mathrm{SU}(N_f)_R$, $H = \mathrm{SU}(N_f)_V$ and we have $\phi^a(a = 1, ..., N_f^2 - 1)$ coordinates describing the Goldstone fields. Left and right chiral transformations are related by parity and thus we can write $\xi(\phi')$ as [64]

$$\xi(\phi') = g_R\xi(\phi)h^\dagger(g,\phi) = h(g,\phi)\xi(\phi)g_L^\dagger \; ; \quad g = (g_L, g_R) \in G. \tag{4.2}$$

The coset space G/H is not a group, but as a manifold it is homeomorphic to $\mathrm{SU}(N_f)$ [65] and as a result we can choose $\xi(\phi)$ to be a matrix valued field in $\mathrm{SU}(N_f)$. It is more convenient however to work with the square $\Sigma(\phi) = \xi(\phi)^2$, for which the transformation is simply

$$\Sigma(\phi) \xrightarrow{G} g_R\Sigma(\phi)g_L^\dagger. \tag{4.3}$$

A convenient parametrization for $\xi(\phi)$ is given by

$$\xi(\phi) \equiv \exp\left(\frac{i\phi}{f}\right), \tag{4.4}$$

where f is a low energy constant (LEC) which can be shown to be equal to the pion decay constant f_π at lowest order in ChPT. We choose a normalization where $f_\pi \approx 131$ MeV. The two conventional normalizations used in ChPT can be related by $f_\pi = f_\pi/\sqrt{2} \approx 93$ MeV. Using this normalization, for $N_f = 3$, ϕ is given by

$$\phi(x) \equiv \sum_{a=1}^{8} \lambda^a \phi^a(x) = \begin{pmatrix} \pi^0/\sqrt{2} + \eta/\sqrt{6} & \pi^+ & K^+ \\ \pi^- & -\pi^0/\sqrt{2} + \eta/\sqrt{6} & K^0 \\ K^- & \overline{K}^0 & -2\eta/\sqrt{6} \end{pmatrix}, \tag{4.5}$$

where ϕ^a are the real pseudo-Goldstone boson fields and λ^a are proportional

to the Gell-Mann matrices. Similarly for $N_f = 2$, ϕ is given by

$$\phi(x) \equiv \sum_{a=1}^{3} \sigma^a \phi^a(x) = \begin{pmatrix} \pi^0/\sqrt{2} & \pi^+ \\ \pi^- & -\pi^0/\sqrt{2} \end{pmatrix}, \qquad (4.6)$$

where σ^a are the Pauli matrices. We can now write down the most general low energy effective Lagrangian for massless QCD, involving $\Sigma(\phi)$ which is consistent with chiral symmetry. To lowest order this is uniquely given by

$$\mathcal{L}_{\text{eff}}^{(2)} = \frac{f^2}{8} \langle \partial_\mu \Sigma \partial^\mu \Sigma^\dagger \rangle, \qquad (4.7)$$

where $\langle ... \rangle$ denotes the N_f-dimensional trace and the coefficient here is chosen to give the conventional normalization to the meson kinetic term.

This effective Lagrangian gives us an effective field theory in terms of Goldstone fields with exact chiral symmetry for massless quarks. In nature we do not however observe exact chiral symmetry. In addition to spontaneous symmetry breaking, chiral symmetry is explicitly broken by non-zero quark masses and by the electroweak interactions. We can take this into account by introducing couplings to external Hermitian matrix valued fields v_μ, a_μ, s, p and treating these as perturbations. These external fields can also be used to compute the realization of Green functions of quark currents in this effective field theory [66, 67]. To this end the QCD Lagrangian for massless quarks ($\mathcal{L}_{\text{QCD}}^0$) is extended to

$$\mathcal{L}_{\text{QCD}} = \mathcal{L}_{\text{QCD}}^0 + \bar{q}\gamma^\mu(v_\mu + a_\mu\gamma_5)q - \bar{q}(s - ip\gamma_5)q. \qquad (4.8)$$

Defining the fields $r_\mu \equiv v_\mu + a_\mu$ and $l_\mu \equiv v_\mu - a_\mu$ the Lagrangian (4.8) is invariant under the following set of *local G* transformations [64]:

$$q_L \to g_L q_L; \quad q_R \to g_R q_R; \quad s + ip \to g_R(s + ip)g_L^\dagger$$
$$l_\mu \to g_L l_\mu g_L^\dagger + ig_L\partial_\mu g_L^\dagger; \quad r_\mu \to g_R r_\mu g_R^\dagger + ig_R\partial_\mu g_R^\dagger. \qquad (4.9)$$

We then build an effective Lagrangian containing these external sources that is invariant under the *local* transformations (4.9). Imposing invariance under local instead of global chiral transformations automatically ensures gauge invariance when the external fields are used to introduce couplings of the Goldstone fields to gauge fields. For the effective Lagrangian to be invariant the external fields have to be introduced through the covariant

derivatives

$$D_\mu \Sigma = \partial_\mu \Sigma - i r_\mu \Sigma + i \Sigma l_\mu, \quad D_\mu \Sigma^\dagger = \partial_\mu \Sigma^\dagger + i \Sigma^\dagger r_\mu - i l_\mu \Sigma^\dagger, \qquad (4.10)$$

and through the field strength tensors

$$F_L^{\mu\nu} = \partial^\mu l^\nu - \partial^\nu l^\mu - i[l^\mu, l^\nu], \quad F_R^{\mu\nu} = \partial^\mu r^\nu - \partial^\nu r^\mu - i[r^\mu, r^\nu]. \qquad (4.11)$$

The lowest order effective Lagrangian that is invariant under (4.9) is then given by [67,68]

$$\mathcal{L}_{\mathrm{eff}}^{(2)} = \frac{f^2}{8} \langle D_\mu \Sigma D^\mu \Sigma^\dagger + \Sigma^\dagger \chi + \chi^\dagger \Sigma \rangle, \qquad (4.12)$$

where

$$\chi = 2B(s + ip), \qquad (4.13)$$

and B is a constant which can be related to the quark condensate. Throughout this chapter we will use the field χ to introduce the quark masses by setting p to zero and $s = M$, where M is the relevant quark mass matrix in the isospin limit, i.e.

$$M = \begin{pmatrix} \hat{m} & 0 \\ 0 & \hat{m} \end{pmatrix} \text{ for } N_f = 2 \text{ and } M = \begin{pmatrix} \hat{m} & 0 & 0 \\ 0 & \hat{m} & 0 \\ 0 & 0 & m_s \end{pmatrix} \text{ for } N_f = 3 \quad (4.14)$$

with $\hat{m} = \frac{1}{2}(m_u + m_d)$. Also from here onwards we will use f and f_0 to denote the LECs in the SU(2) and SU(3) chiral limits respectively.

At next order in momentum $\mathcal{O}(p^4)$ the most general Lagrangian for $N_f = 3$ is given by [67]

$$\begin{aligned}
\mathcal{L}_{\mathrm{eff}}^{(4)} &= L_1 \langle D_\mu \Sigma^\dagger D^\mu \Sigma \rangle^2 + L_2 \langle D_\mu \Sigma^\dagger D_\nu \Sigma \rangle \langle D^\mu \Sigma^\dagger D^\nu \Sigma \rangle \\
&+ L_3 \langle D_\mu \Sigma^\dagger D^\mu \Sigma D_\nu \Sigma^\dagger D^\nu \Sigma \rangle + L_4 \langle D_\mu \Sigma^\dagger D^\mu \Sigma \rangle \langle \Sigma^\dagger \chi + \chi^\dagger \Sigma \rangle \\
&+ L_5 \langle D_\mu \Sigma^\dagger D^\mu \Sigma (\Sigma^\dagger \chi + \chi^\dagger \Sigma) \rangle + L_6 \langle \Sigma^\dagger \chi + \chi^\dagger \Sigma \rangle^2 \\
&+ L_7 \langle \Sigma^\dagger \chi - \chi^\dagger \Sigma \rangle^2 + L_8 \langle \chi^\dagger \Sigma \chi^\dagger \Sigma + \Sigma^\dagger \chi \Sigma^\dagger \chi \rangle \\
&- i L_9 \langle F_R^{\mu\nu} D_\mu \Sigma D_\nu \Sigma^\dagger + F_L^{\mu\nu} D_\mu \Sigma^\dagger D_\nu \Sigma \rangle + L_{10} \langle \Sigma^\dagger F_R^{\mu\nu} \Sigma F_{L,\mu\nu} \rangle \\
&+ H_1 \langle F_{R,\mu\nu} F_R^{\mu\nu} + F_{L,\mu\nu} F_L^{\mu\nu} \rangle + H_2 \langle \chi^\dagger \chi \rangle. \qquad (4.15)
\end{aligned}$$

The numerical values of the LECs L_i and H_i are not determined by chiral symmetry. They parameterize our inability to solve the dynamics

of QCD in the non-perturbative regime. Their values can be fixed by experimental measurements, lattice simulations and other methods. Except for L_3 and L_7 the low-energy coupling constants L_i and H_1 and H_2 are required in the renormalization of the one-loop graphs [67]. It is possible to absorb the one-loop divergences by an appropriate renormalization of the coefficients L_i and H_i [67]

$$L_i = L_i^r + \frac{\Gamma_i}{32\pi^2} R, \tag{4.16}$$

$$H_i = H_i^r + \frac{\Delta_i}{32\pi^2} R, \tag{4.17}$$

where R is defined by

$$R = \frac{2}{d-4} - [\ln(4\pi) - \gamma_E + 1]. \tag{4.18}$$

with d denoting the number of space-time dimensions and $\gamma_E = -\Gamma'(1)$ being the Euler's constant. The constants Γ_i and Δ_i are given by

$$\Gamma_1 = \frac{3}{32}, \quad \Gamma_2 = \frac{3}{16}, \quad \Gamma_3 = 0, \quad \Gamma_4 = \frac{1}{8}, \quad \Gamma_5 = \frac{3}{8},$$
$$\Gamma_6 = \frac{11}{144}, \quad \Gamma_7 = 0, \quad \Gamma_8 = \frac{5}{48}, \quad \Gamma_9 = \frac{1}{4}, \quad \Gamma_{10} = -\frac{1}{4},$$
$$\Delta_1 = -\frac{1}{8}, \qquad\qquad \Delta_2 = \frac{5}{24}. \tag{4.19}$$

The renormalized coefficients L_i^r depend on the scale μ introduced by dimensional regularization and their values at two different scales μ_1 and μ_2 are related by

$$L_i^r(\mu_2) = L_i^r(\mu_1) + \frac{\Gamma_i}{16\pi^2} \ln\left(\frac{\mu_1}{\mu_2}\right). \tag{4.20}$$

The scale dependence of the coefficients and the finite part of the loop-diagrams however compensate each other in such a way that physical observables are scale independent.

The corresponding $\mathcal{O}(p^4)$, most general Lagrangian for $N_f = 2$ is given by [66]

$$\begin{aligned}
\mathcal{L}_{\text{eff}}^{(4)} &= \frac{l_1}{4} \langle D_\mu \Sigma^\dagger D^\mu \Sigma \rangle^2 + \frac{l_2}{4} \langle D_\mu \Sigma^\dagger D_\nu \Sigma \rangle \langle D^\mu \Sigma^\dagger D^\nu \Sigma \rangle \\
&+ \frac{l_3}{16} \langle \chi \Sigma^\dagger + \Sigma \chi^\dagger \rangle^2 + \frac{l_4}{4} \langle D_\mu \Sigma D^\mu \chi^\dagger + D_\mu \chi D^\mu \Sigma^\dagger \rangle \\
&+ l_5 \left[\langle F_{R,\mu\nu} \Sigma F_L^{\mu\nu} \Sigma^\dagger \rangle - \frac{1}{2} \langle F_{L,\mu\nu} F_L^{\mu\nu} + F_{R,\mu\nu} F_R^{\mu\nu} \rangle \right]
\end{aligned}$$

$$
\begin{aligned}
+ \quad & i\frac{l_6}{2}\langle F_{R,\mu\nu}D^\mu\Sigma D^\nu\Sigma^\dagger + F_{L,\mu\nu}D^\mu\Sigma^\dagger D^\nu\Sigma\rangle - \frac{l_7}{16}\langle\chi\Sigma^\dagger - \Sigma\chi^\dagger\rangle^2 \\
+ \quad & \frac{h_1 - h_3}{16}\left\{\langle\chi\Sigma^\dagger + \Sigma\chi^\dagger\rangle^2 + \langle\chi\Sigma^\dagger - \Sigma\chi^\dagger\rangle^2 - 2\langle\chi\Sigma^\dagger\chi\Sigma^\dagger + \Sigma\chi^\dagger\Sigma\chi^\dagger\rangle\right\} \\
+ \quad & \frac{h_1 + h_3}{4}\langle\chi\chi^\dagger\rangle - 2h_2\langle F_{L,\mu\nu}F_L^{\mu\nu} + F_{R,\mu\nu}F_R^{\mu\nu}\rangle. \tag{4.21}
\end{aligned}
$$

In the $N_f = 2$ case the renormalized low energy constants are related to the unrenormalized ones by

$$
\begin{aligned}
l_i &= l_i^r + \gamma_i \frac{R}{32\pi^2} \tag{4.22} \\
h_i &= h_i^r + \delta_i \frac{R}{32\pi^2} \tag{4.23}
\end{aligned}
$$

where

$$
\gamma_1 = \frac{1}{3}, \quad \gamma_2 = \frac{2}{3}, \quad \gamma_3 = -\frac{1}{2}, \quad \gamma_4 = 2, \quad \gamma_5 = -\frac{1}{6}, \quad \gamma_6 = -\frac{1}{3}, \quad \gamma_7 = 0,
$$
$$
\delta_1 = 2, \quad \delta_2 = \tfrac{1}{12}, \quad \delta_3 = 0. \tag{4.24}
$$

4.2 Pion form factor

The electromagnetic form factor of the pion has been studied extensively in both SU(2) and SU(3) ChPT. NLO expressions appear in [66,67] with extensions to NNLO in [69–71] and we now briefly outline the derivation of $f^{\pi\pi}(q^2)$ defined in equation (1.42) in SU(3) ChPT to NLO. The corresponding derivation in SU(2) ChPT is very similar and we will therefore just quote the result in this case.

In order to calculate the form factor in SU(3) ChPT we identify the external vector fields in the chiral Lagrangian with the photon field A_μ

$$
l_\mu = r_\mu = -eQA_\mu, \quad Q = \begin{pmatrix} 2/3 & 0 & 0 \\ 0 & -1/3 & 0 \\ 0 & 0 & -1/3 \end{pmatrix}. \tag{4.25}
$$

With these definitions, the covariant derivative and the field strength tensors of equations (4.10) and (4.11) become

$$
\begin{aligned}
D_\mu\Sigma &= \partial_\mu\Sigma + ieA_\mu[Q,\Sigma], \\
F_{\mu\nu}^L &= F_{\mu\nu}^R = -e(\partial_\mu A_\nu - \partial_\nu A_\mu)Q. \tag{4.26}
\end{aligned}
$$
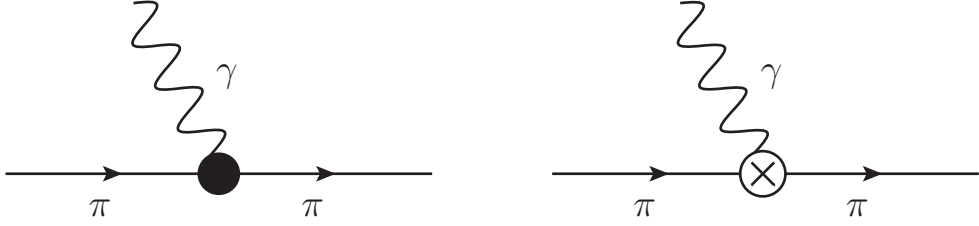
Figure 4.1: Tree level diagrams contributing to the pion electromagnetic form factor in SU(3) ChPT. A ● represents a vertex from $\mathcal{L}_{\text{eff}}^{(2)}$ while a ⊗ represents a vertex from $\mathcal{L}_{\text{eff}}^{(4)}$.

The Feynman rules are then derived by expanding $\Sigma = \exp(2i\phi/f)$ in $\mathcal{L} = \mathcal{L}_{\text{eff}}^{(2)} + \mathcal{L}_{\text{eff}}^{(4)}$ to second order in the Goldstone boson fields ϕ. We can then calculate the current operator for the chiral Lagrangian from taking the derivative

$$J^\mu = -\frac{1}{e}\frac{\partial\mathcal{L}}{\partial A_\mu}\bigg|_{A_\mu=0}, \tag{4.27}$$

and use this to compute the matrix element of equation (1.42) for the chiral Lagrangian. This will allow us to calculate the form factor to NLO.

We can see that to $\mathcal{O}(p^4)$ the $\mathcal{L}_{\text{eff}}^{(2)}$ Lagrangian will give both tree-level and one loop contributions, while the $\mathcal{L}_{\text{eff}}^{(4)}$ Lagrangian will only give a tree level contribution. The contributions to the current operator J_μ at tree level from the $\mathcal{L}_{\text{eff}}^{(2)}$ and $\mathcal{L}_{\text{eff}}^{(4)}$ parts of the Lagrangian are given by

$$J_{2,\mu}^{(2)} = -\frac{i}{2}\langle Q[\phi, \partial_\mu\phi]\rangle, \tag{4.28}$$

$$J_{4,\mu}^{(2)} = -\frac{16iL_4}{f_0^2}\langle Q[\phi, \partial_\mu\phi]\rangle\langle BM\rangle - \frac{16iL_5}{f_0^2}\langle BMQ[\phi, \partial_\mu\phi]\rangle$$
$$-\frac{4iL_9}{f_0^2}\langle Q\partial^\nu[\partial_\mu\phi, \partial_\nu\phi]\rangle. \tag{4.29}$$

The corresponding Feynman diagrams are shown in figure 4.1.

The contributions from these diagrams to the form factor give

$$f_{\text{tree}}^{\pi\pi}(q^2) = 1 + \frac{1}{f_0^2}\left[16(2m_\pi^2 - 2m_K^2 + 3m_\eta^2)L_4 + 16m_\eta^2 L_5 + 4L_9 q^2\right]. \tag{4.30}$$

Here we made use of the relations $m_\pi^2 = 2\hat{m}B$, $m_K^2 = (\hat{m} + m_s)B$ and $m_\eta^2 = 2/3(\hat{m} + 2m_s)B$ which are correct to this order in ChPT.

There are two types of loop diagrams resulting from the expansion of $\mathcal{L}_{\text{eff}}^{(2)}$ in ϕ. These are shown in figures 4.2 and 4.3. The tadpole diagram of figure 4.2 results from the interaction vertex of the photon with four
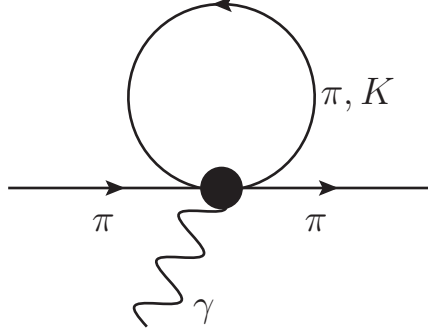
Figure 4.2: One-loop tadpole diagram contributing to the pion electromagnetic form factor in SU(3) ChPT.

Goldstone bosons coming from the part of the current given by

$$J_{2,\mu}^{(4)} = \frac{i}{12 f_0^2} \langle Q \left(\phi^2 [\phi, \partial_\mu \phi] - 2\phi[\phi, \partial_\mu \phi]\phi + [\phi, \partial_\mu \phi]\phi^2 \right) \rangle. \qquad (4.31)$$

This diagram has two contributions, one from a pion loop and one from a kaon loop. The resultant contribution to the form factor is given by [72]

$$f_{\text{tad}}^{\pi\pi}(q^2) = -\frac{10 I(m_\pi^2, \mu^2)}{3 f_0^2} - \frac{5 I(m_K^2, \mu^2)}{3 f_0^2}, \qquad (4.32)$$

where the loop integral $I(m^2, \mu^2)$ is given by

$$
\begin{aligned}
I(m^2, \mu^2) &= \mu^{(4-d)} \int \frac{d^d k}{(2\pi)^d} \frac{i}{k^2 - m^2 + i\epsilon} \\
&= \frac{m^2}{16\pi^2} \left(R + \ln \frac{m^2}{\mu^2} \right) + \mathcal{O}(4 - d), \qquad (4.33)
\end{aligned}
$$

where μ is the renormalization scale and dimensional regularization is used with the $\overline{MS}$ scheme for removal of the pole.

The two-vertex loop diagram of figure 4.3 results from the contraction of the current operator of equation (4.28) with the interaction vertex of four Goldstone bosons given by

$$\mathcal{L}_2^4 = \frac{1}{12 f_0^2} \langle [\phi, \partial_\mu \phi]\phi \partial^\mu \phi) + B \text{Tr}(\phi^4 M) \rangle. \qquad (4.34)$$

The contribution from this diagram to the form factor is [72]

$$f_{\text{ver}}^{\pi\pi}(q^2) = \frac{2 I(m_\pi^2, \mu^2)}{f_0^2} + \frac{I(m_K^2, \mu^2)}{f_0^2} + \frac{1}{f_0^2} \left(4 H_{\pi\pi}(q^2) + 2 H_{KK}(q^2) - \frac{R q^2}{32\pi^2} \right), \qquad (4.35)$$

50
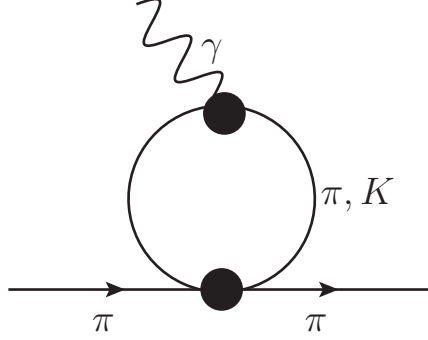
Figure 4.3: One-loop two vertex diagram contributing to the pion form factor in SU(3) ChPT.

where

$$H_{PP}(q^2) = -\frac{q^2}{192\pi^2}\left[\ln\frac{m_P^2}{\mu^2} + \frac{1}{3} + \left(1 - 4\frac{m_P^2}{q^2}\right)H\left(\frac{q^2}{m_P^2}\right)\right], \qquad (4.36)$$

and the function $H(x)$ is given by

$$\begin{aligned}
H(x) &= \int_0^1 \ln[1 + x(y^2 - y)]dy \\
&= -2 + \sqrt{\frac{x-4}{x}}\left[\ln\left(\frac{\sqrt{(x-4)/x}+1}{\sqrt{(x-4)/x}-1}\right)\right], \qquad (4.37)
\end{aligned}$$

for $x < 0$ (we consider only a space-like form factor for which $x = q^2/m_P^2$ is negative) and $(x-4)/x > 1$ so that the logarithm is real.

The result for the renormalized matrix element for the pion is then obtained by adding up all these contributions and multiplying by the wavefunction renormalization constant Z_π. It can be shown that Z_π is given by [72]

$$\begin{aligned}
Z_\pi &= 1 - \frac{1}{f_0^2}\left[16(2m_\pi^2 - 2m_K^2 + 3m_\eta^2)L_4 + 16m_\eta^2 L_5\right] \\
&+ \frac{4I(m_\pi^2, \mu^2)}{3f_0^2} + \frac{2I(m_K^2, \mu^2)}{3f_0^2} + \mathcal{O}(p^4). \qquad (4.38)
\end{aligned}$$

Thus the renormalized expression for the pion electromagnetic form factor to NLO is given by [67, 68]

$$f_{\text{NLO}}^{\pi\pi}(q^2) = 1 + \frac{1}{f_0^2}\left(4L_9^r q^2 + 4H_{\pi\pi}(q^2) + 2H_{KK}(q^2)\right). \qquad (4.39)$$

The derivation of the NLO form factor expression in SU(2) ChPT is

very similar to this derivation with the difference that now only pions are involved in the Feynman diagram loops. The resulting expression is [66]

$$f_{SU(2),\text{NLO}}^{\pi\pi}(q^2) = 1 + \frac{1}{f^2}\left[-2l_6^r\, q^2 + 4H_{\pi\pi}(q^2)\right],\qquad(4.40)$$

where f is the pion decay constant in the SU(2) chiral limit.

We can now calculate the SU(2) and SU(3) NLO expressions for the charge radius of the pion using equation (1.43) to get

$$\langle r_\pi^2\rangle_{SU(2),\text{NLO}} = -\frac{12l_6^r}{f^2} - \frac{1}{8\pi^2 f^2}\left(\ln\frac{m_\pi^2}{\mu^2} + 1\right),\qquad(4.41)$$

$$\langle r_\pi^2\rangle_{SU(3),\text{NLO}} = \frac{24L_9^r}{f_0^2} - \frac{1}{8\pi^2 f_0^2}\left(\ln\frac{m_\pi^2}{\mu^2} + 1\right) - \frac{1}{16\pi^2 f_0^2}\left(\ln\frac{m_K^2}{\mu^2} + 1\right).\qquad(4.42)$$

Comparing the expressions for the charge radius gives the relation between the SU(2) and SU(3) NLO LEC's [67]:

$$l_6^r(\mu) = -2L_9^r(\mu) + \frac{1}{192\pi^2}\left(\ln\frac{\bar{m}_K^2}{\mu^2} + 1\right),\qquad(4.43)$$

where $\bar{m}_K^2$ is the kaon mass in the chiral limit for the light quarks. Using the ρ mass for the renormalization scale, $\mu = m_\rho$, the second term on the right hand side of this relation is very small compared to the expected (power-counting) size of the LECs, so that $l_6^r(m_\rho) \approx -2L_9^r(m_\rho)$. A word of caution should be added however. In deriving equation (4.43) from equations (4.41) and (4.42) we have set $f_0 = f$ which is correct at this order. In ref. [73] it was found that $f/f_0 \simeq 1.23$ and so we may expect significant corrections to (4.43).

4.3 K_{l3} form factor

The form factors $f_+^{K\pi}(q^2)$ and $f_-^{K\pi}(q^2)$ defined in equation (1.38) have been calculated to one and two-loop order in SU(3) ChPT in [68] and [74] respectively and the reader is referred to these papers for detailed derivations. The behaviour of the form factors at $q^2 = 0$ and $q_{\text{max}}^2 = (m_K - m_\pi)^2$ has also been studied using SU(2) ChPT in [75]. For the calculation of $|V_{us}|$ we are particularly interested in the value of $f_+^{K\pi}(q^2)$ at $q^2 = 0$. In this section I give a brief outline of the derivation of $f_+^{K\pi}(0)$ to one-loop order

in SU(3) and SU(2) ChPT.

4.3.1 Derivation in SU(3) ChPT

For the case of K_{l3} decays the external field is the W boson which we introduce by setting l_μ and r_μ to

$$l_\mu = -\frac{g_w}{\sqrt{2}}(W_\mu^+ T + W_\mu^- T^\dagger), \quad r_\mu = 0, \tag{4.44}$$

where g_w is the weak coupling constant, related to the Fermi constant G_F by $G_F/\sqrt{2} = g_w^2/8m_W^2$ and T is the matrix

$$T = \begin{pmatrix} 0 & V_{ud} & V_{us} \\ 0 & 0 & 0 \\ 0 & 0 & 0 \end{pmatrix} \tag{4.45}$$

The calculation then proceeds in an analogous fashion to the pion form factor calculation. We expand in ϕ to derive the Feynman rules, calculate J_μ from

$$J_\mu = \left.\frac{\partial \mathcal{L}}{\partial l_\mu}\right|_{l_\mu=0}, \tag{4.46}$$

and use it to calculate the matrix element by contracting with the external K and π fields. The Feynman diagrams to one-loop order that result are given in figure 4.4. Adding up the contributions from these diagrams, together with wavefunction renormalization results in the following NLO expression for the $f_+^{K\pi}(q^2)$ form factor [67,68]

$$f_+^{K\pi}(q^2) = 1 + \frac{3}{2}H_{K\pi}(q^2) + \frac{3}{2}H_{K\eta}(q^2) + 4\frac{L_9^r}{f_0^2}q^2, \tag{4.47}$$

where

$$H_{PQ}(t) = \frac{t}{f_0^2}\left[\frac{1}{6}(t - 2\Sigma_{PQ})\bar{J}(t) + \frac{\Delta_{PQ}^2}{6t^2}\left(\bar{J}(t) - 4t\bar{J}'(0)\right) - \frac{1}{3}k + \frac{1}{144\pi^2}\right]. \tag{4.48}$$

The constants Σ_{PQ}, Δ_{PQ} and k are given by:

$$\Sigma_{PQ} = m_P^2 + m_Q^2, \quad \Delta_{PQ} = m_P^2 - m_Q^2$$
$$k = \frac{1}{32\pi^2}\frac{m_P^2\ln(m_P^2/\mu^2) - m_Q^2\ln(m_Q^2/\mu^2)}{m_P^2 - m_Q^2}, \tag{4.49}$$
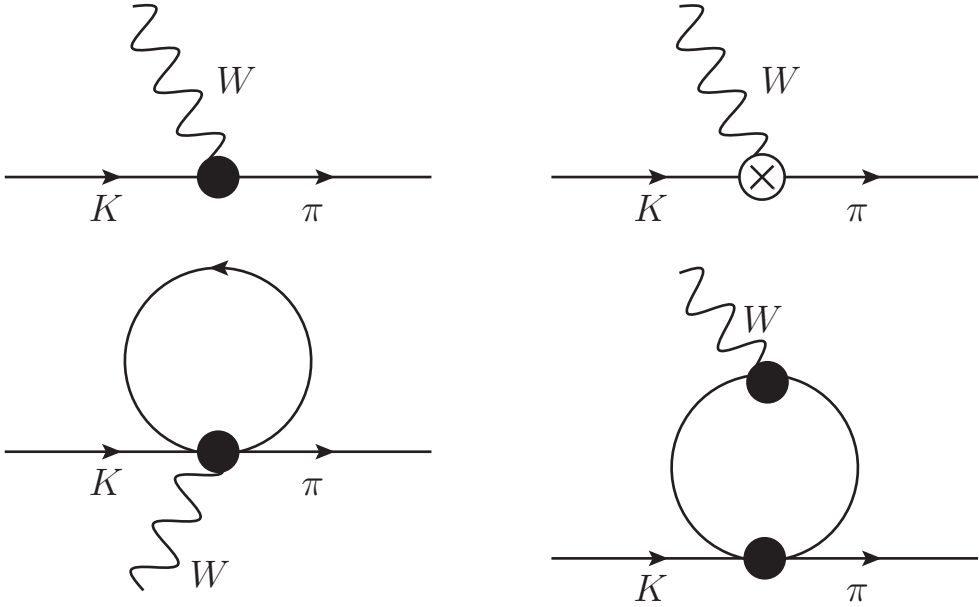
Figure 4.4: Feynman diagrams contributing to the K_{l3} form factor in SU(3) ChPT up to one-loop order.

and the function $\bar{J}(t)$ is given by

$$
\bar{J}(t) = -\frac{1}{16\pi^2} \int_0^1 \ln \left[\frac{m_P^2 - ty(1-y) - (m_P^2 - m_Q^2)y}{m_P^2 - (m_P^2 - m_Q^2)y} \right] dy \tag{4.50}
$$

$$
= \frac{1}{32\pi^2} \left[2 + \frac{\Delta_{PQ}}{t} \ln \frac{m_Q^2}{m_P^2} - \frac{\Sigma_{PQ}}{\Delta_{PQ}} \ln \frac{m_Q^2}{m_P^2} - \frac{\nu}{t} \ln \frac{(t+\nu)^2 - \Delta_{PQ}^2}{(t-\nu)^2 - \Delta_{PQ}^2} \right],
\tag{4.51}
$$

where

$$
\nu^2 = [t - (m_P + m_Q)^2][t - (m_P - m_Q)^2]. \tag{4.52}
$$

From the integral representation in equation (4.50) we can show that the derivative of $\bar{J}(t)$ at $t = 0$ is

$$
\bar{J}'(0) = \frac{1}{32\pi^2} \left[\frac{\Sigma_{PQ}^2}{\Delta_{PQ}^2} + 2\frac{m_P^2 m_Q^2}{\Delta_{PQ}^3} \ln \frac{m_Q^2}{m_P^2} \right]. \tag{4.53}
$$

It is easy to verify that if we let $m_Q = m_P$ then $\bar{J}(t)$ reduces to $H(x)$ of equation (4.37) for $x = t/m_P^2$ and $H_{PQ}(q^2)$ becomes $H_{PP}(q^2)$ of equation (4.36) as we would expect.

54

Using equation (4.50) it is easy to show that

$$\lim_{t \to 0}\{\bar{J}(t)\} = 0; \quad \lim_{t \to 0}\{t\bar{J}(t)\} = 0; \tag{4.54}$$

$$\lim_{t \to 0}\left\{\frac{1}{t}\bar{J}(t)\right\} = \frac{1}{16\pi^2}\int_0^1 \frac{y(1-y)}{m_P^2 - (m_P^2 - m_Q^2)y}dy$$

$$= \frac{1}{32\pi^2}\left[\frac{m_P^4 - m_Q^4 + 2m_P^2 m_Q^2 \ln(m_Q^2/m_P^2)}{(m_P - m_Q)^3(m_P + m_Q)^3}\right]. \tag{4.55}$$

Using these results we can see that if we set $q^2 = 0$ in (4.47) the form factor $f_+^{K\pi}(q^2)$ at NLO reduces to

$$f_+^{K\pi}(0) = 1 + f_2, \tag{4.56}$$

where

$$f_2 = \frac{3}{2}H_{K\pi} + \frac{3}{2}H_{K\eta}, \tag{4.57}$$

and

$$H_{PQ} = -\frac{1}{64\pi^2 f_0^2}\left[m_P^2 + m_Q^2 + 2\frac{m_P^2 m_Q^2}{m_P^2 - m_Q^2}\ln\frac{m_Q^2}{m_P^2}\right]. \tag{4.58}$$

We can see that f_2 is completely specified in terms of m_π, m_K, m_η and f_0, and takes the value $f_2 = -0.023$ at the physical values of the meson masses [26] and using f_π as an approximation for f_0. This is a result of the Ademollo-Gatto Theorem [27], which states that f_2 receives no contribution from local operators appearing in the effective theory.

4.3.2 Derivation in SU(2) ChPT

The K_{l3} form factor has conventionally been studied using SU(3) ChPT. However, following the study of the quark mass dependence of physical quantities computed in a lattice simulation using Domain Wall Fermions in [73], it has been suggested that SU(2) ChPT may be more appropriate for the chiral extrapolations of some quantities. This is mainly due to large one-loop effects in SU(3) ChPT found for the leptonic decay constant of pions with masses in the range in which the simulations were performed. SU(2) ChPT with kaons was introduced by Roessl in [76] for the study of pion-kaon scattering and further developed by the RBC and UKQCD collaborations in [73] for the study of the dependence on the pion mass of the mass of the kaon m_K, the leptonic decay constant f_K and the B_K-parameter describing the non-perturbative QCD effects in $K^0 - \bar{K}^0$ mixing.

It was then applied to K_{l3} decays in [75] and has recently been generalized by Bijnens for $K \to \pi\pi$ decays in [77]. Here we will briefly outline the derivation of $f_+^{K\pi}(0)$ in SU(2) ChPT as given in [75].

Introducing kaons in SU(2) chiral perturbation theory

In order to calculate the K_{l3} form factor in SU(2) ChPT we must add the kaon field as an extra 'heavy meson field' as it is not a pseudo-Goldstone boson in SU(2) chiral perturbation theory. We parametrize the kaon in terms of the physical particle fields as

$$K = \begin{pmatrix} K^+ \\ K^0 \end{pmatrix}. \tag{4.59}$$

Since kaons have isospin $1/2$, the action of the chiral group G on the kaon fields K is defined as [76]

$$K \to hK. \tag{4.60}$$

where $h \in H = SU(2)_V$ is the compensator field defined in equation (4.1). We then systematically construct all independent terms involving the fields Σ, χ and K that are invariant under *local* chiral transformations. For the pion fields the lowest order Lagrangian $\mathcal{L}_{\pi\pi}^{(2)}$ is just given by equation (4.12). For the interaction of kaons with soft pions the lowest order Lagrangian is given by [76]

$$\mathcal{L}_{\pi K}^{(1)} = D_\mu K^\dagger D^\mu K - \bar{m}_K^2 K^\dagger K, \tag{4.61}$$

where the kaon covariant derivative is defined by

$$D_\mu K = \partial_\mu K + \Gamma_\mu K \to h D_\mu K \tag{4.62}$$

$$\text{with} \quad \Gamma_\mu = \frac{1}{2} \left\{ \xi^\dagger (\partial_\mu - i r_\mu) \xi + \xi (\partial_\mu - i l_\mu) \xi^\dagger \right\}. \tag{4.63}$$

As the theory stands, however, we are not yet able to calculate the K_{l3} form factor. This is because we cannot use the external source fields l_μ and r_μ in the same way we did for the SU(3) case to account for the strangeness-changing left handed weak current

$$J_\mu^L = \bar{q}_L \gamma_\mu s_L = \bar{q} \gamma_\mu \frac{1}{2} (1 - \gamma_5) s \quad \text{where } q = u \text{ or } d \tag{4.64}$$

in the underlying QCD theory. To couple strangeness-changing axial cur-

rents to external sources in the ChPT SU(2) Lagrangian, we need to match the left handed current of equation (4.64) to a left handed current in the effective theory with the same chiral transformation properties. We can do this by making q a two component vector with components u and d and introducing a two component constant spurion vector t which projects out u and d as required. The current (4.64) is then invariant under $SU(2)_L$ transformations if t transforms as $t \to g_L t$. The current in the effective theory is now constructed from a linear combination of operators that are linear in t and invariant under $SU(2)_L$. At lowest order the left handed current in the effective theory is then given by [73, 75]

$$J_L^\mu = -L_{A1}(D_\mu K)^\dagger \xi^\dagger t + iL_{A2}K^\dagger A_\mu \xi^\dagger t, \qquad (4.65)$$

where L_{A1} and L_{A2} are low energy constants, A_μ is the pion axial vector field defined by

$$A_\mu = \frac{i}{2}(\xi^\dagger \partial_\mu \xi - \xi \partial_\mu \xi^\dagger) \to hA_\mu h^\dagger, \qquad (4.66)$$

and we have now set the external source fields l_μ and r_μ to zero.

We match the right handed current in the same way by taking the transformation on t to be $t \to g_R t$ and demanding invariance under $SU(2)_R$. This gives

$$J_R^\mu = L_{A1}(D_\mu K)^\dagger \xi t + iL_{A2}K^\dagger A_\mu \xi t. \qquad (4.67)$$

The vector J_μ and axial vector J_μ^5 currents can now easily be determined

$$J_\mu = J_\mu^R + J_\mu^L = L_{A1}(D_\mu K)^\dagger(\xi - \xi^\dagger)t + iL_{A2}K^\dagger A_\mu(\xi + \xi^\dagger)t, \qquad (4.68)$$

$$J_\mu^5 = J_\mu^R - J_\mu^L = L_{A1}(D_\mu K)^\dagger(\xi + \xi^\dagger)t + iL_{A2}K^\dagger A_\mu(\xi - \xi^\dagger)t. \qquad (4.69)$$

K_{l3} form factor at $q^2 = 0$

When considering the K_{l3} form factor at $q^2 = 0$ in SU(2) chiral perturbation theory a problem arises. Consider the momentum p_π of an external pion. Then $2p_\pi . p_K = m_K^2 + m_\pi^2 \approx m_K^2$, so that the energy of the pion in the rest frame of the kaon $E_\pi \approx m_K^2/2$ is not small for $m_K^2 \gg m_\pi^2$. Since SU(2) ChPT is an expansion in powers of masses and momenta of the pions, the fact that the external pion in $K \to \pi$ decays is hard, implies that we cannot neglect operators with an arbitrary number of derivatives on external pion fields, thus complicating the power counting. However, it has been shown in [75] that an expansion in small masses and momenta is

still possible due to the fact that chiral logarithms are caused by internal soft pion propagators, i.e. the momenta of internal pions is of $\mathcal{O}(m_\pi)$. By integrating by parts, they show in [75], that operators with an arbitrary number of covariant derivatives can be related to leading order operators, up to corrections of $\mathcal{O}(m_\pi^2)$, by replacing the low energy constants L_{A1} and L_{A2} with unknown coefficients $\tilde{L}_{A1}$ and $\tilde{L}_{A2}$ which depend on m_s but not on the light quark masses. In this way they are able to calculate the chiral logarithms, i.e. the corrections of $\mathcal{O}(m_\pi^2 \ln(m_\pi^2))$.

To leading order at $q^2 = 0$ the $K \to \pi$ matrix element is thus given by

$$
\begin{aligned}
\langle \pi(p_\pi)| \, \bar{q}\gamma_\mu s \, |K(p_K)\rangle &= \\
&= \langle \pi(p_\pi)| \, \tilde{L}_{A1}(D_\mu K)^\dagger (\xi - \xi^\dagger)t + \tilde{L}_{A2}K^\dagger A_\mu (\xi + \xi^\dagger)t \, |K(p_K)\rangle \quad (4.70)
\end{aligned}
$$

where $\tilde{L}_{A1}$ and $\tilde{L}_{A2}$ are unknown constants that cannot be determined from L_{A1} and L_{A2} alone. Expanding in ϕ one can now use this expression and calculate the matrix element to one-loop order. The resulting NLO expression for the $K \to \pi$ matrix element at $q^2 = 0$ [75] is

$$
\langle \pi(p_\pi)| \, \bar{q}\gamma_\mu s \, |K(p_K)\rangle = F_K p_K^\mu \left[1 - \frac{3}{4}L + c_K m_\pi^2 \right] + F_\pi p_\pi^\mu \left[1 - \frac{3}{4}L + c_\pi m_\pi^2 \right],
$$
$$(4.71)$$

where $F_K = 2\tilde{L}_{A1}/f$, $F_\pi = 2\tilde{L}_{A2}/f$, $c_{K,\pi}$ are LECs and the chiral logarithm L is defined by

$$
L = \frac{m_\pi^2}{16\pi^2 f^2} \ln\left(\frac{m_\pi^2}{\mu^2} \right). \quad (4.72)
$$

From this we deduce that the chiral behaviour of the form factors is given by

$$
f^0(0) = f^+(0) \;\; = \;\; F_+ \left(1 - \frac{3}{4}L + c_+ m_\pi^2 \right), \quad\quad (4.73)
$$

$$
f^-(0) \;\; = \;\; F_- \left(1 - \frac{3}{4}L + c_- m_\pi^2 \right), \quad\quad (4.74)
$$

where $F_\pm = 1/2(F_K \pm F_\pi)$ and $c_\pm = 1/2(c_K \pm c_\pi)$.

4.4 Partial quenching

Partial quenching has become common practice in many lattice QCD simulations. In partially quenched lattice QCD simulations we introduce differ-

ent masses for the sea quarks (the quark masses appearing in the fermion determinant of equation (3.2), used for the gauge configurations generation) and the valence quarks (the quark masses in the Dirac matrix that is inverted to generate the propagators as in equation (3.15)). The advantage of this is that, since the numerical cost of calculating correlators is much smaller than generating gauge configurations, one can calculate lattice correlators for a range of different valence quark masses at a much lower cost than if we had to generate gauge configurations with matching sea quark masses for every valence quark mass.

This unphysical theory corresponding to QCD where the external quarks have different masses to those appearing in loops also has an effective field theory description, known as Partially Quenched Chiral Perturbation Theory (PQChPT), which is a generalisation of the ChPT discussed in this chapter.

In PQChPT, ghost quarks with the same quantum numbers as the valence quarks are introduced into the Lagrangian, in order to ensure that only determinants of the sea quarks appear in the path integral. A theory with N_S sea quarks and N_V valence quarks will now obey a graded $SU(N_S + N_V | N_V)_L \times SU(N_S + N_V | N_V)_R$ chiral symmetry [78]. The $\xi(x)$ field of equation (4.4) is then generalised to include the different mesons that can now be made up of the $2N_V + N_S$ different valence, sea and ghost quarks. It is given by

$$\xi = \exp\left[\frac{i\Phi}{f}\right] \tag{4.75}$$

where Φ is the generalised $(2N_V + N_S) \times (2N_V + N_S)$ meson field matrix which can be written in block form as [78]

$$\Phi \equiv \begin{pmatrix} \phi & \chi^\dagger \\ \chi & \tilde{\phi} \end{pmatrix} \tag{4.76}$$

where ϕ is an $(N_V + N_S) \times (N_V + N_S)$ matrix consisting of the mesons that can be constructed from the normal valence and sea quarks, $\tilde{\phi}$ is an $N_V \times N_V$ matrix containing the mesons made up of ghost quarks only and χ is an $(N_V + N_S) \times N_V$ matrix of Goldstone fermions made up of normal quarks and ghost anti-quarks. All of the operators in PQChPT can then be constructed in terms of $\Sigma = \xi^2$ and other auxiliary matrices such as the

mass matrix

$$M = \text{diag}\left(m_u^{(V)}, m_d^{(V)}, m_s^{(V)}, m_u^{(S)}, m_d^{(S)}, m_s^{(S)}, m_u^{(V)}, m_d^{(V)}, m_s^{(V)}\right), \quad (4.77)$$

where the superscript S stands for sea quark and V for valence quark. The transition from ChPT to PQChPT is then made by replacing ϕ with Φ and traces with supertraces in the ChPT Lagrangians [78] of section 4.1, where the supertrace is similar to a normal trace but a minus sign is introduced for the sum of the diagonal elements in the ghost quark sector.

By constructing a PQChPT in this way the LEC's of the partially quenched Lagrangians share the same numerical values as those in the unquenched theory [79]. Thus partially quenched simulations can be used to determine the LEC's of the unquenched theory.

In this work we have calculated the K_{l3} form factors for both unquenched and partially quenched QCD where the partial quenching is in the strange quark mass only.

Becirevic et al. [80] calculated $f_+^{K\pi}(0)$ at NLO using a PQChPT Lagrangian, as defined in [78, 81], with three dynamical flavours of quarks having two sea quark masses $m_s^{(S)}, m_d^{(S)}$ and two valence quark masses $m_s^{(V)}, m_d^{(V)}$ in the isospin limit. The expression they derive for f_2 using this PQChPT with $N_f = 2+1$ dynamical flavours of quarks is given in the appendix for completeness. We make use of this expression in our analysis of the partially quenched data presented in chapters 6 and 7, setting $m_d^{(V)} = m_d^{(S)}$ as our data is partially quenched in the strange quark only. We note that this expression reduces to the usual unquenched ChPT result of equation (4.57) when we set $m_s^{(V)} = m_s^{(S)}$ and $m_d^{(V)} = m_d^{(S)}$.

4.5   Finite Volume effects in ChPT

The discussions of ChPT in this chapter have thus far assumed an infinite volume. Lattice simulations are however performed in a finite volume, which means the momenta will be discrete. As a result we must sum over all the possible discrete momenta, which will lead to corrections to the chiral logarithms of the ChPT formulae presented in this chapter. For the unquenched case, it can be shown (see for example [82]) that for quark fields obeying periodic boundary conditions, to one loop order the chiral logarithm $m^2 \ln(m^2/\mu^2)$ receives a finite volume correction of

60

$\sim L^{-3/2} \exp(-mL)$. In principle, we should use finite volume ChPT formulae when looking at observables calculated in a finite volume. In practice however, since the finite volume corrections are exponentially small, if we make the volume in which the simulations are performed large enough, we can regard finite volume corrections as negligible when compared to the statistical precision of the simulations and use the infinite volume ChPT formulae as a reasonable approximation. In this work we use infinite volume ChPT formulae in the extrapolations of our lattice data and briefly discuss the systematic errors involved in doing so.

Chapter 5

Boundary Conditions in Lattice QCD

Lattice QCD simulations are performed in a finite volume. One must therefore choose boundary conditions (BCs) for the quark fields, which means that the spatial components of the hadronic momenta will be quantized. The BCs most commonly used for the quarks fields are periodic BCs in the spatial directions

$$\psi(x_i + L) = \psi(x), \ i = 1, 2, 3. \tag{5.1}$$

This leads to the quantized spatial momenta

$$p_i = n_i \frac{2\pi}{L} \tag{5.2}$$

where n_i are integers. The smallest non-zero value of momentum that one can achieve with periodic BCs is therefore $2\pi/L$. This presents a limitation on the momentum resolution that can be achieved in the calculation of momentum dependent quantities such as form factors. For the pion electromagnetic form factor this means that the minimum non-zero value of the momentum transfer $Q^2 = -q^2$ that one can achieve is $Q^2_{\min} = 2m_\pi(\sqrt{m_\pi^2 + (2\pi/L)^2} - m_\pi)$, which for the parameters of our simulation is about $0.15\,\mathrm{GeV}^2$. For the K_{l3} form factor this means that we can only calculate the form factor at $q^2_{\max} = (m_K - m_\pi)^2$, which for our simulations is about $0.06\,\mathrm{GeV}^2$, and at negative values of q^2 thus introducing the need for an interpolation to reach the form factor at $q^2 = 0$.

In [83], Bedaque proposed that by applying twisted BCs one can simulate hadrons with any desired momentum thus improving the momentum resolution in the calculation of momentum dependent quantities. It was

later independently shown in [84] and [85] that one can achieve the same result by applying only partially twisted BCs, which give valence and sea quarks different BCs, thus removing the need for generating a new set of gauge configurations for each value of the twisting angle. A numerical study of the use of partially twisted BCs for the spectrum of pseudo-scalar and vector mesons as well as their leptonic decay constants was subsequently done in [86]. They confirmed the expected momentum shift for mesons with partially twisted BCs and concluded that using partially twisted BCs does not increase statistical errors in any appreciable way. The feasibility of applying partially twisted BCs in the calculation of weak and electromagnetic form factors was then demonstrated in [61]. In this chapter we will define both twisted and partially twisted BCs and look at the consequences of their application. We will then look at the application of partially twisted BCs in the calculation of hadronic form factors.

5.1 Twisted boundary conditions

Periodic BCs are often chosen in lattice field theories as they ensure that the fermion fields are single valued thus avoiding boundary terms. This is however not a necessary condition in order to avoid boundary terms. It is sufficient to only require that observables be single valued, implying that the fermion fields only have to obey the following BCs [85]

$$\psi(x_i + L) = U_i \psi(x_i) \tag{5.3}$$

where U_i is a symmetry of the action and we are not summing over i. We can therefore choose $U_i \in U(N_f)_V$ such that the BCs for the fermion fields are then given by

$$\psi(x_i + L) = U_i \psi(x_i) = e^{i\Theta_i^a T^a} \psi(x_i) \equiv e^{i\theta_i} \psi(x_i) \tag{5.4}$$

where the T^a's are the generators of $U(N_f)_V$. If we now Fourier transform equation (5.4) we can immediately see that imposing twisted BCs implies

$$e^{i(p_i - \frac{\theta_i}{L})L} = 1 \Rightarrow p_i = \frac{\theta_i}{L} + \frac{2\pi n_i}{L}. \tag{5.5}$$

The quark momentum is therefore shifted by θ_i/L when twisted BCs are imposed.

Imposing twisted BCs on the quark fields is equivalent to coupling a constant background vector field B_μ to quark fields satisfying periodic BCs. We can easily see this if we redefine the quark fields such that,

$$\psi(x) \equiv V(x)\tilde{\psi}(x) \qquad \text{where} \qquad V(x) \equiv \exp\left(i\frac{\theta_i}{L}x_i\right) \qquad (5.6)$$

and let the fields $\tilde{\psi}(x)$ satisfy periodic BCs, so that $\psi(x)$ satisfies twisted BCs. We can show that in terms of these fields the Dirac term in the (Euclidean) QCD Lagrangian is given by [85]

$$\mathcal{L} = \bar{\tilde{\psi}}(x)(\gamma^\mu \tilde{D}_\mu + M)\tilde{\psi}(x) \qquad (5.7)$$

where

$$\tilde{D}_\mu = D_\mu + iB_\mu \text{ with } B_i = \frac{\theta_i}{L} \text{ for } i = 1, 2, 3 \text{ and } B_4 = 0. \qquad (5.8)$$

This is the Lagrangian of QCD with quark fields satisfying periodic BCs interacting with a constant background vector field which couples to quarks with charges determined by the phases in the twisted BCs.

In the chiral Lagrangian of equation (4.12) the twisted BCs on the quark fields imply that the chiral field of equation (4.4) satisfies the BCs

$$\Sigma(x_i + L) = U_i\Sigma(x_i)U_i^\dagger. \qquad (5.9)$$

If we again redefine the fields by

$$\Sigma(x) \equiv V(x)\tilde{\Sigma}(x)V^\dagger(x) \qquad (5.10)$$

with $\tilde{\Sigma}(x)$ satisfying periodic BCs, we can show that the chiral Lagrangian becomes [85]

$$\mathcal{L}_{\text{eff}}^{(2)} = \frac{f^2}{8}\langle \tilde{D}_\mu\tilde{\Sigma}\tilde{D}^\mu\tilde{\Sigma}^\dagger + \tilde{\Sigma}^\dagger\chi + \chi^\dagger\tilde{\Sigma}\rangle \qquad (5.11)$$

where

$$\tilde{D}_\mu\tilde{\Sigma} \equiv \partial_\mu\tilde{\Sigma} + i[B_\mu, \tilde{\Sigma}] \qquad (5.12)$$

which again is just the standard chiral Lagrangian for fields satisfying periodic BCs coupled to an external constant vector field B_μ. As shown in [85], this implies that for a charged meson composed of a quark q_1 and an antiquark $\bar{q}_2$, satisfying twisted BCs with twist angles $\vec{\theta}_1$ and $\vec{\theta}_2$ respectively,

65

the corresponding meson momentum is given by

$$\vec{p} = \frac{2\pi}{L}\vec{n} - \frac{\vec{\theta_1} - \vec{\theta_2}}{L}. \tag{5.13}$$

Using the chiral Lagrangian of (5.11), it is shown in [85] that for physical quantities without final state interactions, such as masses, decay constants and form factors with only one final state hadron, the flavour symmetry breaking induced by the twist only affects the finite-volume corrections, which although do depend on the BCs, remain exponentially small as is the case for periodic BCs.

5.2   Partially twisted boundary conditions

The practical difficulty in using twisted BCs in lattice simulations with dynamical quarks is that it requires the generation of a new set of gauge field configurations for every choice of twisting angle. In [85] the effects of applying partially twisted BCs, i.e. imposing twisted boundary conditions for the valence quarks but periodic BCs for the sea quarks, are investigated. They find that breaking the valence-sea symmetry by applying different twists is analogous to the violation of unitarity in partially quenched QCD and that for many physical quantities the use of partially twisted BCs induces finite volume effects which are exponentially small. The physical quantities for which this is true include those with at most a single hadron in the initial and final states. For these processes the finite-volume effects depend on the twisting angles but remain exponentially small. For such physical quantities one can therefore use partially twisted BCs, thus eliminating the need for new simulations for every choice of the twist angles making the technique practically feasible.

With partial twisting the dispersion relation for a meson takes the same form as for full twisting

$$E = \sqrt{m^2 + \left(\vec{p_n} + \frac{\vec{\theta}}{L}\right)^2} \tag{5.14}$$

where m is the meson mass, $\vec{p_n}$ is the Fourier momentum and we have applied a twist $\vec{\theta}$ to the valence quark only, leaving the valence antiquark untwisted, which will be sufficient for the purposes of this work.

5.3 Pseudo-scalar meson form factors with partially twisted BCs

A sketch of the quark-flow diagram for the transition in equation (1.37), with the final-state meson P_f composed of valence quarks $(q_1 \bar{q}_3)$ and the initial-state meson P_i with valence quarks $(q_2 \bar{q}_3)$ is shown in figure 5.1. For $K_{\ell 3}$ decays, each of the three valence quarks has a different flavour, and we can introduce three independent twisting angles for the three flavours. In particular we set the twisting angle of the spectator (anti-)quark q_3 to zero so that it satisfies periodic boundary conditions, which will be sufficient for the purposes of this work, and we give the quark q_2 a twist of $\vec{\theta}_i$ and the quark q_1 a twist of $\vec{\theta}_f$ as shown in figure 5.1. The initial and final state momenta are therefore given by $\vec{p}_i = \vec{p}_{n,i} + \vec{\theta}_i/L$ and $\vec{p}_f = \vec{p}_{n,f} + \vec{\theta}_f/L$ respectively. The momentum transfer between initial and final state mesons is then given by

$$q^2 = (p_i - p_f)^2 = (E_i(\vec{p}_i) - E_f(\vec{p}_f))^2 - (\vec{p}_i - \vec{p}_f)^2. \qquad (5.15)$$

For the electromagnetic form factor of the pion however, q_1 has the same flavour as q_2, and so it would appear that one can not use three independent twist angles in this case. However it was shown in [61], that this is in fact still possible. This is shown in [61] by considering the matrix element $\langle \pi(p_f) | j_\mu | \pi(p_i) \rangle$ in the partially quenched three flavour theory with $m_u^{(V)} = m_d^{(V)} = m_u^{(S)} = m_d^{(S)} = m_s^{(V)}$ and $m_s^{(V)} \neq m_s^{(S)}$ (in which the matrix element is correctly evaluated since the valence strange quark plays no role in its evaluation), and then exploiting the SU(3) flavour symmetry of the valence quark sector to show that in this partially quenched theory the pion's form factor is equivalent to the form factor of the $K \to \pi$ transition (note that the degeneracy of the three flavours of valence quarks in this partially quenched theory implies that there is only a single form factor for the $K \to \pi$ transition). We can therefore use the same strategy as for the $K \to \pi$ transition of giving q_2 a twist of $\vec{\theta}_i$, q_1 a twist of $\vec{\theta}_f$ and q_3 a twist of zero. From here onwards we will refer to the twists as being applied to the mesons as we are only applying twists to the valence quarks in different initial and/or final state mesons.

In order to obtain $q^2 = 0$ for the K_{l3} form factor we set the Fourier momenta of the mesons to zero and make the following two choices of the
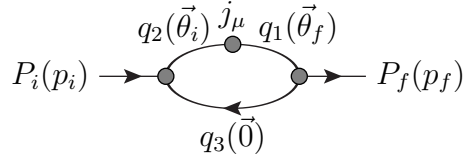
Figure 5.1: Quark flow diagram for a three-point function with initial and final states P_i and P_f, respectively. Our strategy for applying the twisting angles in the three point function is also shown.

twisting angles [61]:

$$
|\vec{\theta}_K| = L\sqrt{\left(\frac{m_K^2+m_\pi^2}{2m_\pi}\right)^2 - m_K^2} \quad \text{and} \quad \vec{\theta}_\pi = \vec{0},
$$

$$
\text{and} \quad |\vec{\theta}_\pi| = L\sqrt{\left(\frac{m_K^2+m_\pi^2}{2m_K}\right)^2 - m_\pi^2} \quad \text{and} \quad \vec{\theta}_K = \vec{0}. \tag{5.16}
$$

The form factors $f_+^{K\pi}(0)$ and $f_-^{K\pi}(0)$ are then calculated by solving the simultaneous linear equations (3.31) using these twist angle choices, which both independently give $q^2 = 0$.

A number of other twisting angles are also used to allow a computation of the K_{l3} form factors in the range $0 < q^2 < q_{\text{max}}^2$ and the pion form factor in the range $0 < Q^2 < Q_{\text{min}}^2$. The choices of twisting angles used is discussed in chapter 6.

Chapter 6

Lattice results at light-quark masses corresponding to $m_\pi = 330\,\mathrm{MeV}$

6.1 Simulation parameters

The computations described in this thesis were performed using a gauge configuration ensemble jointly generated by the RBC-UKQCD collaborations using the QCDOC computers [87–90] at Edinburgh and Brookhaven National Laboratory on a lattice volume of $(L/a)^3 \times T/a \times L_s = 24^3 \times 64 \times 16$. The ensemble used was generated with $N_f = 2 + 1$ dynamical flavours of quarks with an input light quark mass of $am_u = am_d = 0.005$ and strange quark mass of $am_s = 0.04$ using the Iwasaki gauge action described in section 2.2.2 [35, 36] with a coupling of $\beta = 2.13$, and the domain wall fermion action described in section 2.3.3 [43, 44] which is found to have a residual chiral symmetry breaking given by a residual mass of $am_{\mathrm{res}} = 0.00315(2)$ [52].

In [73] the physical quark masses m_{ud}, m_s and the lattice spacing a for this ensemble are determined by comparing the results of SU(2) ChPT fits for the hadron masses m_π, m_K and m_Ω, to their physical values. The inverse lattice spacing is found to be $a^{-1} = 1.73(3)$ GeV ($a = 0.114(2)$fm) [52, 73]. The simulated strange quark mass turned out to be slightly heavier than the physical value $am_s = 0.0343(16)$ found in [73]. The resulting pion mass for this ensemble was found to be $m_\pi \approx 330\,\mathrm{MeV}$. A detailed study of the light-hadron spectrum and other hadronic quantities using these configurations can be found in ref. [73].

set	trajs on $t_{\mathrm{src}}=0$	Δ	t_{src}	N_{meas}
P4	900 – 4460	20	0, 16, 32, 48	700
P3	900 – 4460	20	0, 16, 32	537
$Z_2(4)$	1000 – 6840	40	0, 54, 20, 14, 56, 26, 44, 34	1176
$Z_2(4)'$	1000 – 6440	40	0, 20, 56, 44	548
$Z_2(3)$	1000 – 6840	40	0, 54, 20, 14, 56, 26, 44, 34	1176

Table 6.1: Details of measurements for the different data sets of correlation functions used. The quoted range of trajectories is the one for $t_{\mathrm{src}} = 0$ and Δ is the separation in units of trajectories between subsequent measurements for each source position t_{src}.

The majority of the correlation functions measured on this ensemble for the form factor calculations presented in this thesis were evaluated on the UK Research Councils' HECToR Cray XT4 computer, with the set completed using a University of Edinburgh BlueGene/L system as well as QCDOC. The pion form factor results described in this and the next chapter were published in [4] while the K_{l3} form factor results were recently published in [5].

We distinguish five sets of correlation functions as summarized in table 6.1[1]. Sets P3 and P4 were generated with point sources and sinks. Set P3 is a subset of set P4. The pion form factor correlation function measurements with point sources were performed on the data set P3 and then later a fourth point source was added to make the data set P4 on which we performed the K_{l3} form factor correlation function measurements. For the set P3(P4) measurements were started for three(four) different source positions on trajectories 900, 905, 910 (and 915), respectively, measuring on every 20th trajectory in each case and averaging three(four) consecutive measurements over the sources into one bin in order to reduce autocorrelation effects. For these data sets the initial/final state meson carries Fourier momentum $|\vec{p}| = 0, \frac{2\pi}{L}$ or $\sqrt{2}\frac{2\pi}{L}$ and no twisted boundary conditions are used.

For data sets $Z_2(4)$ and $Z_2(3)$ we use a $\mathbb{Z}(2) \times \mathbb{Z}(2)$ [4,59] stochastic wall source as explained in section 3.2.3 and a point sink with valence strange quark masses $am_s = 0.04$ and $am_s = 0.03$, respectively. The data set $Z_2(4)$ corresponds to a unitary simulation point, i.e. where the sea and valence strange quark masses are the same, while set $Z_2(3)$ corresponds to

[1]Data sets P3, $Z_2(4)$ and $Z_2(4)'$ are the data sets A, B and C respectively in ref. [4]. Data sets $Z_2(4)$ and $Z_2(3)$ are referred to as $Z4PSs4$ and $Z4PSs3$ respectively in ref. [5].

a partially quenched parameter choice. For these data sets we started the measurement chains for the eight source positions specified in table 6.1 on trajectories $1000, 1005, 1010, \ldots, 1035$. Data set $Z_2(4)'$ is a subset of $Z_2(4)$ which starts with four source positions on trajectories $1000, 1010, 1020$ and 1030, respectively. In each case we measured on every 40th trajectory and averaged the correlation functions over the chains into bins of eight measurements for $Z_2(4)$ and $Z_2(3)$, and four measurements for $Z_2(4)'$ to reduce autocorrelation effects. The reason for distinguishing the subset $Z_2(4)'$ originated from the fact that we inadvertently simulated with the wrong sign for the meson twist angles in the remaining correlation functions of set $Z_2(4)$. This however only affects the data where both initial and final state mesons are twisted as can be seen from the equation for the momentum transfer (5.15), and we can therefore use the full set $Z_2(4)$ of correlation functions for calculations where only one of the mesons is twisted. The set $Z_2(4)'$ has the correct twist angle sign and is used for calculations where both initial and final states are twisted.

The correlation functions obtained using stochastic sources were computed with zero Fourier momentum and the momenta of the initial and/or final meson were induced by twisting one of the meson's valence quarks. For each measurement we applied the full twist along one of the spatial directions. In order to reduce correlations we applied twists for the trajectories $1000, 1010, 1020, \ldots$ along the x-direction, for the trajectories 1005, $1025, 1045, \ldots$ along the y-direction and for the trajectories $1015, 1035$, $1055, \ldots$ along the z-direction. In the cases in which both the initial and the final meson carried a twist, $\vec{\theta}_i$ and $\vec{\theta}_f$ were chosen to be anti-parallel.

Our choices of twisting angles are summarized in tables 6.2 and 6.4. In order to obtain $q^2{=}0$ for the K_{l3} form factor we use the twisting angles given by equation (5.16). As input to these formulae we have used the estimates for the central values of the kaon masses $am_K = 0.2990$ ($Z_2(3)$) and $am_K = 0.3328$ ($Z_2(4)$) and for the pion mass $am_\pi = 0.1907$ (for both datasets). These values were determined from a preliminary study of the gauge field ensemble considered here (After a detailed analysis by the RBC/UKQCD collaboration on their data set of choice, called the FPQ data set in [73], the pion mass was quoted as $0.1915(8)$.).

The momenta of the mesons are given by $\vec{p}_K = \vec{\theta}_K/L$ and $\vec{p}_\pi = \vec{\theta}_\pi/L$. In addition to the values of $|\theta_\pi|$ and $|\theta_K|$ in equation (5.16), propagators were generated for other values of the twisting angles. In particular, for
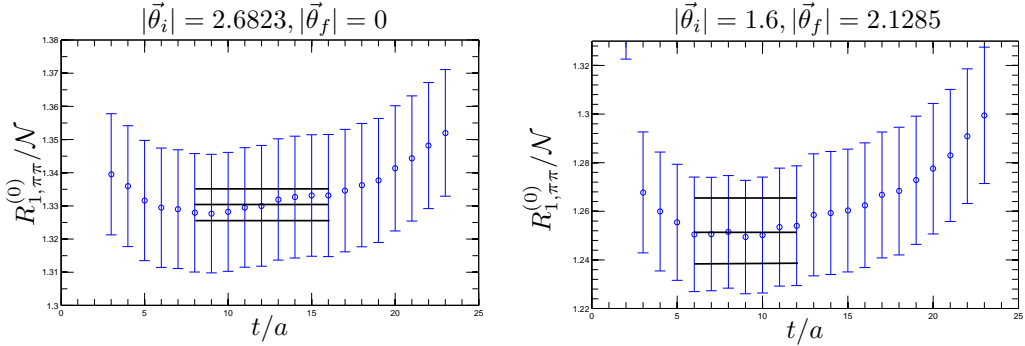
Figure 6.1: Examples for the quality of the plateaus for the ratio $R^{(0)}_{1,\pi\pi}$ with just one of the pions having a twist (left) and with both pions twisted (right).

the kinematical situation where the kaon is at rest and the pion is moving due to the additional *ad hoc* twist angle $\theta_\pi = 1.600$ (chosen to give a q^2 approximately in the middle of the range $0 < q^2 < q^2_{max}$ for both valence strange quark masses) we determined the corresponding values for θ_K which yield the same q^2 also when the pion is at rest. The contractions of these propagators into two- and three-point functions allow a computation of $f^{K\pi}_+(q^2)$ for additional values of the momentum transfer in the range from about $q^2 = 0$ to q^2_{max} (cf. table 6.4). These choices give us the three pion twisting angles 2.6823, 2.1285 and 1.6, which we use to sample the region $0 < Q^2 < Q^2_{min}$ for the pion form factor, as summarized in table 6.2.

All statistical errors presented in this and the next chapter were calculated using the jackknife technique presented in section 3.4.2.

6.2 Results for the pion form factor

We calculated the pion form factor at a range of values of Q^2 using the ratio $R^{(0)}_{1,\pi\pi}$ as defined in equation (3.30). This ratio was chosen as it was found to give the best quality of plateaus. Examples of the plateaus we obtained using this ratio are given in figure 6.1. We performed both uncorrelated and correlated (*frozen* covariance matrix) χ^2 fits to our pion form factor data, and found similar statistical errors for both approaches. For this reason we opted for uncorrelated χ^2 fits and all fits to our pion form factor data presented in this and the next chapter were performed in this way.

The results of our computation of the form factor of a pion with $m_\pi = 330\,\mathrm{MeV}$ for a range of low values of Q^2 (obtained from data sets P3, $Z_2(4)$ and $Z_2(4)'$), are presented in table 6.2 and plotted in figure 6.2. The upper plot of figure 6.2 shows the results for all the Q^2 values at which

set	$|\vec{p}_i|L$	$|\vec{p}_f|L$	$aE_\pi(\vec{p}_i)$	$aE_\pi(\vec{p}_f)$	Q^2 (GeV^2)	$f^{\pi\pi}(q^2)$
$Z_2(4)$	0	0	0.1910(4)	0.1910(4)	0	1
$Z_2(4)$	0	1.6	0.1910(4)	0.2023(4)	0.013	0.9804(15)
$Z_2(4)$	0	2.1285	0.1910(4)	0.2106(4)	0.022	0.9660(24)
$Z_2(4)$	0	2.6823	0.1910(4)	0.2213(4)	0.035	0.9477(36)
$Z_2(4)'$	1.6	1.6	0.2023(6)	0.2023(6)	0.053	0.9189(75)
$Z_2(4)'$	2.1285	1.6	0.2106(5)	0.2023(6)	0.072	0.8943(88)
$Z_2(4)'$	2.1285	2.1285	0.2106(5)	0.2106(5)	0.094	0.867(10)
$Z_2(4)'$	2.6823	1.6	0.2213(5)	0.2023(6)	0.094	0.864(11)
$Z_2(4)'$	2.6823	2.1285	0.2213(5)	0.2106(5)	0.120	0.838(12)
$Z_2(4)'$	2.6823	2.6823	0.2213(5)	0.2213(5)	0.150	0.802(15)
P3	0	0	0.1912(7)	0.1912(7)	0	1
P3	2π	0	0.3242(4)	0.1912(7)	0.152	0.809(14)
P3	$\sqrt{2}\,2\pi$	0	0.4167(3)	0.1912(7)	0.258	0.711(26)

Table 6.2: Table of accessible values of $Q^2 = -q^2$ for the matrix element $\langle \pi(p_f)|j_\mu|\pi(p_i)\rangle$ together with the values of $f^{\pi\pi}(q^2)$. For data sets $Z_2(4)$ and $Z_2(4)'$ we also determined the correlation functions with momenta $|\vec{p}_i| = |\vec{\theta}_i|/L$ and $|\vec{p}_f| = |\vec{\theta}_f|/L$ interchanged.

we calculated the form factor using all three data sets. The lower plot is a zoom into the very low Q^2 region. The vertical dashed line represents the position of the lowest value of Q^2 which can be reached with periodic boundary conditions ($Q^2_{\text{min}} \simeq 0.15\,\text{GeV}^2$). From the figure it is satisfying to observe that at Q^2_{min} the results obtained with partially twisted boundary conditions join smoothly onto the data obtained by performing a Fourier sum with momentum of magnitude $2\pi/L$.

Our results from datasets $Z_2(4)$ and $Z_2(4)'$ are well represented in the range $0 \leq Q^2 \leq Q^2_{\text{min}}$ by the phenomenological pole formula

$$f^{\pi\pi}_{\text{pole}}(q^2) = \frac{1}{1 - q^2/M^2_{\text{pole}}}. \tag{6.1}$$

From the slope of the form factor at $q^2 = 0$ we obtain the pion's electromagnetic charge radius as defined by equation (1.43). The best fit, which is shown as the blue curve in figure 6.2, gives $\langle r^2_\pi \rangle_{330\,\text{MeV}} = 6/M^2_{\text{pole}} = 0.382(37)(12)(15)\,\text{fm}^2 = 0.382(42)\,\text{fm}^2$, where the first error is statistical and the second is due to the uncertainty in the lattice spacing. The third error is to account for our lack of a continuum extrapolation (as we will discuss in chapter 7). This result corresponds to a pole mass of $(aM_{\text{pole}})^2 = 0.202(20)$.

We compare our results to those of the UKQCD/QCDSF collaboration [1] who determined the pion form factor for a number of unphysical
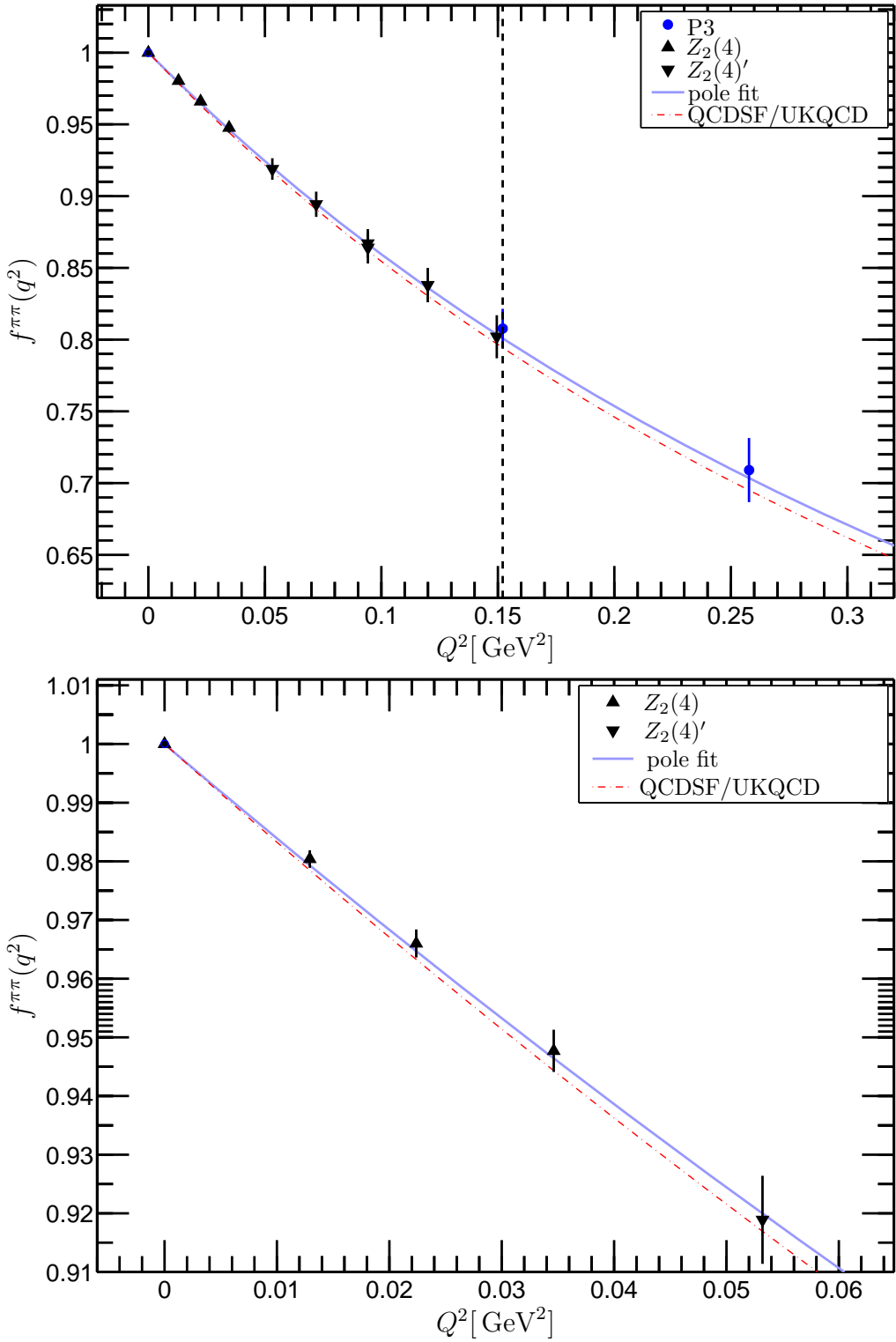
Figure 6.2: Results for the form factor $f^{\pi\pi}(q^2)$ for a pion with $m_\pi = 330\,\text{MeV}$. The upper plot shows the results for all the Q^2 values at which we calculated the form factor using all three data sets. The lower plot is a zoom into the very low Q^2 region. The blue solid curve is a pole fit to the data, while the red dashed curve shows the prediction for a $330\,\text{MeV}$ pion using results from the QCDSF/UKQCD collaboration [1].

pion masses $m_\pi \geq 400\,\mathrm{MeV}$ using periodic boundary conditions. For each pion mass, they fit their data to the pole form in (6.1) and hence determine the dependence of the pole mass M_{pole} on the pion mass. Their results are well described by the ansatz,

$$M^2(m_\pi^2) = c_0 + c_1 m_\pi^2 \,, \tag{6.2}$$

for which they determined $c_0 = 0.517(23)\,\mathrm{GeV}^2$ and $c_1 = 0.647(30)$. Thus, for a pion of mass $330\,\mathrm{MeV}$ they predict $\langle r_\pi^2 \rangle_{330\,\mathrm{MeV}}^{\mathrm{UKQCD/QCDSF}} = 0.396(15)\,\mathrm{fm}^2$. This result, which we also illustrate in figure 6.2, is compatible with ours.

Although the pole formula (6.1) is a good representation of our data for the full range $Q^2 \leq Q^2_{\mathrm{min}}$, we find that the points at the smallest values of Q^2 tend to give a smaller central value for the charge radius. We will take as our best estimates of $\langle r_\pi^2 \rangle_{330\,\mathrm{MeV}}$ the value obtained by applying SU(2) ChPT to the points at small Q^2 as explained in section 7.1 (we find $\langle r_\pi^2 \rangle_{330\,\mathrm{MeV}} = 0.354(31)\,\mathrm{fm}^2$, see table 7.1). If we limit the fits to the points at small Q^2, the slope at $Q^2 = 0$ (and hence the charge radius) is not sensitive to the precise form of the fitting function. To illustrate this we present in table 6.3 the results obtained by fitting our results for the form factor at the lowest three values of Q^2 to the pole form (6.1) as well as to linear, quadratic and cubic polynomials. In the final row of table 6.3 we present the value of $\langle r_\pi^2 \rangle_{330\,\mathrm{MeV}}$ obtained by applying the same fits to all 9 points up to Q^2_{min}.

set	max Q^2	linear	quadratic	cubic	pole
$Z_2(4)$	$0.013\,\mathrm{GeV}^2$	$0.354(28)(11)$	$-$	$-$	$0.361(29)(12)$
$Z_2(4)$	$0.022\,\mathrm{GeV}^2$	$0.354(26)(11)$	$0.353(35)(11)$	$-$	$0.364(27)(12)$
$Z_2(4)$	$0.035\,\mathrm{GeV}^2$	$0.353(25)(11)$	$0.355(32)(11)$	$0.351(41)(11)$	$0.366(27)(12)$
$Z_2(4)'$	$0.150\,\mathrm{GeV}^2$	$0.332(28)(11)$	$0.387(44)(13)$	$0.406(56)(13)$	$0.382(37)(12)$

Table 6.3: Results for $\langle r_\pi^2 \rangle_{330\,\mathrm{MeV}}$ obtained by fitting to linear, quadratic or cubic functions of Q^2 and by using the pole ansatz (6.1). In the first row we use only the single point at the lowest value of Q^2 ($Q^2 = 0.013\,\mathrm{GeV}^2$), in the second we use the two points at the lowest values of Q^2 ($Q^2 = 0.013\,\mathrm{GeV}^2$ and $Q^2 = 0.022\,\mathrm{GeV}^2$) and in the third row we use the points at the lowest three values of Q^2 ($Q^2 = 0.013\,\mathrm{GeV}^2$, $Q^2 = 0.022\,\mathrm{GeV}^2$ and $Q^2 = 0.035\,\mathrm{GeV}^2$). The final row corresponds to fits to all 9 points with $Q^2 \leq Q^2_{\mathrm{min}}$. The two quoted errors are statistical and that due to the uncertainty in the lattice spacing.

6.3 Results for the K_{l3} form factor

In our analysis of the data generated for the calculation of the K_{l3} form factor we computed covariance matrices for the correlation functions and the ratios $R^\mu_{\alpha,K\pi}(\alpha = 1,3)$, for use in the fits (*frozen* covariance matrix). *Unfreezing* the covariance matrix, i.e. using the covariance matrix computed individually for each jackknife sample destabilized the fits. We interpret this as a reflection of the fact that we have an insufficient set of measurements and that the fluctuations of the covariance matrix are therefore large. We found that the results we get with the frozen covariance matrix agree within (similar) errors with the results we would get when neglecting any correlations.

We found that for the spatial component of the vector current in the three-point function, i.e. for $R^{(i)}_{\alpha,K\pi}$, the plateaus for $\alpha = 1,3$ are of comparable quality (cf. figure 6.3) - in the analysis we opted to use $R^{(i)}_{3,K\pi}$. For the time-component however in the cases where only one of the initial and final states carries a twist the quality of the ratios varies. Here we decided to use $R^{(0)}_{1,K\pi}$ for the case where only the pion carries the twist and $R^{(0)}_{3,K\pi}$ in all other cases (cf. figure 6.3).

Table 6.4 summarises the kinematical points which we analysed. The kaon masses for the full statistics of $Z_2(3)$ and $Z_2(4)$ turn out to be $am_K = 0.2987(4)$ and $am_K = 0.3327(4)$, respectively and the pion mass in both cases is $am_\pi = 0.1903(4)$[2]. From table 6.4 we see that there are degeneracies in q^2, i.e. we have data for the same q^2 but from three-point functions with different kinematical parameters for the kaon and pion. With these degeneracies in q^2 we can then just solve the simultaneous equations (cf. equation (3.31)):

$$
\begin{aligned}
R^{(\mu)}_{\alpha,K\pi}(\vec{p}_K, \vec{0}) &= f^+_{K\pi}(q^2)p_{K,\mu} + f^-_{K\pi}(q^2)p_{K,\mu}, \\
R^{(\mu)}_{\alpha,K\pi}(\vec{0}, \vec{p}_\pi) &= f^+_{K\pi}(q^2)p_{\pi,\mu} - f^-_{K\pi}(q^2)p_{\pi,\mu},
\end{aligned}
\tag{6.3}
$$

for each of the μ components to calculate $f^+_{K\pi}(q^2)$ and $f^-_{K\pi}(q^2)$. We find however that by computing the form factors in this way the errors in the form factors are much larger than the errors in the ratios $R^{(\mu)}_{\alpha,K\pi}$. In our analysis we opt instead to perform a χ^2 minimization to find the values of the form factors that best fit the overdetermined system of equations of all

---

[2]While agreeing within errors, the central values differ slightly from those quoted in [73] because the number of measurements and the measurement techniques differ.
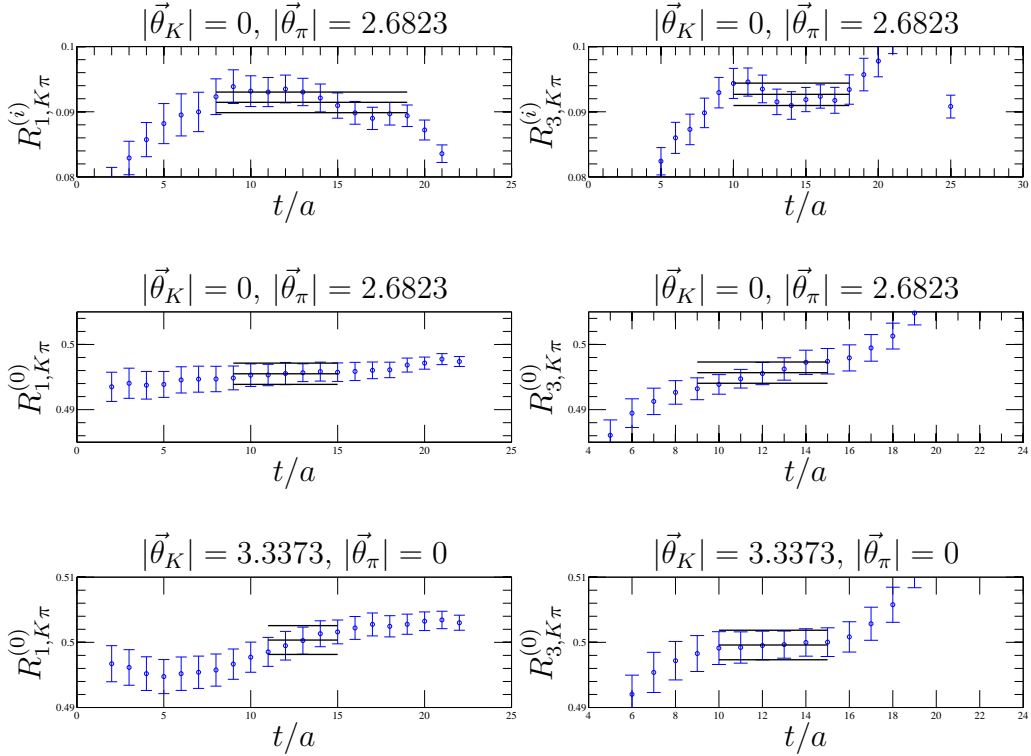
Figure 6.3: Examples for the quality of the ratios $R^{(\mu)}_{\alpha,K\pi}(\alpha = 1, 3)$, once with either the pion/kaon moving and the kaon/pion at rest.

the μ components together. We find that the errors we obtain for the form factors in this way are comparable to the errors in the ratios $R^{(\mu)}_{\alpha,K\pi}$.

The form factor data generated in this work extends the previous data calculated from correlation functions in the data set P4 presented in [2] by a number of new points for $f_0^{K\pi}(q^2)$ in the range $0 \lesssim q^2 \leq q^2_{\max}$ for two valence strange quark masses $am_s = 0.04$ (unitary) and $am_s = 0.03$ (partially quenched). The results are illustrated in the plot in figure 6.4 by the red/blue, right/left-pointing arrows, respectively. The plot also shows the Fourier momentum data points obtained using the point source data set P4 presented in [2] together with a fit to this data using a pole-ansatz,

$$f_0^{K\pi}(q^2)|_{\text{pole}} = \frac{f_+^{K\pi}(0)|_{\text{pole}}}{1 - q^2/M^2} , \tag{6.4}$$

and plots of the results of using the global fit ansatz used in ref. [2], (which we will discuss in section 7.2.1 and is given by equation (7.4)), with the two kaon masses from the $Z_2(4)$ and $Z_2(3)$ data sets.

In the analysis in ref. [2] the results for the form factors at each simulated pion mass are used to determine two estimates for $f_+^{K\pi}(0) = f_0^{K\pi}(0)$,

θ_π	θ_K	q^2/GeV^2	$f_0^{K\pi}(q^2)$	$f_+^{K\pi}(q^2)$	$f_-^{K\pi}(q^2)$
		$am_s = 0.04$			
0	4.6810	0.0002(2)	0.9758(44)	0.9758(44)	-0.0997(93)
2.6823	0	0.0004(3)			
2.1285	0	0.0216(2)	0.9898(34)	0.9975(42)	-0.081(17)
1.6	0	0.0381(2)	1.0030(20)	1.0213(32)	-0.108(11)
0	2.7922	0.0382(2)			
0	0	0.0607(2)	1.0185(15)		
		$am_s = 0.03$			
2.6823	0	-0.0192(3)	0.9677(49)	0.9613(41)	-0.054(14)
0	3.3373	0.0001(5)	0.9867(30)	0.9867(30)	-0.0771(77)
2.1285	0	0.0001(3)			
1.6	0	0.0149(3)	0.9986(21)	1.0066(27)	-0.0852(96)
0	2.5087	0.0150(4)			
0	0	0.0352(4)	1.0124(10)		

Table 6.4: Table of twisting angles used in this study, together with the corresponding values of q^2 and the results for the K_{l3} form factors.

one from an interpolation in q^2 with a pole-ansatz and one from an interpolation of $f_0(q^2)$ with a 2nd order polynomial (cf. table IV in [2]). The systematic error due to the phenomenological interpolation is then estimated by taking the difference between the two results. The new data points for $am_s = 0.04$ nicely agree with both the pole dominance and polynomial fits as can be seen in the following comparison:

results for $am_q = 0.005$, $am_s = 0.04$

$$f_+^{K\pi}(0)|_{\text{pole}} \quad = \quad 0.9774(35) \ [2] \,,$$
$$f_+^{K\pi}(0)|_{\text{polynomial}} \quad = \quad 0.9749(59) \ [2] \,,$$
$$f_+^{K\pi}(0)|_{\text{this work}} \quad = \quad 0.9757(44) \,.$$

In [2] the spread $f_+^{K\pi}(0)|_{\text{pole}} - f_+^{K\pi}(0)|_{\text{polynomial}} \approx 0.0024$ is used as an estimate of the systematic error due to the phenomenological q^2-interpolation. As simulations move closer to the physical pion mass, the value of $q^2_{\text{max}} = (m_K - m_\pi)^2$ increases. Therefore the interpolation to $q^2 = 0$, which crucially depends on the high precision which one is able to achieve for the form factor at q^2_{max}, will become increasingly sensitive to the ansatz one makes. One therefore expects the systematic error due to the interpolation to increase. We emphasise that the approach advocated here entirely
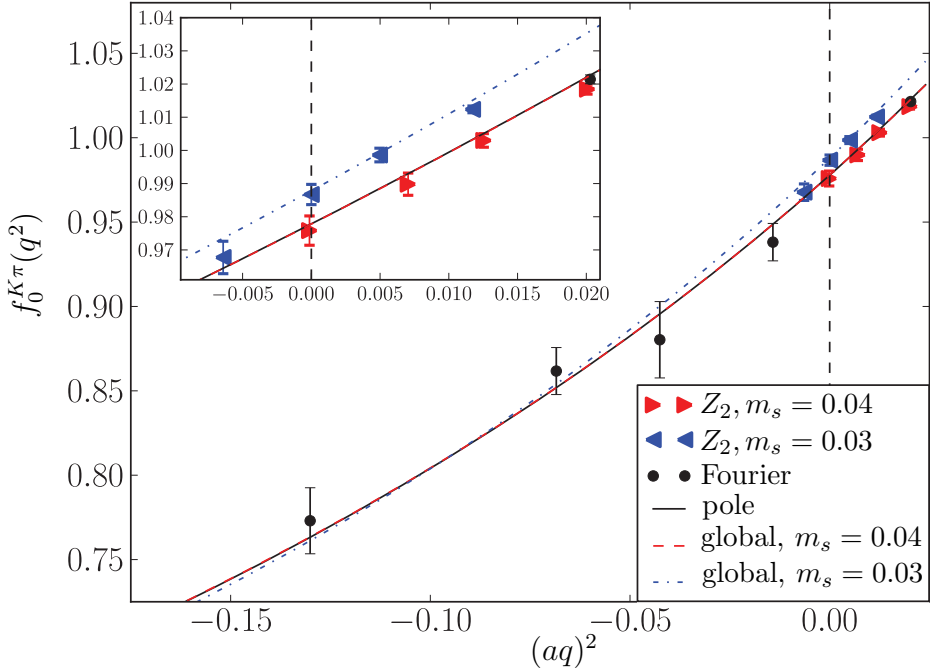
Figure 6.4: Summary of simulation results of $f_0^{K\pi}(q^2)$. The black circles and the (solid line) pole interpolation correspond to the results of [2] while the results represented by the left- and right pointing arrows, correspond to the results of this work for $am_s = 0.04$ and $am_s = 0.03$ respectively. The red and blue dashed curves represent the result from the global fit ansatz of ref. [2] (given by equation (7.4)), once for $m_K^{0.03}$ and $m_K^{0.04}$.

removes this uncertainty.

6.4 Comparison of the cost of using point source and $\mathbb{Z}(2)$-wall source propagators

In this study we have used two different formulations of the source in the computation of the quark propagators. The correlation functions on data sets P3 and P4 have been computed from point source propagators while the correlation functions on data sets $Z_2(4)$, $Z_2(4)'$ and $Z_2(3)$ have been

data set	inversions	Z_V	$f^{\pi\pi}(-Q^2_{\min})$
P3	12888	0.7148(9)	0.809(14)
$Z_2(4)'$	1096	0.7136(8)	0.802(15)

Table 6.5: Comparison of the computational cost of using point and stochastic sources for the calculation of Z_V and $f^{\pi\pi}(-Q^2_{\min})$.

79

	am	n_{props}	n_θ	n_{src}	n_{config}	s-c		N_{tot}	$f_+^{K\pi}(0)$
P4	$2 \times$	2	$\times 1 \times$	4	$\times 175$	$\times 12$	$=$	33600	$0.9774(35)$
$Z_2(4)$	$2 \times$	2	$\times 2 \times$	8	$\times 147$	$\times 1$	$=$	9408	$0.9757(44)$

Table 6.6: Comparison of the computational cost of using point and stochastic sources for the calculation of $f_+^{K\pi}(0)$.

computed using the noise source technique briefly described in section 3.2.3.

In this section we compare the relative computational cost of each approach in order to achieve similar statistical errors for standard observables relevant for the phenomenology of light mesons. We compare the costs for both approaches in the calculations of Z_V, $f^{\pi\pi}(-Q_{\text{min}}^2)$ and $f_+^{K\pi}(0)$. The comparisons are shown in tables 6.5 and 6.6.

Table 6.5 shows the total number of inversions of the Dirac matrix that were required to achieve similar statistical errors with both source types for Z_V and $f^{\pi\pi}(-Q_{\text{min}}^2)$. For point sources 12 spin-colour inversions are necessary per measurement. We used 179 measurements per point source and used 3 point sources. We calculate two propagators per configuration (one normal and one sequential source propagator), thus the total number of inversions using point sources is $179 \times 12 \times 3 \times 2 = 12888$. For the stochastic sources we only require a single spin-colour inversion per measurement. We used 137 measurements per source and used 4 sources, thus we require $137 \times 4 \times 2 = 1096$ inversions using stochastic sources in order to achieve similar statistical errors to those using point sources. This indicates that the same statistical error for Z_V and $f^{\pi\pi}(-Q_{\text{min}}^2)$ can be achieved with only about 1/12th of the computational cost when using the stochastic source technique.

We have also tried to study the error for point-source and stochastic source correlators at fixed cost, i.e. for a given number of inversions. The cost of the 1176 measurements which we carried out with the stochastic sources (data set $Z_2(4)$) corresponds to $1176/12 = 98$ point source measurements. While we could carry out reliable fits to the correlators on data set $Z_2(4)$ this was not the case for the subset of 98 measurements of data set P3 and no quantitative comparison seems possible. This observation shows however that the statistical properties of the correlation functions determined with stochastic source propagators are better at the same computational cost.

80

In table 6.6 we compare the cost of the simulations for the two approaches to the computation of $f_+^{K\pi}(0)$. For data set P4, for each quark mass $am = am_q$, am_s one normal and one sequential source propagator, one twist (periodic boundary conditions), four positions of the point source on 175 configurations and 12 spin-colour inversions were necessary. Since with point sources a Fourier transformation between the source and the point of the current insertion can be performed almost for free, one can directly interpolate to $q^2 = 0$ at no additional cost. This is not the case when using the stochastic source technique as for $Z_2(4)$ and $Z_2(3)$ since we need an inversion of the Dirac matrix for each twist angle we use. However, since we only need a single spin-colour inversion for each choice of twist angle, as we can see from table 6.6 we can achieve a similar precision for $f_+^{K\pi}(0)$ using stochastic sources, with only 28% of the computational cost when using point sources. We also note that in general the quality of plateaus is significantly enhanced when using the stochastic volume source technique.

Chapter 7

Chiral extrapolations to physical light quark masses

7.1 Results of extrapolations for the pion form factor

ChPT describes the behaviour of the pion form factor as a function of both the momentum transfer and the quark masses, providing that these are sufficiently small. In ref. [73], the RBC/UKQCD collaboration use SU(2) and SU(3) ChPT formulae in fits to lattice data for the pion masses and decay constants at a range of quark masses. From these fits they determine a number of LEC's of ChPT, of which f and f_0 the decay constants in the SU(2) and SU(3) chiral limits respectively, are of relevance to this work. They find that although both SU(2) and SU(3) ChPT fit the data, in the SU(3) case the NLO corrections were very large casting doubt on the convergence of the chiral expansion. For this reason, in ref. [73] the main results were obtained using SU(2) ChPT and the result for the decay constant in the chiral limit, $af = 0.0665(47)$, includes both the statistical and systematic errors. The corresponding result for the decay constant in the SU(3) limit, $af_0 = 0.0541(40)$, on the other hand, includes only the statistical error.

Since we only have data for the form factor at one pion mass we will use these values for af and af_0 as input into the ChPT formulae of equations (4.40) and (4.39) respectively and fit our data at fixed quark masses (i.e. for the pion with mass $330\,\text{MeV}$) as a function of q^2 to determine the LECs l_6^r and L_9^r. Having obtained the LECs in this way, we then use the ChPT

$Q^2_{\mathrm{max}}\,[\mathrm{GeV}^2]$	0.013	0.022	0.035
$100\,l_6^r(m_\rho)$	$-0.932(79)(03)(63)(40)$	$-0.933(73)(03)(63)(40)$	$-0.932(71)(03)(63)(40)$
$\langle r_\pi^2\rangle_{330\,\mathrm{MeV}}$	$0.354(28)(12)(00)(14)$	$0.354(26)(12)(00)(14)$	$0.354(25)(12)(00)(14)$
$\langle r_\pi^2\rangle_\chi$	$0.418(28)(12)(04)(14)$	$0.419(26)(12)(04)(14)$	$0.418(25)(12)(04)(14)$
$100\,L_9^r(m_\rho)$	$0.307(26)(03)(49)(13)$	$0.308(24)(03)(49)(13)$	$0.308(23)(03)(49)(13)$
$\langle r_\pi^2\rangle_{330\,\mathrm{MeV}}$	$0.354(28)(12)(00)(14)$	$0.355(26)(12)(00)(14)$	$0.355(25)(12)(00)(14)$
$\langle r_\pi^2\rangle_\chi$	$0.460(28)(12)(16)(14)$	$0.460(26)(12)(16)(14)$	$0.460(25)(12)(16)(14)$

Table 7.1: Results from the SU(2) (top three rows) and SU(3) (bottom three rows) ChPT fits. The charge radii are quoted in fm^2. The first error is statistical, the second is from the uncertainty in the lattice spacing, the third is due to the uncertainty in af for SU(2) fits and af_0 for SU(3) fits (only statistical uncertainty is known for af_0) and the final error is due to the uncertainty from the continuum extrapolation. The three columns correspond to using the data at the lowest, the lowest two and the lowest three non-zero values of Q^2 respectively, while Q^2_{max} denotes the largest value of Q^2 used in the determination.

formulae to determine the form factor (and hence the charge radius) of a physical pion ($m_\pi = 139.57\,\mathrm{MeV}$ [91]).

The results of the SU(2) and SU(3) chiral extrapolations are summarized in table 7.1. The first column corresponds to the result of fitting only to the data point at our lowest value of Q^2 ($Q^2 = 0.013\,\mathrm{GeV}^2$) to determine the single LEC ($l_6^r(m_\rho)$ or $L_9^r(m_\rho)$) and the charge radius. In the second column we use the data points at the lowest two values of Q^2 ($Q^2 = 0.013\,\mathrm{GeV}^2$ and $0.022\,\mathrm{GeV}^2$) and in the final column we fit the data for the lowest three values of Q^2. The results in the three columns do not show any dependence on the chosen fit range at these small values of Q^2.

Based on the experience of ref. [73] and because we only know the statistical error for af_0, we take for our best estimate the result from the fit to the $\mathrm{SU(2)_L \times SU(2)_R}$ expression at NLO including the three data points at $Q^2 = 0.013$, 0.022 and $0.035\,\mathrm{GeV}^2$,

$$l_6^r(m_\rho) = -0.0093(10), \qquad \langle r_\pi^2\rangle_{330\,\mathrm{MeV}} = 0.354(31), \qquad \langle r_\pi^2\rangle_\chi = 0.418(31)\,. \tag{7.1}$$

Comparison of our values for $l_6^r(m_\rho)$ and $L_9^r(m_\rho)$ in table 7.1 with the SU(2)–SU(3) conversion formula in equation (4.43) reveals deviations up to around 50%. By this we mean that the LECs obtained directly from the fits differ from the values extracted using the conversion formula with the other LEC as input. Large SU(3) NLO corrections were seen in the analysis in [73], and indeed the discrepancy can be reduced very significantly by

84

collaboration		technique		$\langle r_\pi^2 \rangle_\chi [\text{fm}^2]$
PDG	[22]			0.452(11)
QCDSF/UKQCD	[1]	$N_f = 2$	Clover	0.441(19)
JLQCD	[92]	$N_f = 2$	Clover	0.396(10)
JLQCD	[93]	$N_f = 2$	Overlap	0.409(44)
RBC/UKQCD	this work	$N_f = 2 + 1$	Domain Wall	0.418(31)
ETMC	[31]	$N_f = 2$	Wilson	0.456(38)

Table 7.2: Comparison of our result for the charge radius of a physical pion to the experimental value and computations by other collaborations (excluding quenched lattice results).

using equations (4.41) and (4.42) without setting $f = f_0$.

In table 7.2 and figure 7.1 we compare our result for the charge radius to the one determined from experiment and to other recent computations. Note that the previous lattice results were obtained with 2 flavours of sea quarks ($N_f = 2$) and using periodic boundary conditions so that the values of Q^2 are much larger than in this work. The value obtained by the ETMC collaboration published in [31] after this work was published also uses twisted boundary conditions (with $N_f = 2$). The minimum value of Q^2 for which they calculate the form factor is however $Q^2 \approx 0.05 \text{ GeV}^2$. We emphasize that in our study we have calculated the form factor at three values of Q^2 lower than this, and our calculation of the charge radius is based on the NLO SU(2) ChPT fit to these three small values of Q^2 for which we are confident in the convergence of the SU(2) ChPT formula.
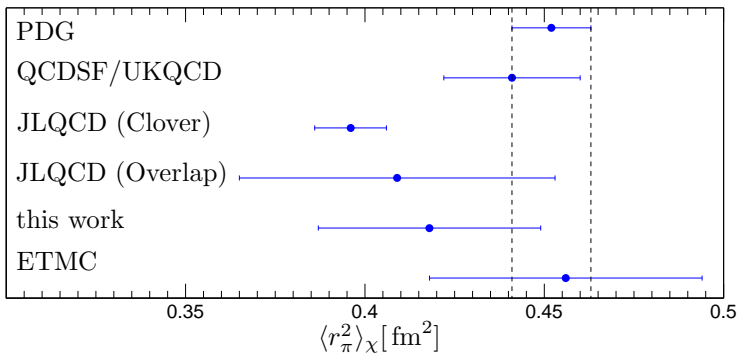

Figure 7.1: Comparison of our result for the charge radius of a physical pion to the experimental value and computations by other collaborations (excluding quenched lattice results).

In figure 7.2 we plot our lattice data for the 330 MeV pion and the form
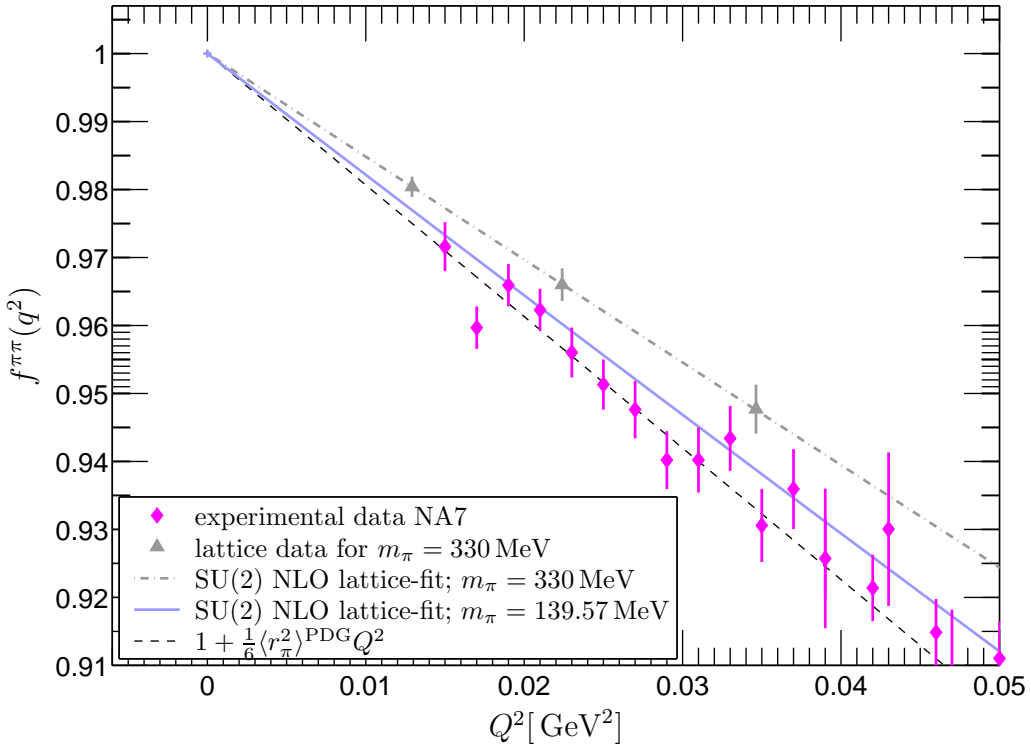
Figure 7.2: Comparison of experimental results (magenta diamonds) for the form factor $f^{\pi\pi}(q^2)$, lattice results at $m_\pi = 330\,\mathrm{MeV}$ (grey triangles and dash-dotted grey line) and the extrapolation of the lattice results to the physical point (blue solid line) using NLO SU(2) chiral perturbation theory. In addition we also represent the PDG world average for the charge radius using the black dashed line.

factor of a physical pion obtained from this data using SU(2) ChPT. The experimental data from ref. [94] is also plotted together with the ChPT formula with the PDG world average for the charge radius (see also table 7.2).

7.1.1 Discussion of systematic errors

Our simulation was performed at a single value of the lattice spacing and we cannot therefore extrapolate our results to the continuum limit. However, our action has $O(a^2)$ discretization errors and we follow [73] by assigning a systematic uncertainty of 4% to measured quantities, representing an estimate of $(a\Lambda_{\mathrm{QCD}})^2$ for our lattice spacing. Thus we assign a 4% error from this source to our values for $1 - f^{\pi\pi}(q^2)$. This relative error is propagated to our results for the LECs and $\langle r_\pi^2 \rangle$, where it appears as the last error quoted in table 7.1.

The ChPT formulae used here are obtained in infinite volume. Jiang and Tiburzi have used partially quenched, partially twisted SU(2) chiral perturbation theory to evaluate the finite-volume effects in the case where only one of the valence quarks is twisted [95]. This is the case for our three points at the lowest values of Q^2 ($Q^2 = 0.013\,\text{GeV}^2$, $Q^2 = 0.022\,\text{GeV}^2$, and $Q^2 = 0.035\,\text{GeV}^2$), which are the points which we use to determine the charge radius and the LECs l_6^r and L_9^r. From figures 7 and 8 of [95] we see that for the pion mass ($m_\pi = 330\,\text{MeV}$) and volume, $(2.74\,\text{fm})^3$, used in our simulation, the finite volume effects in $\langle r_\pi^2 \rangle$ and in $1 - f^{\pi\pi}(q^2)$ are less than 1%. Since the remaining errors quoted for these quantities for a pion with $m_\pi = 330\,\text{MeV}$ are 7–8%, we feel confident in neglecting the finite volume effects in our analysis.

We end this section with a discussion of another source of uncertainty which the use of chiral perturbation theory can help to estimate. The mass of the (sea) strange quark (m_s) in the simulation is different from the physical one ($am_s = 0.04$ in the simulation compared to the physical value $0.0343(16)$ found in ref. [73]). In SU(3) ChPT we use the mass of the kaon as found from our simulation and hence obtain the value of the LEC L_9^r without the need for further corrections. The LEC l_6^r of SU(2) ChPT on the other hand depends on the mass of the strange quark and, since this is our preferred approach, we need to understand the amount by which l_6^r could be shifted due to the different value of m_s. Using equation (4.43) and the value of the mass from [73] to estimate $\bar{m}_K$, we find that the shift in $l_6^r(m_\rho)$ is about 0.9% and is hence negligible compared even to the 9% statistical error (11% total error) that we find for $l_6^r(m_\rho)$ (this is also the case if we use equations (4.41) and (4.42) without setting $f = f_0$, when the relative error grows to 1.3%). We therefore neglect this uncertainty.

We note however that since carrying out the analyses presented in this work the RBC-UKQCD collaboration has adopted the reweighting technique of correcting for the difference in the simulated sea strange quark mass to the physical one [96]. The reweighting technique [97,98] allows us to make small post-simulation changes to the sea quark masses. It involves measuring an observable on a gauge configuration ensemble generated with sea strange quark mass $m_s^{(\text{sim})}$ with a reweighting factor w multiplied, and then relating it to the observable at the target sea strange quark mass m_s via

$$\langle \mathcal{O} \rangle_{m_s} = \frac{\langle \mathcal{O}w \rangle_{m_s^{(sim)}}}{\langle w \rangle_{m_s^{(sim)}}}. \tag{7.2}$$

The reweighting factor $w(U)$ for each configuration U is just the ratio of the determinants of the Dirac matrices $D(U, m_s)$ and $D(U, m_s^{(sim)})$ with the two strange quark masses. This factor is then stochastically evaluated on each configuration using a complex random Gaussian vector.

7.2 Results of extrapolations for the K_{l3} form factor

7.2.1 Extrapolation models

We do not really know how light the quarks must be for the chiral expansion at a fixed order to represent the mass dependence of physical quantities to a given level of precision. In principle, lattice computations at very light quark masses, could answer this question. Our present calculations however, involve masses in a regime where NNLO terms of the SU(3) expansion are non-negligible as was suggested by the studies in [73], and yet we have insufficient data to determine these terms and all the corresponding LECs. We therefore follow the approach in [2] and model higher order contributions using the ansatz

$$f_+^{K\pi}(0) = 1 + f_2(f_0, m_\pi^2, m_K^2) + (m_K^2 - m_\pi^2)^2(A_0 + A_1(m_K^2 + m_\pi^2)), \quad (7.3)$$

where we use the $N_f = 2 + 1$ expression for f_2, partially quenched in the strange quark, as determined in [80] and given in the appendix. The form of this ansatz is motivated by the fact that we know from the Ademollo-Gatto theorem [27] that to leading order $\Delta f \propto (m_s - m_{u,d})^2$, thus we expect equation (7.3), which incorporates the correct $SU(3)_\text{flavour}$ limit, to be a good phenomenological ansatz for the mass dependence of $f_+^{K\pi}(0)$.

In order to gain maximum information from limited data, we incorporate equation (7.3) into a global fit ansatz based on pole dominance (equation (6.4) with a quark mass dependent term included) to simultaneously fit for the q^2 and quark mass dependencies. Our global fit ansatz is [2]

$$f_0^{K\pi}(q^2) = \frac{1 + f_2 + (m_K^2 - m_\pi^2)^2\,(A_0 + A_1(m_K^2 + m_\pi^2))}{1 - q^2/\left(M_0 + M_1(m_K^2 + m_\pi^2)\right)^2}. \quad (7.4)$$

Since the kaon mass appears explicitly, after fitting (7.4) to our lattice data, any values for m_π and m_K can be inserted into equation (7.4) to obtain a

value for $f_0^{K\pi}(q^2)$. Hence, by inserting the physical values for m_π and m_K, we automatically correct for the difference in the sea strange quark mass from its physical value.

In view of the slow convergence of SU(3) chiral perturbation theory observed for some quantities (cf. e.g. [73]) it seems useful to compare the present extrapolation strategy to one incorporating the SU(2) ChPT formula of equation (4.73) derived in [75]. Similarly to the case of SU(3) chiral perturbation theory we use the ansatz,

$$f_0^{K\pi}(q^2) = \frac{F_+(1 - \frac{3}{4}L + c_2 m_\pi^2 + c_4 m_\pi^4)}{1 - q^2/\left(\tilde{M}_0 + \tilde{M}_1 m_\pi^2\right)^2}, \tag{7.5}$$

where the chiral logarithm L is as defined in equation (4.72) and in comparison to the original work we have added an additional term proportional to m_π^4. Note that the parameters in this fit ansatz depend on the value of the strange quark mass.

7.2.2 Results

Combining the data sets P4, $Z_2(3)$ and $Z_2(4)$ and carrying out the global fit (7.4) we find that the data is well described with

$$\begin{aligned} A_0 &= -0.34(9)\text{GeV}^{-4}, & A_1 &= 0.28(12)\text{GeV}^{-6}, \\ M_0 &= 0.94(10)\text{GeV}, & M_1 &= 0.54(18)\text{GeV}^{-1}. \end{aligned} \tag{7.6}$$

Inserting the unitary and partially quenched kaon mass which we simulated here together with these parameters into the phenomenological ansatz (7.4) we can predict the form factor that is to be expected for $am_s = 0.03$ and $am_s = 0.04$ with $am_q = 0.005$ as illustrated in terms of the blue (dot-dashed) and red (dashed) curve in figure 6.4. Both curves are nicely compatible with the new blue and red data points, thus confirming that the ansatz parameterizes the dependence of the form factor on a partially quenched strange quark well.

We can now update the value of $f_+^{K\pi}(0)$ that was calculated in ref. [2] (which uses the physical pion decay constant $f_\pi = 131$ MeV as an approximation for f_0) by inserting the physical pion and kaon masses into (7.4). We find $f_+^{K\pi}(0) = 0.9644(33) \to f_+^{K\pi}(0) = 0.9630(34)$ (statistical errors only) at the physical point.

In figure 7.3 we plot the result of the global fit ansatz (solid black line)
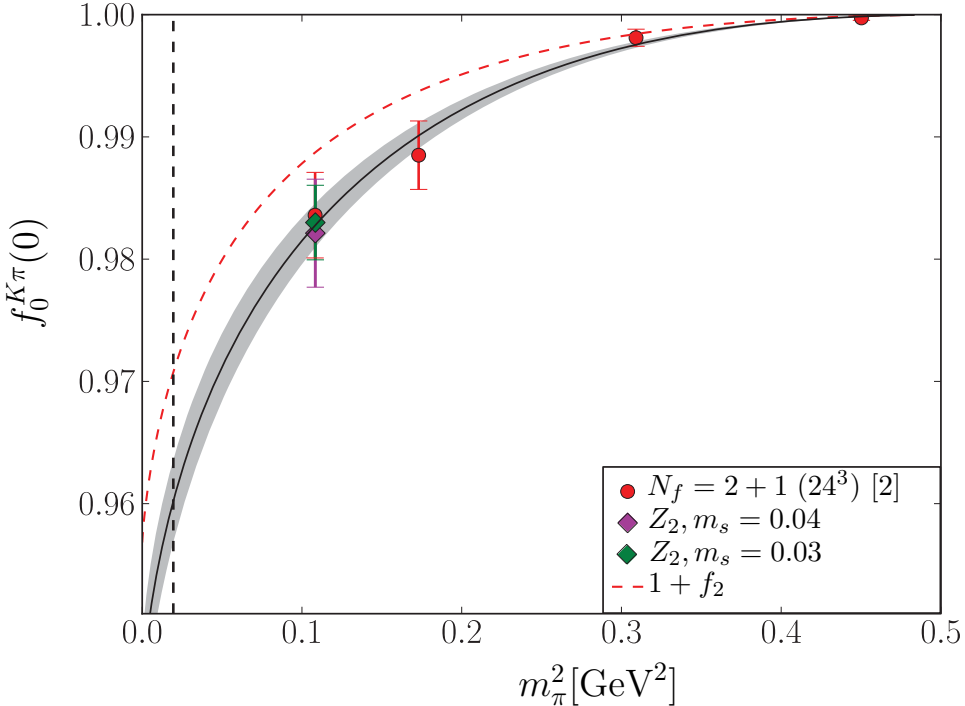
Figure 7.3: Result of global fit based on SU(3) chiral perturbation theory using $f_2(115\text{MeV}, m_K, m_\pi)$. The vertical dashed line is the physical pion mass.

at $q^2 = 0$ as a function of m_π^2 with m_K fixed at its physical value[1]. We also overlay in figure 7.3 the results for $f_+^{K\pi}(0)$ calculated here on the data sets $Z_2(4)$ and $Z_2(3)$ using twisted boundary conditions as well as the results presented in table IV of ref. [2] obtained with pole dominance interpolations to $q^2 = 0$ of Fourier momentum data points on ensembles with $N_f = 2 + 1$ dynamical flavours and sea light quark masses $am_{u,d} = 0.03, 0.02, 0.01$ and 0.005 and the same sea strange quark mass and lattice volume used here[2].

The chiral extrapolation of the lattice data is well constrained by the natural *hinge-point* $f_+^{K\pi}(0)|_{m_K=m_\pi} = 1$. As can be seen in figure 7.3, the data as well as the global SU(3) fit ansatz (7.4) nicely approach this point for $m_\pi \to m_K$. In contrast, in SU(2) chiral perturbation theory one expands the form factor around vanishing pion mass at a fixed strange quark mass [75] (in fact, all strange quark mass dependence resides in the low energy constants). The limit $f_+^{K\pi}(0)|_{m_s=m_q} = 1$ is not naturally implemented

---

[1]Note that in here we use $f_0 = 115$ MeV for the reasons that will be explained in section 7.2.3.

[2]Note however that all the points in this figure have been shifted to the physical sea strange quark mass. Since this is lighter than the simulated sea strange quark, the SU(3) breaking effects are smaller and hence the value of the form factor moves up.

in this expansion. Studies of SU(2) fits to other pion and kaon observables in [73] suggest that such an expansion describes the lattice data reliably only below $m_\pi \approx 400$MeV. Here we only have data for two values of the pion mass below this cut-off and extrapolations are therefore not well constrained. Alternatively one can include data at heavier pion masses. However we find that we cannot obtain reliable fits with these heavier pion masses. Given these considerations, we refrain from presenting fit results based on SU(2) chiral perturbation theory.

7.2.3   Discussion of systematic errors

A potential source of systematic error which to our knowledge has not been taken into account systematically in any previous computation of $f_+^{K\pi}(0)$ is the choice of the decay constant entering in the SU(3) NLO prediction for the form factor as we now explain.

We observe that the interchange symmetry $f_+^{K\pi}(q^2) = f_+^{\pi K}(q^2)$ is held in the SU(3) expansion order by order and also in non-perturbative data to all orders. The SU(3) chiral expansion in terms of the unknown, but in principle unambiguous, LEC f_0 has this symmetry manifest in each term. However, we have the freedom to repartition terms of this expansion between different orders: for example to use an alternative expansion parameter f_0' differing from f_0 beyond leading order

$$f_+^{K\pi}(0) = 1 + f_2(f_0', m_K^2, m_\pi^2) + \dots . \tag{7.7}$$

In fact, the NLO term f_2 is usually quoted as $f_2(f_\pi, m_K^2, m_\pi^2) \simeq -0.023$, with the physical pion decay constant used in place of the unknown LEC f_0. For SU(3) chiral perturbation theory to correspond to QCD when all terms in the chiral expansion are summed, using f_π instead of f_0 must leave the total sum of all terms to all orders in the chiral expansion unchanged. Thus the replacement $f_0 \to f_\pi$ implies that the terms at different orders in the chiral expansion must change in such a way that there is an overall cancellation when we sum the terms to all orders in the chiral expansion.

The replacement $f_0 \to f_\pi$ results in an NNLO correction term

$$\delta_{\mathrm{NNLO}} = f_2(f_0, m_K^2, m_\pi^2) - f_2(f_\pi(f_0, m_{ud}, m_s), m_K^2, m_\pi^2), \tag{7.8}$$

which breaks the symmetry under $\pi \leftrightarrow K$ interchange. The form of the

NNLO terms must therefore change to compensate for this and restore this symmetry.

Using $f_2(f_\pi = 131\mathrm{MeV}, m_K^2, m_\pi^2)$ but *failing* to adjust the forms appearing at NNLO is inconsistent with QCD in the chiral limit as it actively changes the series.

We could alternatively estimate the systematic error in using f_π as an estimate for f_0 by allowing for f_π to vary over a range of values. This allows for the NNLO form to remain unchanged and the interchange symmetry of our global fit ansatz to remain manifest.

This discussion impacts the analysis in [2] in which $f_\pi = 131$ MeV is used and no variation in f_π is allowed, nor is the form of the global fit ansatz at NNLO modified to admit breaking of the mass interchange symmetry.

Lacking a precise value of the decay constant in the SU(3) chiral limit we opt to estimate this systematic error by repeating the global fit for the three choices $f_0 = 100, 115, 131\,\mathrm{MeV}$ which in our opinion cover a conservative range and take for our central value the value obtained using $f_0 = 115$ MeV. For these choices we found for the central values of the form factor $f_+^{K\pi}(0) = 0.9556, 0.9599, 0.9630$, respectively. In each case the fit was of very good quality. This is quite a sizeable variation in the central value which is illustrated in figure 7.4.

We found that the choice of decay constant particularly changes the slope of $f_+^{K\pi}(0)$ with respect to m_π^2 in the region of small pion masses where we do not have data. In order to study the behaviour at NNLO more systematically, one can use the FORTRAN computer code written by Bijnens[3] that can provide SU(3) NNLO terms in terms of numerical integration routines (see also [99] for form factor fits based on this code). Our experience from using the code is that for our limited set of lattice data points there are too many free parameters (low energy constants from the $O(p^4)$ and the $O(p^6)$ chiral Lagrangian) to be able to carry out reliable fits. Lacking a better analytical understanding of NNLO effects we prefer as the central value the one corresponding to $f_0 = 115\,\mathrm{MeV}$. As an estimate for the uncertainty in the chiral extrapolation we use the interval defined by the result for $f_+^{K\pi}(0)$ as obtained when using $f_0 = 100\mathrm{MeV}$ and $f_0 = 131\,\mathrm{MeV}$, respectively. In this way we obtain $f_+^{K\pi}(0) = 0.9599(34)(^{+31}_{-43})(14)$.

The new data presented here confirms the ansatz for the q^2-interpolation

---

[3] the programs for $f_+(q^2)$ and $f_-(q^2)$ used in Ref. [74] are available on request from Johan Bijnens
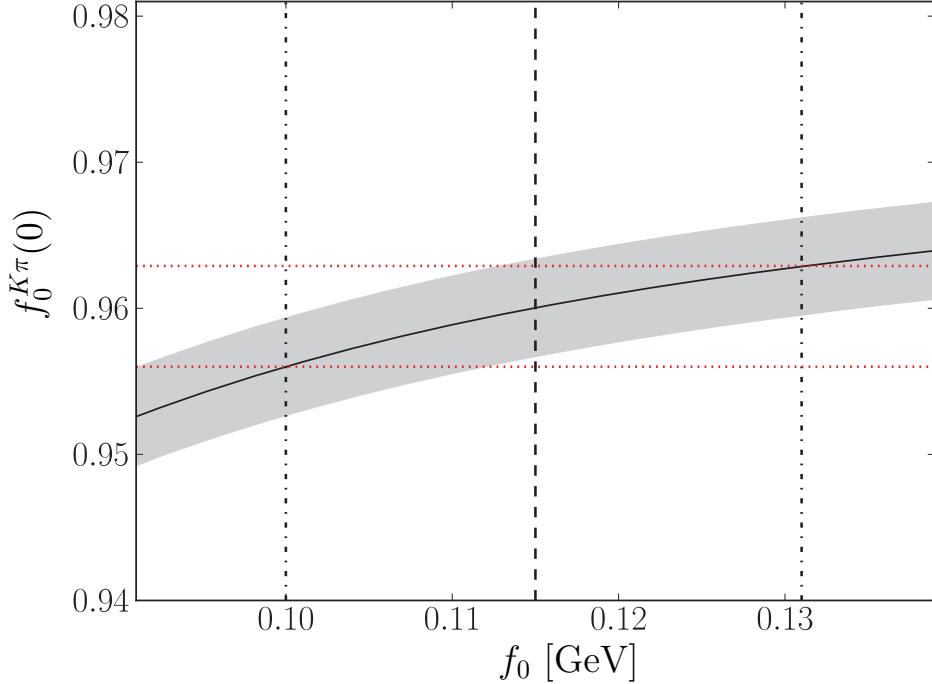
Figure 7.4: Illustration of the dependence of the fit result (with the ansatz in equation (7.4)) on the choice of the decay constant. The horizontal red lines indicate our estimate of the resulting systematic uncertainty.

for the smallest mass used in ref. [2], i.e. $am_q = 0.005$. Since $q^2_{\max}$ increases as m_q decreases, it is at this mass that $q^2_{\max}$ is the largest (and therefore furthest away from $q^2 = 0$) and hence the interpolation is the least constrained. This gives us confidence that the pole ansatz also describes well the form factor data at the other simulated points presented in [2] (where $q^2_{\max}$ is closer to the origin). Further supporting evidence is provided by the result which one obtains when using a polynomial ansatz for the q^2 dependence rather than the pole ansatz (see eqn. (13) in [2]): In this case we obtain a result for the form factor which is by 0.002 smaller and we add this negative shift quadratically into the systematic error. With $\chi^2/\mathrm{d.o.f} = 0.8$ in both cases the fits are of good quality.

Our result is therefore,

$$f_+^{K\pi}(0) \quad = \quad 0.9599(34)\left(^{+31}_{-47}\right)(14)\,, \tag{7.9}$$

where the first error is statistical, the second is due to the chiral extrapola-

tion and the third error is an estimate of the uncertainty due to the finite lattice spacing for which we use the same error estimate used in [2]. We note that the quoted uncertainty due to the chiral extrapolation covers the central value of the result which one obtains when extrapolating instead with $f_2(f_\pi(m_{ud}, m_s), m_K^2, m_\pi^2)$ in (15), i.e. with the decay constant as input that corresponds to each of our simulations points (c.f. [73]). Adding all errors in quadrature we obtain

$$f_+^{K\pi}(0) \;=\; 0.960(^{+5}_{-6}) . \tag{7.10}$$

We believe that the systematic error due to the chiral extrapolation discussed above is conservative but still a more rigid statement would be desirable. To this end a better understanding of the NNLO terms in the chiral expansion and additional simulation points at smaller pion masses are mandatory.

7.2.4 Determining $|V_{us}|$ and testing CKM unitarity

In ref. [3] the most recent value of $|V_{us} f_+^{K\pi}(0)|$ is calculated from the average of the measured decay rates of the possible $K \to \pi l \nu_l$ decay modes. The value quoted is $|V_{us} f_+^{K\pi}(0)| = 0.2163(5)$. Using this value together with our result for $f_+^{K\pi}(0)$ we get

$$|V_{us}| = 0.2253(^{+13}_{-15}). \tag{7.11}$$

Using the current PDG value for $|V_{ud}|$ ($|V_{ud}| = 0.97425(22)$ [23]) we find the deviation from one in the unitarity relation (1.33) to be

$$\delta_{CKM} = 1 - |V_{us}|^2 - |V_{ud}|^2 = 0.0001(^{+7}_{-8}). \tag{7.12}$$

We see therefore that the current results are perfectly consistent with unitarity of the CKM matrix. This is further illustrated in the plot of figure 7.5[4]. In this plot the authors show the results of global fits to $|V_{ud}|, |V_{us}|$ and $|V_{us}/V_{ud}|$ using our result for $f_+^{K\pi}(0)$ (with a symmetrized error) together with the most recent experimental measurements of $|V_{us} f_+^{K\pi}(0)|, |V_{ud}|$ and $|V_{us}|/|V_{ud}| \times f_K/f_\pi$ and the most recent lattice results for f_K/f_π. Two global fit results are shown, one that also assumes the unitarity constraint and

---

[4]Many thanks to M. Antonelli et al. for granting permission to use the plot shown in figure 7.5. This plot was originally published in [3].
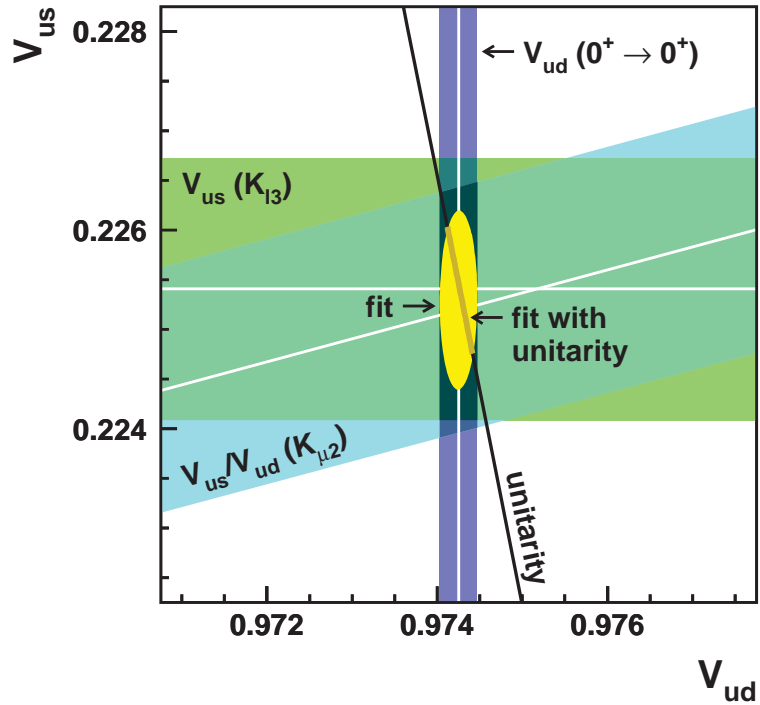
Figure 7.5: Results of global fits to $|V_{ud}|, |V_{us}|$ and $|V_{us}/V_{ud}|$ from ref. [3].

one that doesn't. The unitarity relation (1.33) is also plotted in this figure for comparison. We see also from this figure that the latest results are compatible with unitarity of the CKM matrix.

Chapter 8

Conclusions and Outlook

In this thesis I have presented work done as part of the RBC-UKQCD collaboration, in which we have successfully used partially twisted boundary conditions in lattice QCD simulations, with $N_f = 2+1$ dynamical flavours of quarks, to calculate the electromagnetic (e.m.) form factor of a pion with $m_\pi = 330$ MeV at low values of $Q^2 = -q^2$ and the kaon semi-leptonic decay (K_{l3}) form factors directly at the phenomenologically relevant kinematical point of $q^2 = 0$. The use of partially twisted boundary conditions has allowed us to calculate the pion e.m. form factor at values of Q^2 below those accessible with periodic boundary conditions. Furthermore, using partially twisted boundary conditions makes our computation of $f_+^{K\pi}(0)$, at $m_\pi = 330$ MeV, completely independent of any phenomenological ansatz for the interpolation in the momentum transfer. In this way one significant source of systematic error has been removed in the computation of the K_{l3} form factor.

In our calculation we have used quark propagators computed using single time-slice $\mathbb{Z}(2) \otimes \mathbb{Z}(2)$ stochastic sources. We find that when using these sources we can calculate $f^{\pi\pi}(-Q_{\min}^2)$ and $f_+^{K\pi}(0)$ at 8.5% and 28% respectively, of the computational cost of computing these quantities using the traditional point sources.

We fit our results for the pion form factor at the lowest three values of Q^2 to the NLO SU(3) and SU(2) ChPT formulae, of equations (4.39) and (4.40) respectively, to determine the low energy constants l_6^r and L_9^r. Based on the studies in ref. [73] in which SU(3) NLO corrections are found to be large, we choose to use only the SU(2) ChPT formula to extrapolate our results to calculate the physical form factor and charge radius of the pion (see equation (7.1)). The results which we obtain are in good agreement

with the experimentally determined pion form factor which gives us further confidence in the use of SU(2) chiral perturbation theory in the mass range below 330 MeV (indeed the value of f which we use in the chiral extrapolation was obtained with pion masses up to 420 MeV in ref. [73]).

Although the mass and momentum transfers are sufficiently small to expect that NLO SU(2) ChPT is a good approximation, it would be nice to be able to check this explicitly. It is not clear whether in practice a full NNLO calculation can be performed with sufficient precision (i.e. whether the NNLO LECs will be determined sufficiently accurately) but, as it becomes possible to reach lighter quark masses, in the future we will be able to check the stability of the results. The finite-volume corrections for our mass and volume are small [95] and with our precision can be neglected.

The K_{l3} form factor data generated in this work for both unitary and partially quenched strange quark masses extends the previous data presented in ref. [2] by a number of new points for $f_0^{K\pi}(q^2)$ in the range $0 \lesssim q^2 \leq q_{\max}^2$. The use of these new data points reinforces our confidence in the use of the global fit ansatz of equation (7.4) for a simultaneous fit to both the q^2 and quark mass dependencies of the form factor. Using the global fit ansatz with this new data we update the result presented in [2] where f_π is used as an approximation to f_0 the decay constant in the chiral limit.

We reconsidered the estimates of the systematic uncertainties of the calculation presented in [2]. Currently, chiral extrapolations of lattice results for the kaon semi-leptonic form factor are based on NLO chiral perturbation theory. We show that ambiguities in the parameterisation of the NLO expression can lead to additional systematic effects which we include into our revised estimate of the systematic uncertainties. This ambiguity also applies to any other lattice computation of $f_+^{K\pi}(0)$. We want to stress that the interpretation of lattice data for the $K \to \pi$ form factors would profit from the availability of their expressions at NNLO in chiral perturbation theory in a more transparent form.

One limitation of the current calculation of both the pion and K_{l3} form factors is that it was performed at a single value of the lattice spacing, albeit with an action for which the discretization errors are of $O(a^2)$ and with good chiral and flavour properties.

The RBC-UKQCD collaboration is currently finalizing a set of measurements of correlation functions for both K_{l3} and pion form factor calcula-

tions with partially twisted boundary conditions on a gauge configuration ensemble with the same gauge and fermion actions as used in this work but at a finer lattice spacing and larger volume of $32^3 \times 64 \times 16$. The pion mass measured on this ensemble is lighter than the one in this work ($m_\pi \sim 290$ MeV). A combined analysis of all data is the next step in RBC-UKQCD's program of a precise computation of the $K \to \pi$ and pion form factors in $N_f = 2 + 1$ flavour lattice QCD.

The dominant systematic error in the calculation of the K_{l3} form factor is the chiral extrapolation error. For this reason it would be desirable to perform this calculation at even lighter pion masses. The RBC-UKQCD collaboration is currently generating gauge configuration ensembles with pion masses as low as $m_\pi \sim 180$ MeV. To get down to such low pion masses coarser lattices are being used to allow for a small pion mass while keeping a large volume. This results in a greater residual chiral symmetry breaking by the DWF action which is compensated for by using a new modified Iwasaki gauge action [100]. A calculation of the K_{l3} form factor on these new ensembles would be the natural next step.

We conclude with our determination of $|V_{us}|$. Using our result for $f_+^{K\pi}(0)$ together with the latest experimental result for $|V_{us}f_+^{K\pi}(0)|$ we find $|V_{us}| = 0.2253(^{+13}_{-15})$. Together with the latest determination of $|V_{ud}|$ we find that to within errors the latest results show no deviation from unitarity in the first row of the CKM matrix.

Appendix

This appendix presents the PQChPT expression for f_2, the NLO correction to $f_+^{K\pi}(0)$, for $N_f = 2 + 1$ dynamical flavours of quarks with sea quark masses of $m_s^{(S)}, m_d^{(S)}$ and valence quark masses of $m_s^{(V)}, m_d^{(V)}$ as calculated by Becirevic et al. in [80]. The meson masses in this partially quenched theory at leading order are given by

$$m_\pi^2 = 2Bm_d^{(V)}, \qquad m_K^2 = B\left(m_s^{(V)} + m_d^{(V)}\right)$$
$$m_{dd}^2 = 2Bm_d^{(S)}, \qquad m_{ss}^2 = 2Bm_s^{(S)}$$

where B is the LEC of the leading order Lagrangian as in equation (4.12). The expression for f_2 in this PQChPT is given by

$$
\begin{aligned}
f_2^{pq} =\; & m_K^2 \Big[(2m_K^2 - m_\pi^2)\Big(6m_K^2(2m_K^2 - m_\pi^2)^2 \\
& - m_{ss}^2((2m_K^2 - m_\pi^2)(11m_K^2 - m_\pi^2) + 4m_K^2 m_{ss}^2)\Big) \\
& - 2\Big((5m_K^2 - m_\pi^2)(2m_K^2 - m_\pi^2)^2 - 3(2m_K^2 - m_\pi^2)(3m_K^2 - m_\pi^2)m_{ss}^2 \\
& + (3m_K^2 - m_\pi^2)m_{ss}^4 \Big)m_{dd}^2 + \Big(m_\pi^2 m_{ss}^2 + m_K^2(4m_K^2 - 2m_\pi^2 - 3m_{ss}^2)\Big)m_{dd}^4 \Big] \times \\
& \times \frac{\ln\left(\frac{2m_K^2 - m_\pi^2}{m_\pi^2}\right)}{32\pi^2 f_0^2 (m_K^2 - m_\pi^2)^2 (3m_\pi^2 + 2m_{ss}^2 + m_{dd}^2 - 6m_K^2)^2} \\
& - \frac{m_K^4(m_K^2 - m_{ss}^2)(m_K^2 - m_{dd}^2)\ln\left(\frac{m_K^2}{m_\pi^2}\right)}{8\pi^2 f_0^2 (m_K^2 - m_\pi^2)^2 (3m_K^2 - 2m_{ss}^2 - m_{dd}^2)} \\
& + \frac{(2m_K^2 - m_\pi^2 + m_{ss}^2)(m_\pi^2 + m_{ss}^2)\ln\left(\frac{2m_K^2 - m_\pi^2 + m_{ss}^2}{m_\pi^2 + m_{ss}^2}\right)}{128 f_0^2 (m_K^2 - m_\pi^2)} \\
& + \frac{(2m_K^2 - m_\pi^2 + m_{dd}^2)(m_\pi^2 + m_{dd}^2)\ln\left(\frac{2m_K^2 - m_\pi^2 + m_{dd}^2}{m_\pi^2 + m_{dd}^2}\right)}{64\pi^2 f_0^2 (m_K^2 - m_\pi^2)} \\
& - \frac{3m_K^2(m_K^2 - m_\pi^2)^2(m_{ss}^2 - m_{dd}^2)^2(2m_{ss}^2 + m_{dd}^2)\ln\left(\frac{2m_{ss}^2 + m_{dd}^2}{3m_\pi^2}\right)}{4\pi^2 f_0^2 (3m_K^2 - 2m_{ss}^2 - m_{dd}^2)(2m_{ss}^2 + m_{dd}^2 - 3m_\pi^2)^2(3m_\pi^2 + 2m_{ss}^2 + m_{dd}^2 - 6m_K^2)^2} \\
& + \frac{26m_K^4 - (2m_{ss}^2 + m_{dd}^2 + 3m_\pi^2)(m_{ss}^2 + 2m_{dd}^2)}{64\pi^2 f_0^2 (3m_\pi^2 + 2m_{ss}^2 + m_{dd}^2 - 6m_K^2)} \\
& - \frac{m_K^2(39m_\pi^4 - 8m_{ss}^4 - 18m_\pi^2(m_{ss}^2 + 2m_{dd}^2) + m_{dd}^2(18m_{ss}^2 + 5m_{dd}^2))}{64\pi^2 f_0^2 (3m_\pi^2 - 2m_{ss}^2 - m_{dd}^2)(3m_\pi^2 + 2m_{ss}^2 + m_{dd}^2 - 6m_K^2)} \; .
\end{aligned}
$$

We use this formula for lattice QCD data partially quenched in the strange quark, by setting $m_{dd}^2 = m_\pi^2$. This expression reduces to the unquenched result of equation (4.57) if we also set $m_{ss}^2 = 2m_K^2 - m_\pi^2$ corresponding to setting $m_s^{(V)} = m_s^{(S)}$.

Bibliography

[1] **QCDSF/UKQCD** Collaboration, D. Brommel *et al.*, *The pion form factor from lattice QCD with two dynamical flavours*, Eur. Phys. J. **C51** (2007) 335–345, [`hep-lat/0608021`].

[2] P. A. Boyle *et al.*, *Kl3 semileptonic form factor from 2+1 flavour lattice QCD*, Phys. Rev. Lett. **100** (2008) 141601, [`0710.5136`].

[3] M. Antonelli *et al.*, *An evaluation of $|V_{us}|$ and precise tests of the Standard Model from world data on leptonic and semileptonic kaon decays*, The European Physical Journal C - Particles and Fields (2010) 1–26, [`1005.2323`].

[4] P. Boyle, J. Flynn, A. Jüttner, C. Kelly, C. Maynard, H. Pedroso de Lima, C. Sachrajda, and J. Zanotti, *The pion's electromagnetic form factor at small momentum transfer in full lattice QCD*, JHEP **07** (2008) 112, [`0804.3971`].

[5] P. Boyle, J. Flynn, A. Jüttner, C. Kelly, C. Maynard, H. Pedroso de Lima, C. Sachrajda, and J. Zanotti, *$K \to \pi$ form factors with reduced model dependence*, The European Physical Journal C - Particles and Fields **69** (2010) 159–167, [`1004.0886`].

[6] P. Boyle, J. Flynn, A. Jüttner, C. Kelly, C. Maynard, H. Pedroso de Lima, C. Sachrajda, and J. Zanotti, *K_{l3} and pion form factors using partially twisted boundary conditions*, PoS **LATTICE2008** (2008) 287, [`0812.4265`].

[7] M. Gell-Mann, *A schematic model of baryons and mesons*, Physics Letters **8** (1964), no. 3 214 – 215.

[8] S. L. Glashow, *Partial-symmetries of weak interactions*, Nuclear Physics **22** (1961), no. 4 579 – 588.

[9] S. Weinberg, *A Model of Leptons*, *Phys. Rev. Lett.* **19** (1967) 1264–1266.

[10] A. Salam, *Weak and Electromagnetic Interactions*, . Originally printed in *Svartholm: Elementary Particle Theory, Proceedings Of The Nobel Symposium Held 1968 At Lerum, Sweden*, Stockholm 1968, 367-377.

[11] P. W. Higgs, *Broken symmetries, massless particles and gauge fields*, *Phys. Lett.* **12** (1964) 132–133.

[12] P. W. Higgs, *Spontaneous Symmetry Breakdown without Massless Bosons*, *Phys. Rev.* **145** (1966) 1156–1163.

[13] F. Englert and R. Brout, *Broken symmetry and the mass of gauge vector mesons*, *Phys. Rev. Lett.* **13** (Aug, 1964) 321–323.

[14] G. S. Guralnik, C. R. Hagen, and T. W. B. Kibble, *Global conservation laws and massless particles*, *Phys. Rev. Lett.* **13** (Nov, 1964) 585–587.

[15] D. J. Gross and F. Wilczek, *Ultraviolet behaviour of non-abelian gauge theories*, *Phys. Rev. Lett.* **30** (1973) 1343–1346.

[16] N. Cabibbo, *Unitary Symmetry and Leptonic Decays*, *Phys. Rev. Lett.* **10** (1963) 531–533.

[17] M. Kobayashi and T. Maskawa, *CP Violation in the Renormalizable Theory of Weak Interaction*, *Prog. Theor. Phys.* **49** (1973) 652–657.

[18] M. Artuso *et al.*, *B, D and K decays*, *Eur. Phys. J.* **C57** (2008) 309–492, [0801.1833].

[19] M. Raidal *et al.*, *Flavour physics of leptons and dipole moments*, *Eur. Phys. J.* **C57** (2008) 13–182, [0801.1826].

[20] A. Juttner, *Progress in kaon physics on the lattice*, *PoS* **LAT2007** (2007) 014, [0711.1239].

[21] M. E. Peskin and D. V. Schroeder, *An Introduction to quantum field theory*, . Reading, USA: Addison-Wesley (1995) 842 p.

[22] **Particle Data Group** Collaboration, K. Nakamura *et al.*, *Review of particle physics*, *J. Phys.* **G37** (2010).

[23] J. C. Hardy and I. S. Towner, *Superallowed $0^+ \rightarrow 0^+$ nuclear beta decays: A new survey with precision tests of the conserved vector current hypothesis and the standard model, Phys. Rev.* **C79** (2009) 055502, [`0812.1202`].

[24] W. J. Marciano and A. Sirlin, *Radiative corrections to π_{l2} decays, Phys. Rev. Lett.* **71** (1993) 3629–3632.

[25] V. Cirigliano and I. Rosell, *$\pi/K \rightarrow e\nu$ branching ratios to $O(e^2 p^4)$ in Chiral Perturbation Theory, JHEP* **10** (2007) 005, [`0707.4464`].

[26] H. Leutwyler and M. Roos, *Determination of the Elements V_{us} and V_{ud} of the Kobayashi-Maskawa Matrix, Z. Phys.* **C25** (1984) 91.

[27] M. Ademollo and R. Gatto, *Nonrenormalization Theorem for the Strangeness Violating Vector Currents, Phys. Rev. Lett.* **13** (1964) 264–265.

[28] D. Becirevic *et al.*, *The $K \rightarrow \pi$ vector form factor at zero momentum transfer on the lattice, Nucl. Phys.* **B705** (2005) 339–362, [`hep-ph/0403217`].

[29] D. Becirevic *et al.*, *SU(3)-breaking effects in kaon and hyperon semileptonic decays from lattice QCD, Eur. Phys. J.* **A24S1** (2005) 69–73, [`hep-lat/0411016`].

[30] **ETMC** Collaboration, S. Simula, *Pseudo-scalar meson form factors with maximally twisted Wilson fermions at $N_f = 2$, PoS* **LAT2007** (2007) 371, [`0710.0097`].

[31] R. Frezzotti, V. Lubicz, and S. Simula, *Electromagnetic form factor of the pion from twisted-mass lattice QCD at $N_f = 2$, Phys. Rev.* **D79** (2009) 074506, [`0812.4042`].

[32] K. G. Wilson, *Confinement of quarks, Phys. Rev.* **D10** (1974) 2445–2459.

[33] K. Symanzik, *Continuum limit and improved action in lattice theories : (i). principles and ϕ^4 theory, Nuclear Physics B* **226** (1983), no. 1 187 – 204.

[34] K. Symanzik, *Continuum limit and improved action in lattice theories : (ii). o(n) non-linear sigma model in perturbation theory*, Nuclear Physics B **226** (1983), no. 1 205 – 227.

[35] Y. Iwasaki and T. Yoshie, *Renormalization group improved action for SU(3) lattice gauge theory and the string tension*, Phys. Lett. **B143** (1984) 449.

[36] Y. Iwasaki, *Renormalization Group Analysis of Lattice Theories and Improved Lattice Action: Two-Dimensional Nonlinear O(N) Sigma Model*, Nucl. Phys. **B258** (1985) 141–156.

[37] **RBC and UKQCD** Collaboration, D. J. Antonio *et al.*, *First results from 2+1-flavor domain wall QCD: Mass spectrum, topology change and chiral symmetry with L(s) = 8*, Phys. Rev. **D75** (2007) 114501, [`hep-lat/0612005`].

[38] **RBC** Collaboration, D. J. Antonio *et al.*, *Localization and chiral symmetry in 3 flavor domain wall QCD*, Phys. Rev. **D77** (2008) 014509, [`0705.2340`].

[39] R. Gupta, *Introduction to lattice QCD*, `hep-lat/9807028`.

[40] K. G. Wilson, *Quarks and Strings on a Lattice*, . New Phenomena In Subnuclear Physics. Part A. Proceedings of the First Half of the 1975 International School of Subnuclear Physics, Erice, Sicily, July 11 - August 1, 1975, ed. A. Zichichi, Plenum Press, New York, 1977, p. 69, CLNS-321.

[41] H. B. Nielsen and M. Ninomiya, *No Go Theorem for Regularizing Chiral Fermions*, Phys. Lett. **B105** (1981) 219.

[42] P. H. Ginsparg and K. G. Wilson, *A Remnant of Chiral Symmetry on the Lattice*, Phys. Rev. **D25** (1982) 2649.

[43] D. B. Kaplan, *A Method for simulating chiral fermions on the lattice*, Phys. Lett. **B288** (1992) 342–347, [`hep-lat/9206013`].

[44] Y. Shamir, *Chiral fermions from lattice boundaries*, Nucl. Phys. **B406** (1993) 90–106, [`hep-lat/9303005`].

[45] V. Furman and Y. Shamir, *Axial symmetries in lattice QCD with Kaplan fermions, Nucl. Phys.* **B439** (1995) 54–78, [`hep-lat/9405004`].

[46] P. M. Vranas, *Chiral symmetry restoration in the Schwinger model with domain wall fermions, Phys. Rev.* **D57** (1998) 1415–1432, [`hep-lat/9705023`].

[47] T. Blum *et al.*, *Quenched lattice QCD with domain wall fermions and the chiral limit, Phys. Rev.* **D69** (2004) 074502, [`hep-lat/0007038`].

[48] A. D. Kennedy, *Algorithms for dynamical fermions,* `hep-lat/0607038`.

[49] N. Metropolis, A. W. Rosenbluth, M. N. Rosenbluth, A. H. Teller, and E. Teller, *Equation of state calculations by fast computing machines, The Journal of Chemical Physics* **21** (1953), no. 6 1087–1092.

[50] E. Marinari, G. Parisi, and C. Rebbi, *Monte carlo simulation of the massive schwinger model, Nuclear Physics B* **190** (1981), no. 4 734 – 750.

[51] **HPQCD** Collaboration, C. T. H. Davies *et al.*, *High-precision lattice QCD confronts experiment, Phys. Rev. Lett.* **92** (2004) 022001, [`hep-lat/0304004`].

[52] **RBC and UKQCD** Collaboration, C. Allton *et al.*, *2+1 flavor domain wall qcd on a (2 fm)^3 lattice:light meson spectroscopy with l_s = 16, Phys. Rev.* **D76** (2007) 014504, [`hep-lat/0701013`].

[53] M. A. Clark and A. D. Kennedy, *Accelerating Dynamical Fermion Computations using the Rational Hybrid Monte Carlo (RHMC) Algorithm with Multiple Pseudofermion Fields, Phys. Rev. Lett.* **98** (2007) 051601, [`hep-lat/0608015`].

[54] A. D. Kennedy, I. Horvath, and S. Sint, *A new exact method for dynamical fermion computations with non-local actions, Nucl. Phys. Proc. Suppl.* **73** (1999) 834–836, [`hep-lat/9809092`].

107

[55] M. A. Clark, *The rational hybrid Monte Carlo algorithm*, *PoS* **LAT2006** (2006) 004, [`hep-lat/0610048`].

[56] G. Martinelli and C. T. Sachrajda, *A lattice study of nucleon structure*, *Nucl. Phys.* **B316** (1989) 355.

[57] **UKQCD** Collaboration, M. Foster and C. Michael, *Quark mass dependence of hadron masses from lattice QCD*, *Phys. Rev.* **D59** (1999) 074503, [`hep-lat/9810021`].

[58] **UKQCD** Collaboration, C. McNeile and C. Michael, *Decay width of light quark hybrid meson from the lattice*, *Phys. Rev.* **D73** (2006) 074506, [`hep-lat/0603007`].

[59] P. A. Boyle, A. Juttner, C. Kelly, and R. D. Kenway, *Use of stochastic sources for the lattice determination of light quark physics*, *JHEP* **08** (2008) 086, [`0804.1501`].

[60] S.-J. Dong and K.-F. Liu, *Stochastic estimation with Z(2) noise*, *Phys. Lett.* **B328** (1994) 130–136, [`hep-lat/9308015`].

[61] P. A. Boyle, J. M. Flynn, A. Juttner, C. T. Sachrajda, and J. M. Zanotti, *Hadronic form factors in lattice QCD at small and vanishing momentum transfer*, *JHEP* **05** (2007) 016, [`hep-lat/0703005`].

[62] S. R. Coleman, J. Wess, and B. Zumino, *Structure of phenomenological Lagrangians. 1*, *Phys. Rev.* **177** (1969) 2239–2247.

[63] C. G. Callan, Jr., S. R. Coleman, J. Wess, and B. Zumino, *Structure of phenomenological Lagrangians. 2*, *Phys. Rev.* **177** (1969) 2247–2250.

[64] A. Pich, *Chiral perturbation theory*, *Rept. Prog. Phys.* **58** (1995) 563–610, [`hep-ph/9502366`].

[65] H. Leutwyler, *On the foundations of chiral perturbation theory*, *Ann. Phys.* **235** (1994) 165–203, [`hep-ph/9311274`].

[66] J. Gasser and H. Leutwyler, *Chiral Perturbation Theory to One Loop*, *Ann. Phys.* **158** (1984) 142.

[67] J. Gasser and H. Leutwyler, *Chiral Perturbation Theory: Expansions in the Mass of the Strange Quark, Nucl. Phys.* **B250** (1985) 465.

[68] J. Gasser and H. Leutwyler, *Low-Energy Expansion of Meson Form-Factors, Nucl. Phys.* **B250** (1985) 517–538.

[69] J. Bijnens, G. Colangelo, and P. Talavera, *The vector and scalar form factors of the pion to two loops, JHEP* **05** (1998) 014, [hep-ph/9805389].

[70] J. Bijnens, G. Colangelo, and G. Ecker, *Renormalization of chiral perturbation theory to order p^6, Annals Phys.* **280** (2000) 100–139, [hep-ph/9907333].

[71] J. Bijnens and P. Talavera, *Pion and kaon electromagnetic form factors, JHEP* **03** (2002) 046, [hep-ph/0203049].

[72] T. E. Rudy, H. W. Fearing, and S. Scherer, *Off-shell electromagnetic form factors of pions and kaons in chiral perturbation theory, Phys. Rev. C* **50** (Jul, 1994) 447–459.

[73] **RBC-UKQCD** Collaboration, C. Allton *et al.*, *Physical Results from 2+1 Flavor Domain Wall QCD and SU(2) Chiral Perturbation Theory, Phys. Rev.* **D78** (2008) 114509, [0804.0473].

[74] J. Bijnens and P. Talavera, *K_{l3} decays in chiral perturbation theory, Nucl. Phys.* **B669** (2003) 341–362, [hep-ph/0303103].

[75] **RBC** Collaboration, J. M. Flynn and C. T. Sachrajda, *SU(2) chiral perturbation theory for Kl3 decay amplitudes, Nucl. Phys.* **B812** (2009) 64–80, [0809.1229].

[76] A. Roessl, *Pion kaon scattering near the threshold in chiral SU(2) perturbation theory, Nucl. Phys.* **B555** (1999) 507–539, [hep-ph/9904230].

[77] J. Bijnens and A. Celis, *$K \to \pi\pi$ Decays in SU(2) Chiral Perturbation Theory, Phys. Lett.* **B680** (2009) 466–470, [0906.0302].

[78] C. W. Bernard and M. F. L. Golterman, *Partially quenched gauge theories and an application to staggered fermions*, Phys. Rev. **D49** (1994) 486–494, [`hep-lat/9306005`].

[79] J. Bijnens, N. Danielsson, and T. A. Lahde, *Three-flavor partially quenched chiral perturbation theory at NNLO for meson masses and decay constants*, Phys. Rev. **D73** (2006) 074509, [`hep-lat/0602003`].

[80] D. Becirevic, G. Martinelli, and G. Villadoro, *The Ademollo-Gatto theorem for lattice semileptonic decays*, Phys. Lett. **B633** (2006) 84–88, [`hep-lat/0508013`].

[81] S. R. Sharpe and N. Shoresh, *Partially quenched chiral perturbation theory without* Φ_0, Phys. Rev. **D64** (2001) 114510, [`hep-lat/0108003`].

[82] A. Hasenfratz, K. Jansen, J. Jersk, H. A. Kastrup, C. B. Lang, H. Leutwyler, and T. Neuhaus, *Goldstone bosons and finite size effects: A numerical study of the o(4) model*, Nuclear Physics B **356** (1991), no. 1 332 – 363.

[83] P. F. Bedaque, *Aharonov-Bohm effect and nucleon nucleon phase shifts on the lattice*, Phys. Lett. **B593** (2004) 82–88, [`nucl-th/0402051`].

[84] P. F. Bedaque and J.-W. Chen, *Twisted valence quarks and hadron interactions on the lattice*, Phys. Lett. **B616** (2005) 208–214, [`hep-lat/0412023`].

[85] C. T. Sachrajda and G. Villadoro, *Twisted boundary conditions in lattice simulations*, Phys. Lett. **B609** (2005) 73–85, [`hep-lat/0411033`].

[86] **UKQCD** Collaboration, J. M. Flynn, A. Juttner, and C. T. Sachrajda, *A numerical study of partially twisted boundary conditions*, Phys. Lett. **B632** (2006) 313–318, [`hep-lat/0506016`].

[87] **QCDOC** Collaboration, P. A. Boyle, C. Jung, and T. Wettig, *The QCDOC supercomputer: Hardware, software, and performance*, ECONF **C0303241** (2003) THIT003, [`hep-lat/0306023`].

[88] P. A. Boyle *et al.*, *Hardware and software status of QCDOC*, *Nucl. Phys. Proc. Suppl.* **129** (2004) 838–843, [`hep-lat/0309096`].

[89] P. Boyle *et al.*, *The QCDOC project*, *Nucl. Phys. Proc. Suppl.* **140** (2005) 169–175.

[90] P. A. Boyle *et al.*, *Overview of the qcdsp and qcdoc computers*, *IBM J. Res. Dev.* **49** (2005), no. 2 351–365.

[91] **Particle Data Group** Collaboration, W. M. Yao *et al.*, *Review of particle physics*, *J. Phys.* **G33** (2006) 1–1232.

[92] **JLQCD** Collaboration, S. Hashimoto *et al.*, *Pion form factors in two-flavor QCD*, *PoS* **LAT2005** (2006) 336, [`hep-lat/0510085`].

[93] **JLQCD** Collaboration, S. Aoki *et al.*, *Pion form factors from two-flavor lattice QCD with exact chiral symmetry*, *Phys. Rev.* **D80** (2009) 034508, [`0905.2465`].

[94] **NA7** Collaboration, S. R. Amendolia *et al.*, *A Measurement of the Space - Like Pion Electromagnetic Form-Factor*, *Nucl. Phys.* **B277** (1986) 168.

[95] F. J. Jiang and B. C. Tiburzi, *Flavor Twisted Boundary Conditions, Pion Momentum, and the Pion Electromagnetic Form Factor*, *Phys. Lett.* **B645** (2007) 314–321, [`hep-lat/0610103`].

[96] C. Jung, *Status of dynamical ensemble generation*, `1001.0941`.

[97] M. Luscher and F. Palombi, *Fluctuations and reweighting of the quark determinant on large lattices*, *PoS* **LATTICE2008** (2008) 049, [`0810.0946`].

[98] A. Hasenfratz, R. Hoffmann, and S. Schaefer, *Reweighting towards the chiral limit*, *Phys. Rev.* **D78** (2008) 014515, [`0805.2369`].

[99] V. Bernard and E. Passemar, *Chiral Extrapolation of the Strangeness Changing $K \to \pi$ Form Factor*, *JHEP* **04** (2010) 001, [`0912.3792`].

[100] D. Renfrew, T. Blum, N. Christ, R. Mawhinney, and P. Vranas, *Controlling Residual Chiral Symmetry Breaking in Domain Wall Fermion Simulations*, *PoS* **LATTICE2008** (2008) 048, [`0902.2587`].